

EFFECT OF GIGANTOL ON TUMORIGENICITY OF NON-SMALL CELL LUNG CANCER  
CELLS VIA CANCER STEM CELL SIGNAL SUPPRESSION



A Dissertation Submitted in Partial Fulfillment of the Requirements  
for the Degree of Doctor of Philosophy in Pharmacology and Toxicology

Department of Pharmacology and Physiology

FACULTY OF PHARMACEUTICAL SCIENCES

Chulalongkorn University

Academic Year 2019

Copyright of Chulalongkorn University

ผลของใจแกนทอลต่อการก่อเนื่องอกของเซลล์มะเร็งปอดชนิดไม่ใช่เซลล์เล็กผ่านการกดสัญญาณ  
เซลล์ต้นกำเนิดมะเร็ง



วิทยานิพนธ์นี้เป็นส่วนหนึ่งของการศึกษาตามหลักสูตรปริญญาเภสัชศาสตรดุษฎีบัณฑิต  
สาขาวิชาเภสัชวิทยาและพิษวิทยา ภาควิชาเภสัชวิทยาและสรีรวิทยา  
คณะเภสัชศาสตร์ จุฬาลงกรณ์มหาวิทยาลัย  
ปีการศึกษา 2562  
ลิขสิทธิ์ของจุฬาลงกรณ์มหาวิทยาลัย

Thesis Title EFFECT OF GIGANTOL ON TUMORIGENICITY OF NON-SMALL  
CELL LUNG CANCER CELLS VIA CANCER STEM CELL SIGNAL  
SUPPRESSION

By Miss Nattanan Losuwannarak

Field of Study Pharmacology and Toxicology

Thesis Advisor Professor PITHI CHANVORACHOTE, Ph.D.

---

Accepted by the FACULTY OF PHARMACEUTICAL SCIENCES, Chulalongkorn  
University in Partial Fulfillment of the Requirement for the Doctor of Philosophy

..... Dean of the FACULTY OF  
PHARMACEUTICAL SCIENCES  
(Assistant Professor RUNGPETCH SAKULBUMRUNGSIL, Ph.D.)

DISSERTATION COMMITTEE

..... Chairman  
(Associate Professor SUREE JIANMONGKOL, Ph.D.)

..... Thesis Advisor  
(Professor PITHI CHANVORACHOTE, Ph.D.)

..... Examiner  
(Associate Professor VARISA PONGRAKHANANON, Ph.D.)

..... Examiner  
(Assistant Professor SUPANNIKAR TAWINWUNG, Ph.D.)

..... External Examiner  
(Associate Professor Uraiwan Panich, M.D., Ph.D., FCFPT)

ณัฐนันท์ โล่สุวรรณรักษ์ : ผลของใจแกนทอลต่อการก่อเนื้องอกของเซลล์มะเร็งปอดชนิดไม่ใช้  
เซลล์เล็กผ่านการกดสัญญาณเซลล์ต้นกำเนิดมะเร็ง. ( EFFECT OF GIGANTOL ON  
TUMORIGENICITY OF NON-SMALL CELL LUNG CANCER CELLS VIA CANCER STEM  
CELL SIGNAL SUPPRESSION) อ.ที่ปรึกษาหลัก : ศ. ภก. ดร.ปิติ จันทรวรรโชติ

มะเร็งปอดเป็นสาเหตุสำคัญของการเสียชีวิตจากโรคมะเร็ง การเจริญของก้อนมะเร็งเป็นกระบวนการสำคัญที่กระตุ้นให้โรคดำเนินไป คุณลักษณะสำคัญที่ส่งเสริมการเจริญของก้อนมะเร็งคือเซลล์มะเร็งต้นกำเนิดและการเพิ่มจำนวนของเซลล์มะเร็ง มีรายงานว่าการรักษาแบบมุ่งเป้าไปที่วิถีสัญญาณที่ส่งเสริมความเป็นเซลล์ต้นกำเนิดหรือการเพิ่มจำนวนเซลล์เป็นวิธีการที่มีแนวโน้มที่ดีในการรักษาโรคมะเร็ง ใจแกนทอลซึ่งเป็นสารประกอบกลุ่มโอบิเจน (Dendrobium Draconis) มีฤทธิ์ยับยั้งฟิโนไทป์เซลล์มะเร็งต้นกำเนิดในหลอดทดลอง อย่างไรก็ตามยังไม่มีการศึกษาผลของใจแกนทอลที่มีต่อการเกิดเนื้องอก การเพิ่มจำนวนเซลล์มะเร็ง และวิถีสัญญาณที่ส่งเสริมความเป็นเซลล์ต้นกำเนิดรวมถึงการเพิ่มจำนวนเซลล์มะเร็ง การศึกษานี้ใช้การปลูกถ่ายเนื้องอกไวรัสพันธุ์ในหนูไร้ขนเพื่อศึกษาผลของใจแกนทอลต่อความสามารถในการเกิดเนื้องอกและใช้การทดสอบการเกิดโคโลนีในหลอดทดลองเพื่อศึกษาผลของใจแกนทอลต่อการเพิ่มจำนวนเซลล์ นอกจากนี้ยังใช้การวิเคราะห์ทางโปรตีโอมิกส์มาช่วยในการวิเคราะห์หาไกลโกลิเซโกลของใจแกนทอลต่อฟิโนไทป์ดังกล่าว ผลการทดลองในหนูไร้ขนแสดงให้เห็นว่าก้อนเนื้องอกที่เกิดจากเซลล์ที่ได้รับใจแกนทอลมีมวลและความหนาแน่นของก้อนเนื้องอกลดลงเทียบกับก้อนเนื้องอกควบคุมภายในหนูตัวเดียวกัน ยิ่งไปกว่านั้นก้อนเนื้องอกที่เกิดจากเซลล์ที่ได้รับใจแกนทอลมีจำนวนเซลล์มะเร็งที่กำลังแบ่งตัวซึ่งถูกระบุโดยการย้อมติด Ki-67 น้อยกว่ากลุ่มควบคุมอย่างมีนัยสำคัญ ส่วนผลต่อการเพิ่มจำนวนเซลล์ ใจแกนทอลชะลออัตราการเจริญของเซลล์รวมทั้งลดจำนวนโคโลนีของเซลล์มะเร็งปอดได้อย่างมีนัยสำคัญ ผลการวิเคราะห์ทางโปรตีโอมิกส์บ่งชี้ว่าใจแกนทอลยับยั้งโปรตีนสัญญาณในวิถี PI3K/Akt/mTOR และ JAK/STAT ซึ่งเป็นวิถีที่ควบคุมคุณสมบัติของเซลล์มะเร็งต้นกำเนิด และยับยั้ง c-Myc ซึ่งเป็นทรานสคริปชันแฟกเตอร์ที่ส่งเสริมการเพิ่มจำนวนเซลล์และรักษาความเป็นเซลล์ต้นกำเนิด เนื่องจากเป็นที่ทราบกันว่า Akt ควบคุม c-Myc ผ่านการยับยั้ง GSK3 $\beta$  การทำเวสเทิร์นบลอตพร้อมกับการตกตะกอนภูมิคุ้มกันจึงถูกนำมาใช้เพื่อยืนยัน ซึ่งพบว่าใจแกนทอลส่งเสริมการทำงานของ GSK3 $\beta$  และส่งผลให้เพิ่มการทำลาย c-Myc โดยเพิ่มการเกิดสารเชิงซ้อนของ c-Myc กับ ubiquitin โดยสรุป การศึกษานี้เผยให้เห็นกลไกใหม่ในการต้านมะเร็งของใจแกนทอลซึ่งคือการยับยั้งวิถี PI3K/Akt/mTOR และ JAK/STAT รวมทั้งเหนี่ยวนำการทำลาย c-Myc ทาง ubiquitin-proteasome โดยผ่านการทำงานของ GSK3 $\beta$  ส่งผลให้ลดอัตราการเจริญของก้อนมะเร็งและเสถียรภาพของก้อนมะเร็งที่เกิดขึ้นในร่างกาย ข้อมูลดังกล่าวสนับสนุนศักยภาพของใจแกนทอลที่จะพัฒนาต่อไปเพื่อใช้เป็นยารักษาโรคมะเร็งปอด

สาขาวิชา เกษัตริศาสตร์และพิษวิทยา

ลายมือชื่อนิสิต .....

ปีการศึกษา 2562

ลายมือชื่อ อ.ที่ปรึกษาหลัก .....

# # 5976456333 : MAJOR PHARMACOLOGY AND TOXICOLOGY

KEYWORD: gigantol, cancer stem cell, lung cancer, cell proliferation, tumorigenicity, tumor xenograft, proteomics

Nattanan Losuwannarak : EFFECT OF GIGANTOL ON TUMORIGENICITY OF NON-SMALL CELL LUNG CANCER CELLS VIA CANCER STEM CELL SIGNAL SUPPRESSION. Advisor: Prof. PITHI CHANVORACHOTE, Ph.D.

Lung cancer is a major cause of cancer-related death. Tumor growth is a fundamental process of cancer progression. Vital characteristics that potentiate tumor growth are cancer stem cell (CSC) and enhance cell proliferation. Previous studies reported that targeting on CSC-promoting pathways or proliferative signals was a promising strategy in cancer treatment. Gigantol, a bibenzyl compound from *Dendrobium draconis*, was reported to have a suppressive activity on CSC phenotypes, *in vitro*. However, the effects of gigantol on tumorigenicity *in vivo*, cancer cell proliferation and related CSC-promoting and proliferation regulatory mechanisms have not been explored. In this study, ectopic tumor xenograft in nude mice was utilized to gain understanding on how gigantol attenuated CSCs and tumorigenicity capacity, and proliferation assay and colony formation assay were used to evaluate an anti-proliferative effect of gigantol. Proteomics analysis was used to identify molecular mechanisms of gigantol on the CSC-phenotype and proliferation regulation. The results of tumor xenografts showed that the tumor raised from gigantol-treating cells had lower tumor weight and density than its own paired untreated control within each mouse. Moreover, the tumors raised from gigantol-pretreated cells showed significantly lower proliferative tumor cells, indicating by Ki-67 labeling. For proliferation, gigantol reduced growth rates and colony forming units of lung cancer cells. The proteomics analysis revealed that gigantol suppressed functional proteins manipulating the CSC properties, which were signaling proteins in PI3K/Akt/mTOR and JAK/STAT pathways. Also, c-Myc, a proliferation- and stemness-promoting transcription factor, was down-regulated by gigantol. It was known that Akt controls c-Myc by inhibiting GSK3 $\beta$ . Western blot analysis and immunoprecipitation were used to confirm, and the results showed that gigantol facilitated GSK3 $\beta$  function, which enhanced c-Myc degradation by increasing c-Myc-ubiquitin complex. In conclusion, this study reveals novel insights into the anti-tumor mechanisms of gigantol focused on CSC targeting, destabilizing tumor integrity, and suppressing tumor growth via suppression of the PI3K/Akt/mTOR and JAK/STAT pathways, as well as, induction of GSK3 $\beta$ -mediated c-Myc ubiquitin-proteasome degradation. This data supports the potential of gigantol to be developed as a drug for lung cancer.

Field of Study: Pharmacology and Toxicology

Student's Signature .....

Academic Year: 2019

Advisor's Signature .....

## ACKNOWLEDGEMENTS

I would like to express my sincere gratefulness to my advisor, Associate Professor Dr. Pithi Chanvorachote for his valuable support, knowledge supervision, and encouragements. He never hesitates to provide an opportunity for his students to access the experience the world outside through his numerous collaborations. He also arouses my critical thinking and encourages me to my best. I would never make it to this point without his support.

I would like to show an appreciate to Associate Professor Dr. Sittiruk Roytrakul and Mr. Yodying Yingchutrakul from BIOTEC for knowledge and skills in proteomics technique, as well as, Associate Professor Dr. Nakarin Kitkumtorn, Assistant Professor Dr. Asada Leelahavanichkul, and Dr. Panomwat Amornphimoltham for knowledge and skills in in vivo technique.

Also, I would like to give my gratitude to all teachers and staffs from the Department of Pharmacology and Physiology, Faculty of Pharmaceutical Sciences, Chulalongkorn University for their advices and tireless helps throughout my study.

I would like to thank all colleagues in my laboratory, particularly Mr. Arnatchai Maiuthed, Miss Sucharat Tungsukruthai, Miss Korrakod Petsri, Miss Rapeepun Soonnarong, Miss Nicharat Sriratanasak, and Miss Nongyao Nonpanya for their helps. This thesis could not be completed without their support.

Lastly, I am grateful to the 90th Anniversary of Chulalongkorn University, Rachadapisek Sompote Fund of Chulalongkorn University.

Nattanan Losuwannarak

## TABLE OF CONTENTS

	Page
ABSTRACT (THAI).....	iii
ABSTRACT (ENGLISH).....	iv
ACKNOWLEDGEMENTS.....	v
TABLE OF CONTENTS.....	vi
LIST OF TABLES.....	ix
LIST OF FIGURES.....	xi
LIST OF ABBREVIATIONS.....	xiv
CHAPTER I INTRODUCTION.....	1
BACKGROUND AND RATIONALE.....	1
RESEARCH QUESTIONS.....	5
OBJECTIVES.....	5
HYPOTHESIS.....	6
EXPECTED BENEFITS.....	6
CHAPTER II LITERATURE REVIEWS.....	7
Lung cancer.....	7
Cancer stem cells.....	9
Lung CSCs.....	10
Signaling pathways in CSCs and therapeutic implications.....	11
PI3K/Akt pathway in CSCs.....	13
JAK/STAT3 pathway in CSCs.....	16
Tumorigenicity.....	20

Tumor subcutaneous xenograft model .....	21
Proteomics analysis .....	25
Gigantol.....	26
CHAPTER III METHODOLOGY .....	29
1. Cell line cultures.....	29
2. Animals.....	29
3. Chemicals and reagents.....	30
4. Equipments .....	31
5. Cell viability test: MTT assay .....	31
6. Cell death determination assay .....	32
7. Cancer cell preparation for subcutaneous xenograft inoculation .....	32
8. Subcutaneous tumor xenograft procedure .....	33
9. Immunohistochemistry staining of Ki-67 and $\alpha$ -SMA of the tumor slides.....	34
10. Sample preparation for proteomics analysis .....	35
11. Liquid chromatography-tandem mass spectrometry (LC-MS/MS).....	35
12. Bioinformatics and proteomics data analysis.....	36
13. Proliferation assay.....	37
14. Colony formation assay.....	37
15. Western Blot Analysis.....	38
16. Cycloheximide (CHX) chasing assay.....	39
17. Immunoprecipitation Assay.....	40
18. Statistical analysis.....	40
EXPERIMENTAL DESIGN.....	42



Part I: Determination of the non-toxic concentration of gigantol in human lung cancer cell lines .....	42
Part II: Investigation of effects of non-toxic concentration of gigantol on cell proliferation and tumorigenicity in human lung cancer H460 cell line.....	43
Part III: Investigation of effects of gigantol on underlying mechanisms involved in CSC-like phenotype and cell proliferation in human lung cancer H460 cell line .....	45
CHAPTER IV RESULTS .....	48
Part I: Non-cytotoxic concentration evaluation of gigantol in human lung cancer cell lines .....	48
Part II: Investigation of effects of non-toxic concentration of gigantol on cell proliferation and tumorigenicity in human lung cancer H460 cell line.....	51
Part III: Investigation of effects of gigantol on underlying mechanisms involved in CSC-like phenotype and cell proliferation in human lung cancer H460 cell line .....	64
CHAPTER V DISCUSSION .....	93
REFERENCES .....	105
APPENDIX.....	126
VITA.....	137

## LIST OF TABLES

	Page
<b>Table 1.</b> The pairwise percentage of identity in Akt domains of each isoform .....	14
<b>Table 2.</b> Activation of STATs in human solid tumors .....	19
<b>Table 3.</b> The details of antibodies used in Western blot analysis .....	39
<b>Table 4.</b> First 10 ranking enrichment terms from the GO biological process of down- and up-regulated proteins in gigantol-treated cells .....	67
<b>Table 5.</b> List of genes involved with protein phosphorylation and differentially regulated by gigantol treatment in H460 lung cancer cells .....	68
<b>Table 6.</b> List of genes associated with regulation of cell proliferation and differentially regulated by gigantol treatment in H460 lung cancer cells .....	80
<b>Table 7.</b> Hub proteins that controls cell proliferation which were down-regulated by gigantol treatment in H460 lung cancer cells.....	83
<b>Table 8.</b> Hub proteins that controls cell proliferation which were up-regulated by gigantol treatment in H460 lung cancer cells. ....	84
<b>Table 9.</b> The percentage of H460, A549, H292 and BEAS-2B cell viability .....	126
<b>Table 10.</b> The percentage of apoptotic cells of H460 cells.....	126
<b>Table 11.</b> Relative protein levels of CSC markers of H460 cells .....	127
<b>Table 12.</b> Body weights of nude mice observed from day 0 to 13.....	127
<b>Table 13.</b> Tumor volumes (mm <sup>3</sup> ) of untreated and gigantol-pretreated groups measured from day 7 to 13. ....	128
<b>Table 14.</b> Means of tumor volume (mm <sup>3</sup> ) of untreated and gigantol-pretreated groups from day 7 to 13 .....	128
<b>Table 15.</b> Tumor weights (mg) of untreated and gigantol-pretreated groups observed on day 13.....	129

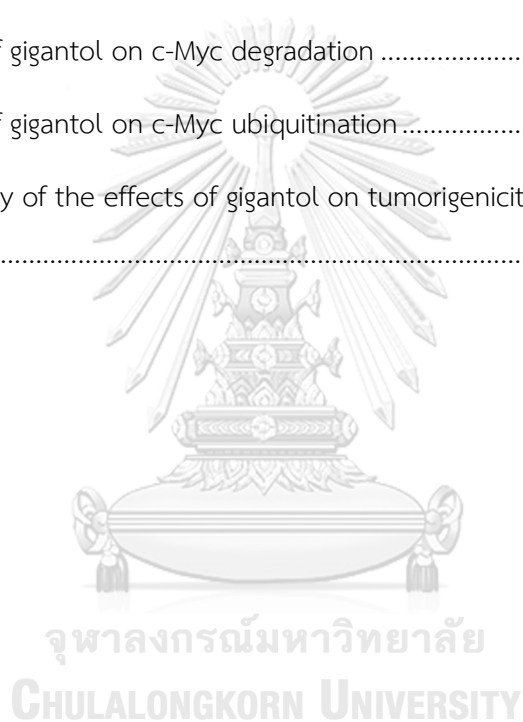
<b>Table 16.</b> Tumor volume (mm <sup>3</sup> ) of dissected untreated and gigantol-pretreated groups measured on day 13. ....	129
<b>Table 17.</b> Tumor densities of untreated and gigantol-pretreated groups from dissected tumor weights and volumes measured on day 13. ....	130
<b>Table 18.</b> The percentage of necrotic areas in Hematoxylin and eosin-stained tumor slides. ....	130
<b>Table 19.</b> The percentage of Ki-67 positive cells .....	131
<b>Table 20.</b> Relative ratios of the protein levels of p-Akt (S473) and total Akt and p-STAT3 (S727) and total STAT3 of H460 cells.....	131
<b>Table 21.</b> Relative protein levels of CSC markers, CD133 and ALDH1A1, and relative ratios of the protein levels of p-Akt (S473) and total Akt and p-STAT3 (S727) and total STAT3 of H460, A549, and H292 cells.....	132
<b>Table 22.</b> Relative growth rates of H460, A549, and H292 cells.....	133
<b>Table 23.</b> The percentage of colony numbers of H460, A549, and H292 cells from colony formation assay .....	134
<b>Table 24.</b> Relative protein levels of c-Myc of lung cancer cells .....	134
<b>Table 25.</b> Relative protein levels of p-GSK3 $\beta$ (S9)/GSK3 $\beta$ of lung cancer cells.....	135
<b>Table 26.</b> Relative protein levels of c-Myc of lung cancer cells from CHX chasing assay.....	135
<b>Table 27.</b> Relative protein levels of c-Myc of lung cancer cells after treatment with MG132 or MG132 with gigantol for 1 hour. ....	136
<b>Table 28.</b> Relative protein levels of ubiquitin of lung cancer cells from the c-Myc immunoprecipitated lysates.....	136

## LIST OF FIGURES

	Page
<b>Figure 1.</b> Akt1 structure.....	14
<b>Figure 2.</b> Depicted PI3K/Akt signaling pathway .....	16
<b>Figure 3.</b> The domain structure of the seven STAT-family members.....	18
<b>Figure 4.</b> JAK/STAT3 signaling pathway .....	19
<b>Figure 5.</b> Scheme shows a process of tumorigenesis.....	20
<b>Figure 6.</b> Gigantol structure and plant specimen of <i>Dendrobium droconis</i> Rchb.f. ....	27
<b>Figure 7.</b> Scheme showing the experimental design of <i>in vivo</i> subcutaneous xenograft experiment.....	33
<b>Figure 8.</b> Schematic diagram of conceptual framework. ....	41
<b>Figure 9.</b> Schematic diagram of the experimental design.....	47
<b>Figure 10.</b> Cytotoxic effect of gigantol on lung cancer cells. and normal lung epithelial cells.....	49
<b>Figure 11.</b> Hoechst 33342 and propidium iodide staining of apoptotic cells of H460 cells after gigantol treatment .....	50
<b>Figure 12.</b> Anti-proliferative effect of gigantol on lung cancer cells using MTT assay	52
<b>Figure 13.</b> Anti-proliferative effect of gigantol on lung cancer cells using colony formation assay.....	53
<b>Figure 14.</b> Effect of gigantol on CSC markers in H460 cells.....	54
<b>Figure 15.</b> Graph showing mice body weights .....	56
<b>Figure 16.</b> Graphs demonstrating the tumor growth rate.....	57
<b>Figure 17.</b> Images of dissected tumors and graph showing tumor weights and tumor volumes.....	58
<b>Figure 18.</b> Graph showing the tumor densities.....	59

<b>Figure 19.</b> Hematoxylin and eosin staining showing intratumor morphology and graph showing percentages of necrotic areas.....	60
<b>Figure 20.</b> Immunohistochemistry staining demonstrating Ki-67 positive cells and graph showing the means of %Ki-67 positive cells.....	62
<b>Figure 21.</b> Immunohistochemistry staining of $\alpha$ -SMA showing vessel distribution among the tumor mass.....	63
<b>Figure 22.</b> Schematic diagram of the proteomic workflow for verification of the CSC-related signaling pathways affected by gigantol.....	65
<b>Figure 23.</b> Venn diagram showing the difference in proteins expressions between the control and gigantol-treated H460 cells .....	66
<b>Figure 24.</b> Networks presenting the functional protein-protein interactions of the down-regulated proteins related to protein phosphorylation and the enriched signaling pathways .....	72
<b>Figure 25.</b> Networks presenting the functional protein-protein interactions of the up-regulated proteins related to protein phosphorylation and the enriched signaling pathways .....	73
<b>Figure 26.</b> Heatmap representing the levels of proteins associated with the signaling pathways regulating the pluripotency of stem cells in the control and gigantol-treated H460 cells.....	74
<b>Figure 27.</b> Effect of gigantol on CSC-regulatory signaling proteins in H460 cells.....	76
<b>Figure 28.</b> Effect of gigantol on CSC-regulatory signaling proteins and CSC markers in A549 and H292 cells.....	77
<b>Figure 29.</b> Bioinformatic analysis process for verification of the proliferation-regulatory proteins affected by gigantol.....	79
<b>Figure 30.</b> The protein-protein interaction network of the differentially expressed proteins associated with regulation of cell proliferation.....	82

<b>Figure 31.</b> The protein-protein interaction network of hub proteins with differential expression status .....	83
<b>Figure 32.</b> Effect of gigantol on c-Myc levels in H460, A549, and H292 cells .....	85
<b>Figure 33.</b> PPI network showing the relationship between c-Myc, GSK3 $\beta$ , and ubiquitin .....	86
<b>Figure 34.</b> Effect of gigantol on GSK3 $\beta$ in H460, A549, and H292 cells.....	87
<b>Figure 35.</b> Effect of gigantol on c-Myc stability and c-Myc half-life evaluated by CHX chasing assay .....	90
<b>Figure 36.</b> Effect of gigantol on c-Myc degradation .....	91
<b>Figure 37.</b> Effect of gigantol on c-Myc ubiquitination .....	92
<b>Figure 38.</b> Summary of the effects of gigantol on tumorigenicity and cell proliferation of lung cancer cells.....	104



## LIST OF ABBREVIATIONS

ABCG2	=	ATP binding cassette subfamily G member 2
Akt	=	protein kinase B
ALDH1A1	=	aldehyde dehydrogenase 1 family member A1
$\alpha$ -SMA	=	$\alpha$ -smooth muscle actin
CHX	=	cycloheximide
CSC	=	cancer stem cell
DMSO	=	dimethylsulfoxide
EMT	=	epithelial-to-mesenchymal transition
FBS	=	fetal bovine serum
GO	=	gene ontology
GSK3 $\beta$	=	glycogen synthase kinase 3 beta
H&E	=	hematoxylin and eosin
IgG	=	Immunoglobulin G
IHC	=	immunohistochemistry
IL-6	=	interleukin 6
JAK	=	Janus kinase
LUAD	=	lung adenocarcinoma
LUSC	=	lung squamous cell carcinoma
MDR	=	multidrug resistance
mTOR	=	mammalian target of rapamycin
MTT	=	3-(4,5-Dimethylthiazol-2-yl) 2,5-diphenyltetrazolium bromide

NFKB	=	nuclear factor kappa B
NOD/SCID	=	nonobese diabetic/severe combined immunodeficiency
NSCLC	=	non-small cell lung carcinoma
OCT4	=	octamer-binding transcription factor 4
PBS	=	phosphate buffer saline
PI	=	propidium iodide
PI3K	=	phosphatidylinositol 3-kinase
PIP2	=	phosphatidylinositol (3,4)-bisphosphate
PIP3	=	phosphatidylinositol (3,4,5)-trisphosphate
RIPA	=	radioimmunoprecipitation assay
SCLC	=	small cell lung carcinoma
SDS	=	sodium dodecyl sulfate
SDS-PAGE	=	sodium dodecyl sulfate-polyacrylamide gel electrophoresis
SOX2	=	sex determining region Y-box 2
STAT	=	signal transducer and activator of transcription
TIC	=	tumor-initiating cell
WNT	=	wingless-type



## CHAPTER I

### INTRODUCTION

#### BACKGROUND AND RATIONALE

Tumorigenicity, practically defined as the ability to initiate and sustain tumors and in an *in vivo* environment, is a crucial feature of the malignant behavior of tumor cells. Evading growth suppressor and sustaining proliferation are among the hallmarks of cancer leading to a disease progression (1). Cell proliferation is an increase in the number of cells as a result of cell growth and cell division, and a rapid proliferation is considered as an aggressive factor of cancer which correlated with poor prognosis (2, 3). Dysregulated activation of proliferative signals and oncogenes are known to drive carcinogenesis and tumor growth (4, 5). Targeting cells with rapid proliferative rate shows benefits in most patients (6). There are several oncogenes that control cancer cell growth. Regarding oncogene, c-Myc, a member of MYC proto-oncogene, is a central transcription factor that controls cell proliferation, differentiation, and apoptosis. Amplification or overexpression of c-Myc occurs in various cancers, including lung cancer, was shown to relate with poor survival (7). An inhibition of c-Myc may offer the effective therapeutic treatment via tumor growth suppression (8, 9). However, targeted therapy against c-Myc is still unidentified due to its lack of inhibitory binding site, modulation c-Myc level via targeting its up-stream regulators is a potential strategy (7). GSK3 $\beta$  showed prominent tumor suppressor properties in lung cancer (10). Akt-dependent GSK3 $\beta$  phosphorylation at Ser9 was shown to correlate with poor survival rate of lung cancer patients (11). GSK3 $\beta$  suppresses cancer cell

proliferation by inhibit various oncoproteins, including c-Myc. The active GSK3 $\beta$  mediates degradation of c-Myc via phosphorylation at Thr58 (12). Indirect attenuation of c-Myc stabilization may offer the effective therapeutic treatment via tumor growth suppression.

However, cell proliferation is not the only factor that help maintain tumor growth. In fact, tumor needs a heterogeneity of the tumor population to enhance tumor microenvironment. A new paradigm shift in the field of cancer cell biology is being driven by the concept of a key cancer cell population controlling the whole tumor, termed “cancer stem cells (CSCs)” (13). CSCs from various types of cancers share a number of conservation properties, such as self-renewal ability, the generation of multiple types of differentiated cancer cells to drive tumor growth and heterogeneity, and resistance to chemotherapy via an upsurge of the DNA repair system and drug efflux transporter (14). In lung adenocarcinoma, CSCs from patients were found to be less than 1.5% of the whole tumor cell population (15), but this small subpopulation was still substantial for tumorigenesis and tumor relapse (16). The CSCs have a slow proliferative rate and can survive as a dormancy in stressful condition. Once they are activated by exogenous stimuli or an appropriate microenvironment, the CSCs start self-renewal and asymmetric division in order to generate tumor bulk consisting of proliferative cells and angiogenic cells, which release essential signals that promote tumor growth and CSC maintenance (13).

The suggesting therapeutic strategies targeting CSCs, including CSC direct eradication, CSC differentiation into tumor bulk cells, deletion of the supportive signals from a CSC niche, and suppression of CSC pathways, could lead to effective cancer therapy (17). The key driving pathways of CSCs, such as the PI3K/AKT/mTOR and JAK/STAT3

signals, were found to be significantly increased in cancers with high CSC properties, and hence investigations of many small molecules targeting such pathways are ongoing in clinical trials (18, 19). Protein kinase B (PKB) or Akt, which is frequently up-regulated in lung cancer plays a key role in cell survival and proliferation (20). The activation of Akt was shown to be related with cisplatin resistance in lung cancer cells (21). The roles of Akt on the properties of CSCs and their survival have been demonstrated in several key studies (22, 23). Likewise, signal transducer and activator of transcription 3 (STAT3) activation has been associated with poor prognosis as well as augmented CSCs (24). A higher level of phosphorylated STAT3 (active STAT3) contributed to epithelial-to-mesenchymal transition (EMT) as well as increased CSC-like phenotypes of non-small cell lung cancer cells (NSCLCs), while the inhibition of STAT3 caused the opposite effects (25). Instead of bulk non-CSC tumor clearance, the targeting of Akt and STAT3 is believed to be a promising anti-cancer strategy that could lead to the tumor collapse and prevention of the relapse of the disease (26, 27).

Recently, natural compounds from plants have garnered increasing attention either as potential drugs or lead compounds in drug discovery research (28, 29). The key benefits of natural compounds are the abundance of plants, compound diversity, and cost effectiveness. In focusing on CSCs and tumor growth inhibition, previous studies have reported the promising activities of the bibenzyl derivative chrysotoxine in the suppression of Akt and Src (30). *In vivo* studies further revealed that the bibenzyl derivative moscatilin reduced tumor volumes of lung and esophageal cancer xenografts (31, 32). Gigantol, a bibenzyl compound, is one of the polyphenolic components frequently found in

traditional Chinese medicine, and has been shown to have several pharmacological effects, e.g., anti-inflammatory, amelioration of diabetic nephropathy and cataract, and anti-cancer (33-35). *In vitro* studies reported that gigantol triggered the apoptotic cell death of lung cancer cell lines but was not toxic to keratinocytes (36).

The previous studies revealed several effects of non-toxic concentrations of gigantol on NSCLCs (37-40). Pretreatment of 5 to 20  $\mu\text{M}$  of gigantol showed a reduction of the tumor-forming capacity of NSCLCs, represented by significantly suppressing the anchorage-independent growth. The number and size of the colonies from gigantol-pretreated lung cancer cells were smaller than the controls, indicating that gigantol suppressed tumor growth (37). In addition, with a single pretreatment of gigantol, the ability of cancer cells to form spheroids in a detached condition, a hallmark assay for detecting CSCs, was abundantly suppressed (37). These data indicated that the cancer cells had lost their self-renewal capability, which was confirmed by Western blot results showing the down-regulation of octamer-binding transcription factor 4 (OCT4) and Nanog, essential transcription factors for self-renewal and CSC-like phenotype maintenance (37). Altogether, gigantol has the potential to attenuate tumorigenesis. However, certain information regarding the tumor growth attenuation mechanism and key evidence in animal models are still required. Moreover, activity of tumor growth suppression of gigantol is largely unknown.

Proteomic analysis is a systematic identification and quantification of the complete protein profile that benefit the investigation of molecular pharmacology by monitoring the affected proteins in response to drug or active compound leading to the identification of

major drug mechanism (41). In the present study, an *in vitro* proliferation assay and colony formation assay, as well as, an *in vivo* subcutaneous xenograft model were performed to help illustrate a clearer picture of how gigantol could suppress lung tumor growth. Furthermore, the proteomic analysis of tumor growth related pathways, especially involving the cell proliferation and stemness maintenance, was evaluated. This data may benefit the development of gigantol for novel cancer treatment as well as provide the overall information of cellular proteins affected by this compound.

#### RESEARCH QUESTIONS

1. Do the stemness suppressed lung cancer cells have lower tumorigenicity than the untreated ones?
2. Can gigantol reduce lung cancer cell proliferation capacity?
3. What are the molecular mechanisms of gigantol, which result in the attenuation of stemness maintenance and proliferation of lung cancer cells?

#### OBJECTIVES

This study aims to:

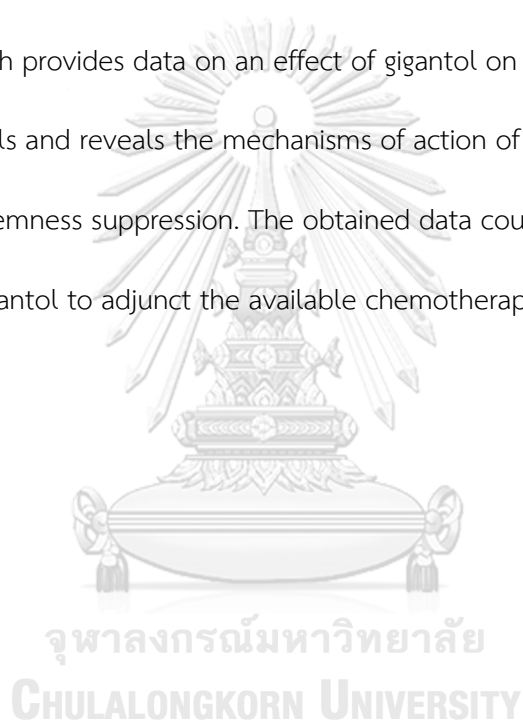
1. Investigate the effect of gigantol on tumorigenicity of lung cancer cells using an *in vivo* model.
2. Investigate the effect of gigantol on cell proliferation of lung cancer cells using an *in vitro* model?
3. Define the proliferative and CSC-related signals affected by gigantol treatment.

## HYPOTHESIS

Gigantol reduces tumorigenicity of lung cancer cells through the suppression of lung CSCs, as well as, proliferation capacity of lung cancer cells via the inhibition of the CSC- and proliferation-related signals, including PI3K/Akt and JAK/STAT pathways.

## EXPECTED BENEFITS

This research provides data on an effect of gigantol on tumorigenicity of non-small cell lung cancer cells and reveals the mechanisms of action of gigantol on lung cancer cell proliferation and stemness suppression. The obtained data could be beneficial on the development of gigantol to adjunct the available chemotherapy for lung carcinoma.



## CHAPTER II

### LITERATURE REVIEWS

#### Lung cancer

Lung cancer is the second most common cancer worldwide and in Thailand. Moreover, it is the major cause of cancer death (42). The lung cancer 5-year survival rate of localized (within the lung) is 56%, which is much lower than other common cancer sites, such as colorectal (90%), breast (99%), and prostate (99%). Moreover, the late-stage 5-year survival rate is never more than 5% (43). It was reported that patients who have detected lung cancer at a stage I and received a surgical resection within one month after diagnosis had more than 90% survival rate, while the patients who did not receive the treatment die from lung cancer within five years after diagnosis (44). In fact, 84% percent of lung cancer cases are diagnosed at a late stage (45). Besides, more than half of the stage I-III lung cancer patients had a local or distant recurrence after cancer treatments (46).

The most diagnostic type of lung cancer is non-small cell lung carcinoma (NSCLC), which is counted as around 85%, and the other 15% is small cell lung carcinoma (SCLC) (47). NSCLC is mainly categorized into two subtypes, which are lung adenocarcinoma (LUAD) and lung squamous cell carcinoma (LUSC). If the cancer cell morphology and squamous cell biomarkers are not enough to match both subtypes, the lung tumor then is diagnosed as a large cell carcinoma. Half of the NSCLC diagnostic subtype is LUAD, while LUSC is one-quarter (48).

The treatment selection is based on the stage and tumor subtypes, small- or non-small cell, and then squamous or non-squamous for NSCLC. Early-stage lung cancer can be cured by surgery with or without chemotherapy for NSCLC or chemoradiotherapy for SCLC. First-line treatment for advanced-stage lung cancer is platinum-based therapy for both NSCLC and SCLC. If the advanced lung expresses certain genetic mutations such as EGFR exon 19 deletion or exon 21 (L858R) substitution mutations or ALK-positive, targeted therapy may become the first-line therapy (49).

Because lung cancer has no specific symptoms and normal annual check-up does not include chest CT screening, people usually unaware of the disease and mostly come up with a late-staged disease (50). Advanced stage of lung cancer associated with poor prognosis. At this advanced stage, the disease generally unresectable, and chemo- and/or radiotherapy is the first-line treatment. The efficacy of conventional chemotherapy was usually limited when the adverse events caused early discontinuation of the treatment, especially in the elderly (51). Other treatments, such as immunotherapy for the PD1 receptor, can be considered as second-line therapy for advanced-stage NSCLC (52). The response rate of advanced-stage lung cancer to conventional chemotherapy is low, and the tumor usually relapses after the treatment cessation. Median time-to-treatment failure of the conventional chemotherapy was around three months (51), and 5-year survival was only 5% (43). The approved targeted therapy and immunotherapy also showed disappointing outcomes (53). The causes of cancer treatment failure, cancer progression, and tumor relapse are now clarified as cancer stem cells.



## Cancer stem cells

The concept of cancer stem cell was first proposed by Bonnet and Dick in 1997 and described that only leukemic tumor-initiating cells, which expressed the same cell-surface  $CD34^+ CD38^-$  as normal hematopoietic stem cell showed the high capacity of self-renewal and differentiation into leukemic progenitors when inoculated into NOD/SCID mice. These cells generated leukemia in a manner of hierarchical organization in NOD/SCID mice. (54). Then, the CSCs from various solid tumors were identified using the specific cell-surface markers, started with CD44 and CD24 of breast tumor CSCs in 2003 (55, 56). After abundant data of CSCs were consolidated, the static CSC hierarchical model was shifted to the dynamic clonal evolution model, which was described that the CSC-like properties (or stemness) could be acquired by the differentiated cancer cells (57). Not only oncogenic genetic mutations, but non-CSCs can acquire the stem-like traits via exposure to specific stimuli or specific conditions, such as hypoxia, cytokines, or nitric oxide in tumor microenvironments (58-60).

The CSCs from different types of cancer share key conservation properties of pluripotent stem cells, which are an ability of self-renewal and a capacity to generate the multi-lineage differentiated cancer cell types, resulting in the tumor heterogeneity and a potential to repopulate a new tumor (61, 62). A lot of experimental and clinical data revealed that the CSCs or high CSC-like phenotype cancer cells were the cause of tumor initiation, metastasis, anticancer drug/radiation resistance, and cancer relapse (63). There are several biological functions of the CSCs that contribute these aggressiveness of the cancer cells, including an acquisition of epithelial-mesenchymal transition (EMT)

phenotype switching, an upsurge of multidrug resistance (MDR) or detoxification proteins, an ability of quiescence that the CSCs can survive as a dormancy, a resistance to cell death, and up-regulation of signaling pathways of CSC-driven chemoresistance (13, 64). There are several methods developed for determination of the CSC phenotype of the cancer cells, such as tumorigenicity *in vivo* models, Hoechst 33342 efflux in side-population (SP), ALDH activity measurement, anchorage-independent growth using soft agar assay, spheroid formation in CSC-selective medium, and sorting by CSCs' specific cell-surface markers (56).

### Lung CSCs

In LUAD, CSCs from patients were found to be less than 1.5% of the whole tumor cell population (15). To define lung CSCs is challenged. Several studies tried to link the lung CSC markers with its original lung stem cell by introducing various stimuli and observe that which normal lung cells transformed into cancer cells. For LUAD, the most common form of lung cancer, tumor-initiating cells were proposed to be transformed from Clara cells, which were multipotent stem cells, and alveolar type II cells (AT2 cells). The  $Kras^{G12D}$  mutated lung cells of mice which transformed to cancer cells were positive for the Clara cell antigen (CCA or CC10), the biomarker of Clara cells, or the surfactant apoprotein-C (SP-C), the biomarker of AT2 cells, and the mixed expression of both antigens (65). Only progenitor cells that had  $Sca-1^{pos} CD45^{neg} Pecam^{neg} CD34^{pos}$  population contained stem cell-like properties, which were defined by colonies formation and limiting dilution analysis (66).

Later, various cell-surface proteins had been verified as the CSC markers for lung cancer, including CD133, CD166, CD117, CD90, CD44, CXCR4, and EpCAM (67, 68). ABCG2, an ATP-binding cassette transporter, was identified in various types of cancer, including carcinomas of the digestive tract, lung, breast, ovarian, and melanoma (69). The expression level of ABCG2 is also associated with a high pathological grade of tumor and poor prognosis outcomes of patients (70). The elevated level of ABCG2 caused resistance to conventional chemotherapy. ALDH1A1, a detoxification enzyme, was commonly up-regulated in CSCs. A cancer cell with a high level of ALDH1A1 usually exhibited features of CSCs, including increased capacity for proliferation, self-renewal, differentiation, and expression of the CSC surface marker, CD133 (71). The transcription factors which regulated the expression of stemness genes are also used to characterize CSCs. OCT4, SOX2, and Nanog are transcription factors mostly analyzed. They are essential for the maintenance of pluripotent embryonic stem cells and germ cells (72).

### **Signaling pathways in CSCs and therapeutic implications**

The principle of the first era of anticancer drugs was to eradicate to highly proliferative rate cells, and the results showed some failures, especially in solid tumors. Besides, these drugs caused a lot of adverse events (73). After that, the concept of targeting dependent oncogene of cancer cells was raised with targeted therapy. This concept aimed to more specifically target the cancer cells by inhibition of the mutated genes that caused overexpression of oncogenic proteins or amplification of oncogenic

pathways. The targeted therapy was successful in the reduction of drug-induced toxicities, but the success rate of patients' survival was not satisfying (74).

After an accumulating data revealed that CSC was the main cause of treatment failure and cancer relapse or recurrence, the concept of cancer treatment was revised, and the CSC-targeted therapy was developed (17). Instead of targeting the oncogenic pathways in common cancer cells, CSC-regulating pathways were verified, and small molecules that targeted the CSCs' pathways were tested (75). Several laboratory studies of CSC-regulating pathway-targeted drugs showed promising results in CSC eradication or attenuation, and clinical trials that targeted CSCs through CSC-regulating pathway suppression in advanced-stage cancers were ongoing (76-81).

Normal stem cells utilize some signaling pathways for the purpose of regulation of self-renewal and differentiation processes. Also, CSCs use similar signaling pathways in order to preserve their stem cell-like phenotype. In general, signaling pathways involved in CSCs' preservation are PI3K/Akt, Janus family tyrosine kinase (JAK)/signal transducer and activator of transcription (STAT), nuclear factor kappa B (NF $\kappa$ B), Notch, Hedgehog, and Wnt/ $\beta$ -catenin pathways (82). These pathways are required to maintain the stem cell-like phenotypes in many types of cancer, including lung cancer (24, 83). An activation of the mentioned pathways enhances the CSC-like phenotypes of cancer cells, while an inhibition caused the stemness suppression (25). Targeting CSC-regulatory pathways might not be effective for non-CSC eradication, but this strategy precisely targeted the CSCs and inhibited tumor formation. For instance, rapamycin, an mTOR inhibitor, in combination with triciribine, a tricyclic purine nucleoside which prevents Akt phosphorylation, effectively

decreased the 3D sphere-forming units by extinguishing CSC population in glioblastoma and neuroblastoma, while showed minimal effect on the survival of non-CSC in 2D culture model (26). Also, verteporfin, a porphyrin derivative, showed inhibitory effect on YAP1 and STAT3, two oncogenes that promote CSC properties which especially up-regulated in lung adenocarcinoma, and resulted to reduced proliferation and enhanced cisplatin sensitization, both in *in vitro* model and patient-derived xenograft mice models (27).

There were some clinical trials that proved the efficacy of CSC-targeted drugs in advanced lung cancer. For instance, MK2206, an allosteric Akt inhibitor, improved some responses in erlotinib-resistant NSCLC patients in phase II study (84, 85). A phase I trial of OPB-51602, a STAT3 inhibitor, in patients with drug-resistant solid tumors demonstrates promising antitumor activity, particularly in NSCLC (86). Tarextumab, a fully human IgG2 antibody targeting Notch 2 and 3 receptors, in combination with etoposide and platinum in patients with untreated extensive-stage small-cell lung cancer, was well-tolerated and showed a dose-dependent antitumor activity in a phase I study (87). Also, there was a case report of erlotinib-resistant metastatic NSCLC patients who responded to vismodegib therapy for six months (88). These clinical results reinforced the direction of new anticancer drug development for CSC-targeted therapy.

### **PI3K/Akt pathway in CSCs**

The PI3K/Akt pathway is a signal transduction pathway that promotes cell survival and growth in response to extracellular signals. Key proteins involved are PI3K (phosphatidylinositol 3-kinase) and Akt (Protein Kinase B). Akt, a serine/threonine kinase,

has three isoforms, Akt1, Akt2, and Akt3. Akt1 (PKB $\alpha$ ) is ubiquitous in all tissues, promotes survival pathways by inhibiting apoptotic processes, and was first identified as an oncogene in cancer. Akt2 (PKB $\beta$ ) also promotes cell survival and growth, but via different pathways from Akt1. Akt1 and Akt2 are isoforms that overexpressed in a variety of human tumors (89). Akt3 (PKB $\gamma$ ) is found mainly in brain, heart, testis, kidneys, lungs, and skeletal muscles and its role in cancer is unclear (90).

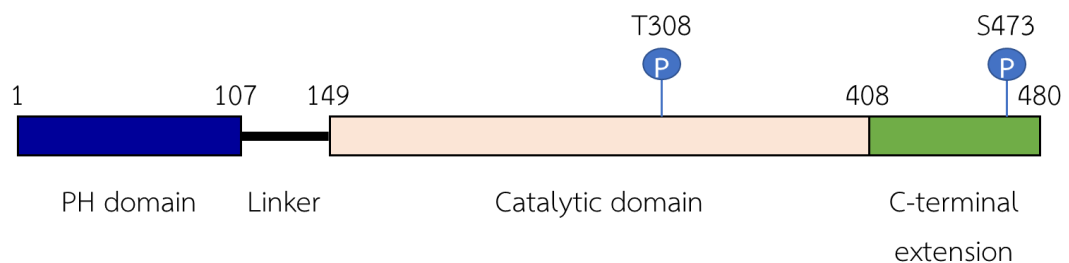


**Figure 1.** Akt1 structure consisted of an N-terminal pleckstrin homology (PH) domain, a catalytic domain and a C-terminal extension (91).

**Table 1.** The pairwise percentage of identity in Akt domains of each isoform. PH – Pleckstrin Homology domain, LINK – linker region, CAT – kinase catalytic domain, EXT – C-terminal extension (91).

Pair	PH	LINK	CAT	EXT
AKT1/AKT2	80	46	90	66
AKT1/AKT3	84	40	88	76
AKT2/AKT3	76	17	87	70

The three Akt isoforms belong to the class of AGC kinases and comprise of three conserved domains, an N-terminal pleckstrin homology (PH) domain, a kinase catalytic (CAT) domain and a C-terminal extension (EXT) containing a regulatory hydrophobic motif (HM) (Figure 1). Among the Akt isoforms, the PH domains are around 80% identical, The

CAT domain is around 90% identical, and the C-terminal extension (EXT) is around 70% identical. The linker (LINK) region connecting the PH domain to the CAT domain is poorly conserved among the Akt isoforms (17–46% identical; Table 1) (91). The phosphorylation of threonine and serine residues is essential to optimize the kinase activity of the three Akt isoforms. These threonine and serine residues are located in slightly different sites in Akt1, Akt2, and Akt3. In Akt1, the most vital regulatory amino acid residues are threonine 308 and serine 473, while in Akt2, the amino acid residues are threonine 309 and serine 474, and in Akt3, the amino acid residues are threonine 305 and serine 472 (92).

Once the growth factors bind and activate a cell surface receptor, PI3K is then phosphorylated. The activated PI3K phosphorylates phosphatidylinositol (3,4)-bisphosphate (PIP<sub>2</sub>) on the plasma membrane, forming second messenger phosphatidylinositol (3,4,5)-trisphosphate (PIP<sub>3</sub>) (93). Akt is recruited to the membrane by interaction with PIP<sub>3</sub> docking sites, so that it can be fully activated by various kinases, such as PDK1, PDK2 and ILK (Figure 2). Akt phosphorylates as many as 100 different substrates, leading to a wide range of effects on cells. Activated Akt mediates downstream responses, including cell survival, growth, proliferation, cell migration and angiogenesis, by phosphorylating a range of intracellular proteins (Figure 2) (94).

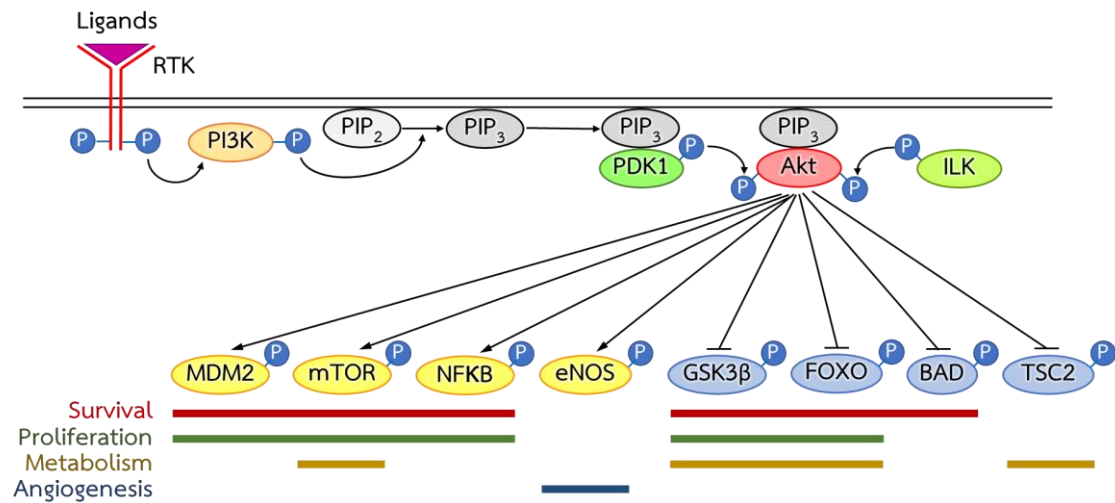


**Figure 2.** Depicted PI3K/Akt signaling pathway, Akt substrates and involving cellular functions (93, 95).

PI3K/Akt pathway is necessary to maintain the CSC-like phenotype as well as their survival, in tumor-initiating cells (TICs). When PI3K activity was blocked, or when Akt (mainly the Akt1 isoform) was knocked down, the survival and population size of TICs (measured as CD44<sup>High</sup>/CD24<sup>Low</sup> population) were severely reduced (96). PI3K activation promotes survival, maintenance of stemness, and tumorigenicity of CD133<sup>+</sup>/CD44<sup>+</sup> prostate cancer stem-like cell populations, as well as, promotes cell proliferation, migration, and invasion in ALDH<sup>+</sup>/CD44<sup>High</sup> head and neck squamous CSCs (97).

### JAK/STAT3 pathway in CSCs

The JAK/STAT pathway is a signal transduction pathway that stimulates cell proliferation, differentiation, cell migration and apoptosis. This pathway can be activated by a wide range of cytokines and growth factors. Key proteins involved in JAK/STAT signaling are Janus kinases (JAKs) and signal transducer and activator of transcription proteins



(STATs). In mammals, JAK family consists of four members: JAK1, JAK2, JAK3 and TYK2. While, STAT family consists of seven members: STAT1, STAT2, STAT3, STAT4, STAT5A, STAT5B and STAT6 (Figure 3). The amino-terminal domain mediates the interaction between two STAT dimers to form a tetramer. This interaction is not essential for STAT function but can stabilize the binding of two STAT dimers to adjacent sites in DNA. The coiled-coil domain is involved in interactions with regulatory proteins and other transcription factors. The DNA-binding domain makes direct contact with STAT-binding sites in gene promoters, which have the consensus core sequence T(N<sub>4,6</sub>)AA. Reciprocal interactions between the SRC-homology 2 (SH2) domain of one STAT monomer and the phosphotyrosine residue of another mediates dimer formation, which is required for the binding of STATs to DNA. The transactivation domain is involved in the transcriptional activation of target genes through interactions with other proteins, such as histone acetyltransferases. This carboxy-terminal domain contains a site of serine phosphorylation that enhances transcriptional activity in some STATs. STAT5a and STAT5b are closely related proteins that are encoded by distinct genes (98).

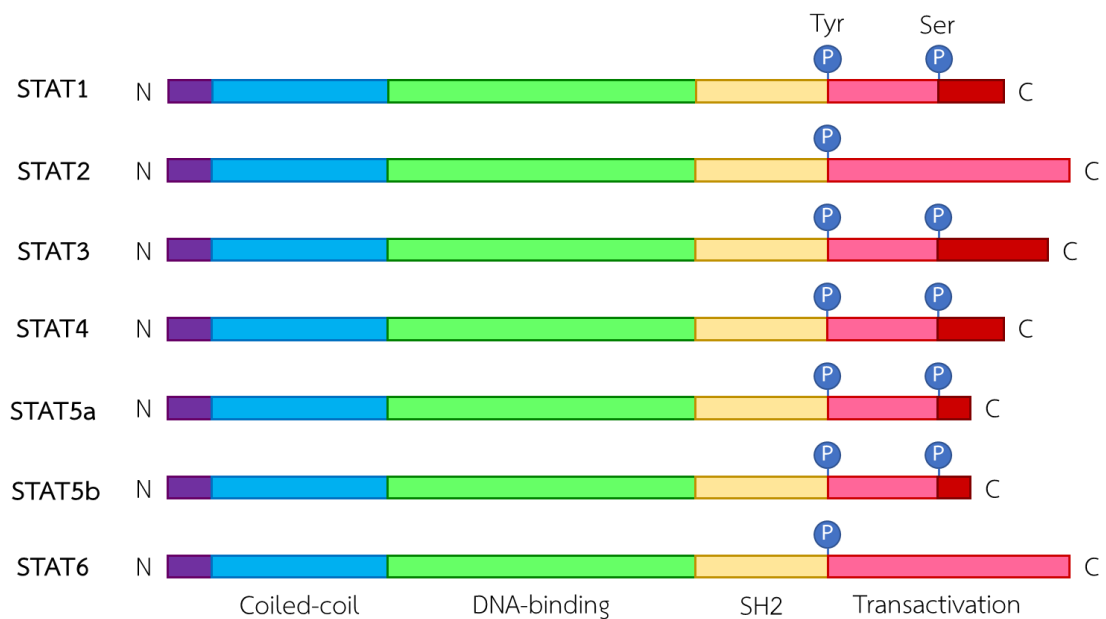


**Figure 3.** The domain structure of the seven STAT-family members. N – amino-terminal domain, SH2 – SRC-homology2 domain, C – carboxy terminal domain. (97)

The binding of extracellular ligand leads to pathway activation via dimerization of the receptor subunits that allow the two cytoplasmic JAKs associated with them to trans-phosphorylate one another. Trans-phosphorylated JAKs subsequently phosphorylate downstream substrates, including both the receptor and the STATs, the latent transcription factors that locate in the cytoplasm until they are activated. Activated STATs form dimers and enter the nucleus, then bind to specific regulatory sequences of target genes and activate or repress transcription of the target genes, such as SOCS, Nmi, Bcl-XL, p21, MYC, NOS2 (Figure 4). (99, 100)

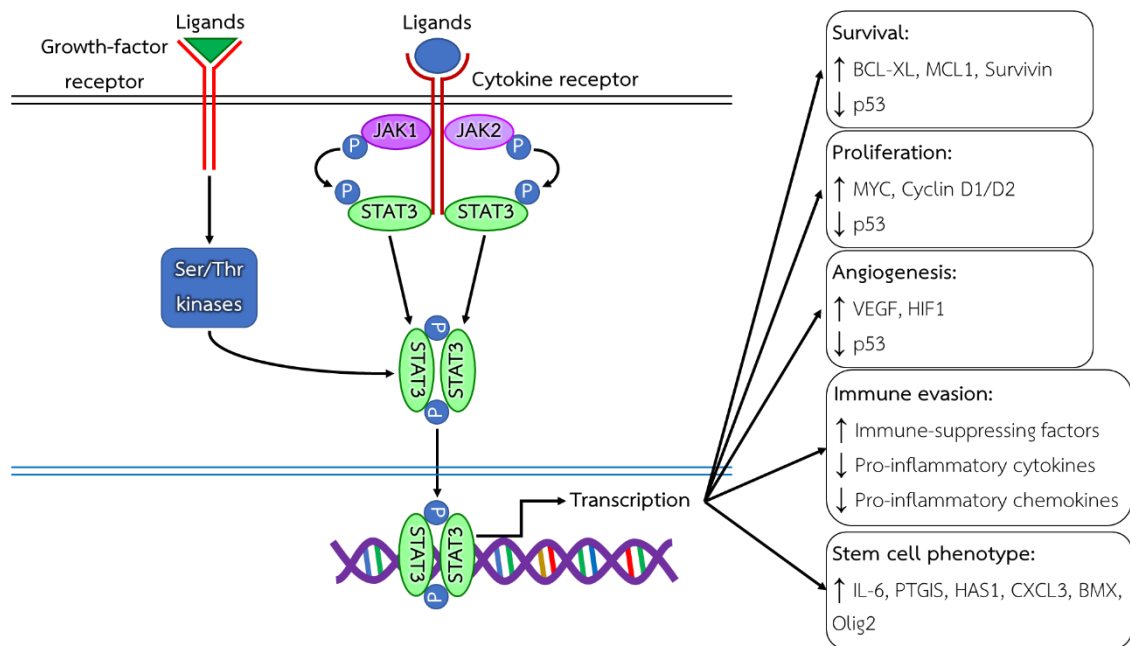


**Figure 4.** JAK/STAT3 signaling pathway and biological functions controlled by STAT3. (98, 101)

**Table 2.** Activation of STATs in human solid tumors. (98)

Tumor type	Activated STAT
Breast cancer	STAT1, STAT3, STAT5
Head and neck cancer	STAT1, STAT3, STAT5
Melanoma	STAT3
Ovarian cancer	STAT3
Lung cancer	STAT3
Pancreatic cancer	STAT3
Prostate cancer	STAT3

STAT proteins, particularly STAT3 and STAT5, are found overactivated in various types of solid tumors and blood malignancies. Persistent STAT3 signaling in tumor cells activate the gene-expression patterns that induces cancer-cell survival, proliferation, tumor angiogenesis and suppresses anti-tumor immune responses, leading to tumor progression

(Figure 4). STAT3 has been reported to be crucial for lung cancer progression and is a promising target for cancer therapy (Table 2) (98). The STAT3 is mainly activated via the phosphorylation at Tyr705 by JAK. However, the phosphorylation at Ser727 by Akt or ERK1/2 is also required for nuclear localization and maximized transcriptional activity (102, 103). The IL-6/JAK/STAT3 is an essential cascade for promoting self-renewal of CSCs and aggressive phenotypes of cancer cells such as chemoresistance, EMT, and pro-oncogenic inflammation (101).

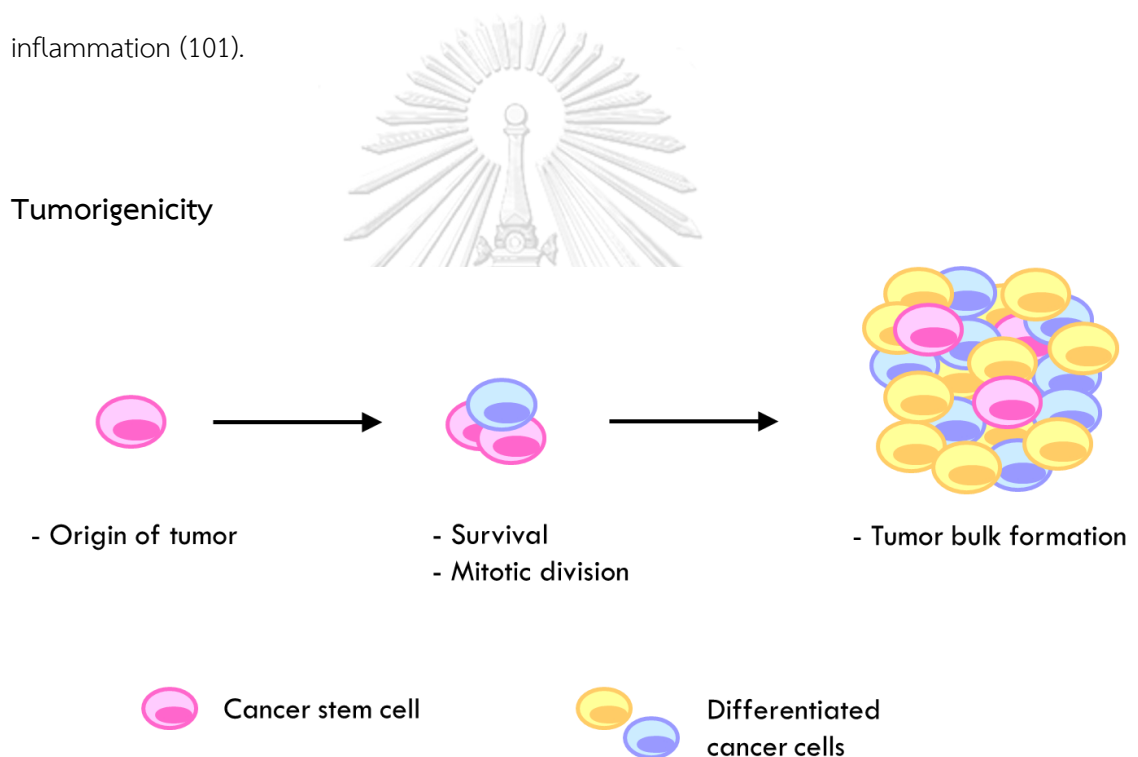


**Figure 5.** The scheme shows a process of tumorigenesis.

Tumorigenicity is “the capacity of a cell population inoculated into an animal model to produce a tumor by proliferation at the site of inoculation and/or at a distant site by metastasis” (WHO Technical Report Series No. 978, Annex 3, 2013) (104). The tumorigenesis is a multistep process which consists of many biological activities and requires a heterogeneity of the tumor cells, including the transformation of the normal cell

to cancer progenitor or cancer stem cell, promotion of cell survival, mitotic proliferation, and tumor bulk formation (Figure 5) (105, 106).

It is strongly evidenced that the PI3K/Akt pathway associated with these aggressive phenotypes (107). Inhibition of PI3K/Akt signaling resulted in the suppression of cell proliferation, chemoresistance, and a reduction of immune escape (20, 21). Moreover, JAK/STAT, Notch, Hedgehog, Wnt, and NF $\kappa$ B pathways were also showed a correlation with these hallmarks of cancer (108-112).

### **Tumor subcutaneous xenograft model**

Animal tumor xenograft experiments are necessary to confirm the consistency of the *in vitro* assay results and to demonstrate any unpredicted effects in the living body.

Tumor formation and metastasis consist of multistep processes and complex interactions between cancer cells and tumor microenvironment, as well as the host immune system.

Therefore, tumor formation assay is required for studying tumor biology and anticancer drug development. The most used animal species is mouse because it is a mammal, easy to handle, and transplantable with human cells. Various tumor transplant methods and mouse strains have been developed for different purposes of evaluation. The immunocompetent mice can be used for a mouse cancer cell transplant model, but those mice rarely develop a tumor from human cancer cells. Athymic nude mice are immunocompromised mice strains that lack T cells and partial defects in B cell development due to the defective development of the thymic epithelium. However, the innate immunity, such as NK cells, in nude mice is intact, and the leakage of T cells

increases with age (113). By the way, the nude mice give a good success rate of tumor formation in many types of human cancer cell lines and patient-derived tumors (114) and are widely used for tumorigenicity test.

The transplantation models for therapeutics study are subcutaneous- and orthotopic tumor transplantation. The advantages of the subcutaneous method are that the administration of cancer cells is simple without anesthetic (but anesthetic is required for tissue transplantation), and the tumors can be easily monitoring. Moreover, this method facilitates the use of bilateral transplantation. The disadvantages of this method are that the tumor grows in an ectopic site (except skin cancer), so the tumor microenvironment interaction may be limited, and vascularization may be poorly formed. Moreover, metastasis rarely develops from the subcutaneous tumors, so it is not suitable for an anti-metastasis treatment. In order to investigate the interaction between tumor cells and stromal or vascular cells, as well as a spontaneous metastasis, the orthotopic method is developed. The advantages of this method are that the full metastasis cascades and the tumors in metastatic sites can be observed. The disadvantages of the orthotopic method are that the delicate surgical procedure is required, the risk of infection is high, pilot studies must be performed to determine the time frame of the experiment, and the monitoring may be difficult if real-time imaging is not used (115). In case that the treatment effects only tumor establishment and the spontaneous metastasis will not be observed, the subcutaneous transplantation method may be considered. Besides, the bilateral tumor transplant can be done in case that there is no post-treatment after the

transplantation, and the purposes of tumor analysis are to compare the incidence of tumor initiation and tumor growth rate between two different populations of cancer cells.

In order to study an effect of a treatment that suppresses tumorigenicity of cancer cells, the cancer cells can be pretreated with drugs, radiation, or other therapeutic procedures that are supposed to reduce the tumor-initiating cells in the cancer population transplanted. This study design is widely utilized in many studies of CSC-targeted therapy development (116) or treatments that affect the tumor formation of the overall cancer population (117).

#### **c-Myc and cancer cell proliferation**

Sustaining proliferative signaling and anti-growth signal evasion are the fundamental ability of cancer cells leading to a disease progression. Cell proliferation is a multistep developmental process involves cell growth and cell division, resulting an increase in the number of cells. Normal cells, especially epithelial cells, are in quiescent state unless exogenous mitogenic signals from extracellular matrix or adjacent cells transmit into cells. In contrast, cancer cells can proliferate independent to extracellular stimulation by generate their own growth signals. Self-sufficiency of growth signals was the first cancer hallmark identified by researchers for mutations of dominant oncogenes had been verified. For example, mutated Ras proteins trigger a flux of mitogenic signals with no stimulation by their upstream regulators (1, 118). Some major signaling pathways that sustain cancer proliferation were found being effective targets for blocking tumor

proliferation, including PI3K/Akt, Wnt/ $\beta$ -catenin, Ras/MAPK, NF $\kappa$ B, Notch, and Hedgehog pathways (119).

Several growth signals were deregulated in human tumors. MYC was a proto-oncogene first discovered its role in tumor cell transformation and essential for tumorigenesis. c-Myc, a major member of MYC products, is overexpression in more than half of human cancers. c-Myc functions as a transcription factor that controls a variety of biological processes in cancer cells, such as, cell proliferation, differentiation, senescence, and apoptosis. However, for tumorigenesis, c-Myc activation alone is not enough to drive tumor proliferation. Some synergistic genetic events, such as, loss of p53 or overexpression of Bcl-2 are required. An inhibition of c-Myc caused senescence or apoptosis in many types of cancers, including lymphoma, osteosarcoma, and hepatocellular carcinoma. Although c-Myc is considered as an undruggable protein because it is a transcription factor with essential for several biological functions, an inhibition of c-Myc using small interfering RNA, short hairpin RNA, and antisense oligonucleotides showed a promising effect in cancer treatment (120).

Because c-Myc is a potent regulator of cell proliferation and cell fate decision, a restricted regulation in order to keep a proper level of c-Myc is vital in normal cells. c-Myc is mainly controlled by Threonine 58 in the N-terminus, which are targeted by GSK3 $\beta$ . Therefore, c-Myc phosphorylation is indirectly regulated by PI3K/Akt pathway, which suppresses GSK3 $\beta$  through Akt-dependent GSK3 $\beta$  phosphorylation at Ser9. GSK3 $\beta$  functioned as a tumor suppressor in lung cancer (10). The level of Ser9 phosphorylated GSK3 $\beta$  correlated with poor survival rate of lung cancer patients (11). The Thr58



phosphorylation of c-Myc by GSK3 $\beta$  is required for the recognition by the ubiquitylation machinery, resulting to c-Myc degradation by the ubiquitin proteasome pathway (12). Some natural compounds that targeted c-Myc stability via blocking the upstream regulators that control c-Myc degradation showed an inhibitory effect on lung tumor growth both *in vitro* and *in vivo* models (8). Indirect attenuation of c-Myc stabilization may offer the effective therapeutic treatment via tumor growth suppression.

### Proteomics analysis

Proteomics is a high-throughput method for the study of proteins in biological systems. This technique provides an entire view of protein expression in a system by identification and quantification of the proteins from a given sample. Proteomics data can be contributed to a variety of information due to the categories of database and the selected analytical software. Nowadays, there are various free web-based and off-lined bioinformatics tools available for the researchers.

Proteomics can be used to study the effect of drug treatment on the proteome of the cancer cells. Proteomics analysis compares the total proteins between the samples from the control and the treatment groups, and then the differential expression of the interesting proteins can be analyzed. The advantage of this method is that the whole map of the drug's effects can be observed (41).

## Gigantol

Natural compounds from plants have been good resources for drug discovery research, especially in Thailand, according to the abundance of biological diversities (28, 29). The natural bibenzyl derivatives from orchids have been reported for anticancer effects, including moscatilin, batatasin III, chrysotoxine, and gigantol. These bibenzyls mostly triggered cancer cell death via apoptosis pathway (30, 121-123). Earlier *in vivo* studies reported that 50-100 mg/kg moscatilin, intraperitoneally injected twice a week, significantly inhibited tumor growth of lung and esophageal cancer xenograft in nude mice (31, 32). Moreover, moscatilin attenuated neoangiogenesis evaluated by *in vitro* HUVEC tube formation and *in vivo* Matrigel plug assay (31). Interestingly, previous studies reported that non-toxic concentrations of several bibenzyl compounds had an inhibitory effect on aggressive phenotypes of lung cancer cells. The non-toxic concentrations of moscatilin inhibited EMT, an essential phenotype for cancer metastasis, inhibited migration and invasion, and sensitized anoikis, a type of cell death in attachment-free condition, in lung cancer cells (122, 123). As well, low doses of batatasin III inhibited lung cancer proliferation, migration and invasion (121). Earlier studies have reported the suppressive activities of non-toxic concentrations of Chrysotoxine on lung CSCs and 3D spheroid formation via the mechanisms of Akt and Src signaling blockade (30).

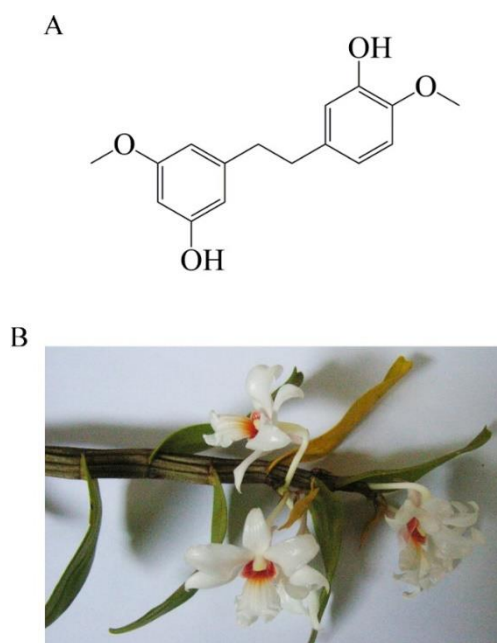


**Figure 6.** (A) Gigantol structure. (B) Plant specimen of *Dendrobium droconis* Rchb.f.

Gigantol is a bibenzyl that was first identified from *Cymbidium giganteum* and can be found in various genera of the Orchidaceae, e.g., *Cymbidium*, *Vanda*, *Dendrobium* (Figure 6) (124). It is one of the polyphenolic components in Traditional Chinese Medicine and has demonstrated several effects, e.g., anti-inflammatory, amelioration of diabetic nephropathy and cataract, and anticancer (33-35). *In vitro* studies reported that gigantol triggered apoptotic cell death of lung cancer cell lines, but not in a human keratinocytes cell line (HaCat) (36). Many studies have shown that non-toxic concentrations of gigantol can decrease aggressive behaviors of cancer cells, which were described by various biological assays such as anoikis-resistance, migration, invasion, anchorage-independent growth and spheroid formation (37-40).

Interestingly, the previous studies revealed several effects of non-toxic concentrations of gigantol on the NSCLC phenotype *in vitro*. It was reported that a 48-hour pretreatment of 5-20  $\mu\text{M}$  of gigantol significantly reduced anchorage-independent growth,

which represented tumor-forming capacity of NSCLC. Gigantol reduced the tumor's ability to form spheroids, a critical hallmark of CSCs. With single pretreatment of gigantol, the cancer cells could not abundantly form primary spheroids after seven days, and even after 30 days of secondary spheroid formation, the cancer cells still could not recover this ability. These data indicated that the cancer cells had lost self-renewal capability, which was confirmed by western blot results of down-regulation of OCT4 and Nanog, essential transcription factors for self-renewal and CSC-like phenotype maintenance (34). Also, pretreatment of non-toxic doses of gigantol diminished EMT-like phenotype, as could be seen from the reduction of mesenchymal cell morphologies and migration and invasion behaviors (39). The previous results have shown that gigantol down-regulated Slug, an important EMT transcription factor which led to anoikis sensitization and survival pathway suppression (40).

In sum, gigantol has the potential to be developed as a CSC-targeted drug in lung cancer. Though the effect of gigantol on tumorigenicity in an animal model has not been explored, and certain information regarding the signaling pathways that regulate cancer stemness is still limited.

## CHAPTER III

### METHODOLOGY

#### 1. Cell line cultures

Human NSCLC H460, A549, H292, and normal bronchus epithelial cell BEAS-2B lines were purchased from the American Type Culture Collection (Manassas, VA, USA). H460, A549, and H292 were cultured in Roswell Park Memorial Institute (RPMI) 1640 medium, while BEAS-2B was cultured in Dulbecco's Modified Eagle medium (DMEM) in a humidified atmosphere with 5% CO<sub>2</sub> at 37 °C. The media were supplemented with 10% fetal bovine serum (FBS), 2 mM L-glutamine, and 100 units/ml of each penicillin and streptomycin.

#### 2. Animals

Six-week old male BALB/cAJcl nude mice were purchased from Nomura Siam International (Samut Prakan, Thailand). Five mice were maintained in one cage under strictly hygiene housing with controlled temperature (23 ± 2 °C) and light/dark cycle (12 h light/12 h dark) at the Animal House of Faculty of Medicine, Chulalongkorn University. The study was approved by the Institutional Animal Care and Use Committee of the Faculty of Medicine, Chulalongkorn University, Bangkok, Thailand (ethical reference number CULAC 001/2561). Animal welfare and experimental procedures were strictly carried out in accordance with The Eighth Edition of the Guide for the Care and Use of Laboratory

Animals (NRC 2011) (125). All efforts were made to minimize animals' suffering and to reduce the number of animals used.

### 3. Chemicals and reagents

Gigantol was extracted from stems of *Dendrobium draconis* Rchb.f., as previously described (126) and dissolved in dimethylsulfoxide (DMSO) at the indicated working concentrations. 3-(4,5-Dimethylthiazol-2-yl) 2,5-diphenyltetrazolium bromide (MTT), Hoechst 33342, propidium iodide (PI), bovine serum albumin (BSA), dimethyl sulfoxide (DMSO), cocktail protease inhibitor, hematoxylin, and eosin were purchased from Sigma chemical, Inc. (Chemical Express, Bangkok, Thailand). RPMI-1640 medium, DMEM, phosphate buffer saline (PBS), glutamine, penicillin, and streptomycin were purchased from Gibco company (Gibthai, Bangkok, Thailand). Primary antibodies against CD133, ALDH1A1, total Akt, phosphorylated Akt (Ser473), total STAT3, phosphorylated STAT3 (Ser727), GSK3 $\beta$ , phosphorylated GSK3 $\beta$  (Ser9), c-Myc, and GAPDH, horseradish peroxidase (HRP) labeled secondary antibodies, and RIPA lysis buffer were purchase from Cell Signaling Technology (Theera Trading, Bangkok, Thailand). Pentobarbital sodium injection was purchased from Ceva Sante Animal (VET AGRITECH, Nonthaburi, Thailand). 3,3'-Diaminobenzidine tetrahydrochloride hydrate was purchased from TCI Co., LTD (Chemical Express, Bangkok, Thailand). Primary antibodies of Ki-67 and  $\alpha$ -SMA and matched secondary antibodies were purchased from DAKO (Medicare Supply, Bangkok, Thailand).

#### 4. Equipments

Automated cell counter (TC20, Bio-Rad, Singapore), autopipette 0.2-2  $\mu$ l, 2-20  $\mu$ l, 20-200  $\mu$ l, 100-1000  $\mu$ l (Pipetteman, Gilson, Middleton, WI, USA), fluorescence microplate reader (ClarioStar, BMG Labtech, Germany), fluorescence microscope (Nikon eclipse Ts2 with Nikon DS Fi3 camera), brightfield microscope (Nikon Eclipse E600 with Nikon DXM1200F camera), centrifuge (CF-10 Wise spin, Korea), biological safety cabinet class II A2 (Airtech, Taiwan), Humidified incubator (Thermo scientific, Waltham, MA, USA), pH meter (SevenCompactS220, Mettler-Toledo, Zürich, Switzerland), vortex mixer (Scientific industries, NY, USA), ImageQuant LAS 4000 biomolecular imager (GE Healthcare, Chicago, Illinois, United States), and cell culture plates (6-well and 96-well), centrifuge tubes (15 and 50 ml) and pipette tips (Corning, NY, USA).

#### 5. Cell viability test: MTT assay

Cell viability was determined by plating cells at a density of 10,000 cells per well in 96-well plates. Cells were allowed to adhere overnight, the medium was removed, and medium with various concentrations of gigantol (0-200  $\mu$ M) was added. After 24 hours of treatment, the number of viable cells was measured with the use of MTT assay. The medium was aspirated, and 0.4 mg/ml of MTT in PBS was added to each well. The plate was then incubated at 37 °C, 5% CO<sub>2</sub> for 3 hours. Afterward, the resulting formazan crystal was dissolved in 100  $\mu$ l of DMSO and subjected to a 570 nm absorbance reading via a microplate reader.

## 6. Cell death determination assay

Nuclear co-staining with Hoechst 33342 and propidium iodide (PI) was used to determine apoptotic and necrotic cell death. Cells were treated with gigantol, as described in cell viability assay. Then, the cells were incubated with 10  $\mu\text{M}$  of Hoechst 33342 and 5  $\mu\text{M}$  PI for 30 minutes at 37 °C. The cells were visualized and imaged under a fluorescence microscope. An apoptotic cell can be detected by Hoechst 33342 nuclear staining, showing condensed nucleus and fragmented nuclei of apoptotic bodies. A necrotic cell can be detected by PI staining.

## 7. Cancer cell preparation for subcutaneous xenograft inoculation

The human lung cancer cells were prepared prior to the tumor establishment. H460 cells were cultured in completed medium with 20  $\mu\text{M}$  of gigantol or vehicle for 48 hours (5 individual sets of cancer cell cultures). Then, the 70% confluent monolayer lung cancer cells were trypsinized, suspended in Hank's saline buffer solution, and counted by TC20 automated cell counter (Bio-rad). Each cell suspension was adjusted to a concentration of viable  $5 \times 10^6$  cells per 100  $\mu\text{l}$ . The cancer cell suspensions were kept on ice and rapidly transferred to an *in vivo* subcutaneous xenograft operation.



## 8. Subcutaneous tumor xenograft procedure

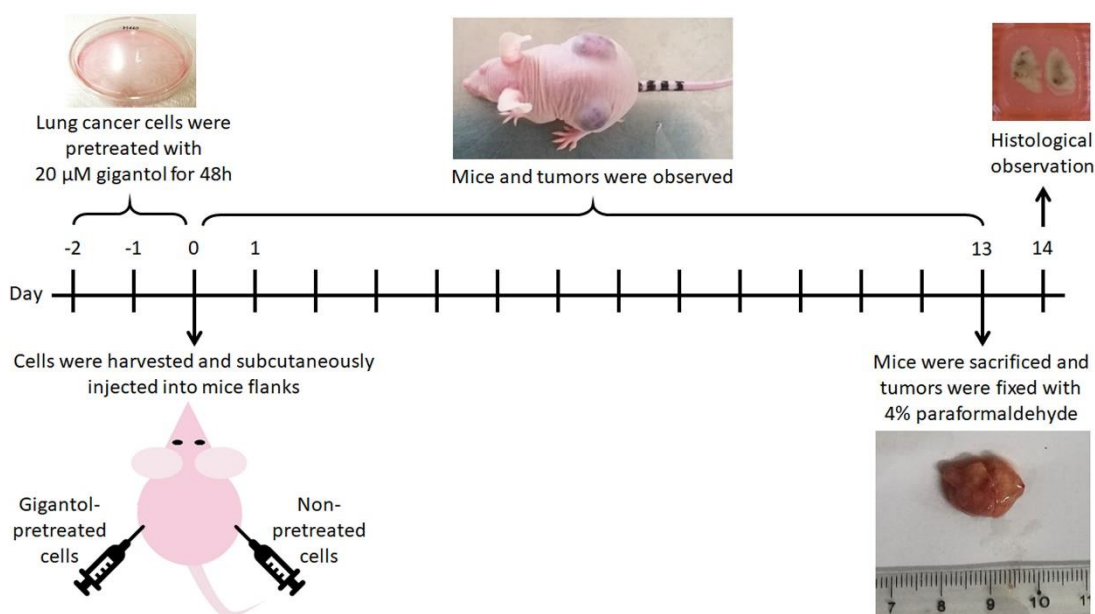


**Figure 7.** The scheme shows the experimental design of in vivo subcutaneous xenograft experiment.

A mouse was assigned to bear both control and its paired gigantol-treated tumor in order to minimize variation between animal bodies (Figure 7). One flank of a mouse was inoculated subcutaneously with viable  $5 \times 10^6$  cells of untreated cells and another flank with gigantol pretreated cells. Mice were weighed, and the tumors were observed every two days. When a tumor was palpable, the mouse was observed daily. Vernier Caliper was used to measure the most length and its own orthogonal most width of each tumor. Tumor volumes were calculated by the formula:  $(\text{length} \times \text{width} \times \text{width}) / 2$ . Tumor growth rates were verified by means of plotting calculated tumor volumes by days. Mice were not exposed to gigantol throughout the experiment. Once control or treatment tumor reached its endpoint size (20 mm in diameter), the tumor-bearing mouse was euthanized by intraperitoneal injection of pentobarbital sodium solution ( $> 150 \text{ mg/kg}$ )

(127), and then the tumors were dissected, washed with ice-cold PBS, weighed, and photographed accompanied with a ruler. The tumors were weighed and immediately fixed with 4% paraformaldehyde for 24 hours. Tumors were embedded in paraffin blocks, sliced and stained with hematoxylin and eosin (H&E) for further histologic observation. The H&E staining showed the intratumor structure and common cellular histology. Necrotic and total areas of tumor slices were determined using ImageJ software (128).

### 9. Immunohistochemistry staining of Ki-67 and $\alpha$ -SMA of the tumor slides

Two pairs of tumor slides were selected for staining with Ki-67 (dilution 1:300) and  $\alpha$ -smooth muscle actin ( $\alpha$ -SMA; dilution 1:100) antibodies and then visualized by incubation with 3,3'-Diaminobenzidine. Slides were observed under a brightfield microscope.

The level of Ki-67 assessment was modified from Jang (2017) (129). Areas with the highest (hot spot) and the lowest (cold spot) numbers of positive cells (indicated by dark brown staining in the nucleus) were selected, and the percentages of the positive cells compared to total cells were calculated. Averages of %Ki-67 positive cells were calculated from the summed total and Ki-67 positive cells from all hot spots and cold spots of the two mice.

For tumor cells with EMT phenotype, the tumor cells with a dark brownish cytosolic staining were detected. For angiogenesis determination, edge and center areas of each tumor were imaged, and the number of mature blood vessels (indicated by a circular lining of cells labeled with a high signal of  $\alpha$ -SMA) were counted.

## 10. Sample preparation for proteomics analysis

H460 cells were treated with 20  $\mu\text{M}$  gigantol or 0.004% DMSO (vehicle) for 24 hours. The cells were lysed with 0.5% sodium dodecyl sulfate (SDS). The total protein amount collected from each sample was measured with Lowry assay with bovine serum albumin as a standard (130). Equal protein amount from 3 independent biological samples was pooled. Fifty micrograms of protein from control or gigantol treated cells were subjected to in-solution digestion. Samples were completely dissolved in 10 mM ammonium bicarbonate (AMBIC), reduced disulfide bonds using 5 mM dithiothreitol (DTT) in 10 mM AMBIC at 60  $^{\circ}\text{C}$  for 1 hour and alkylated of sulfhydryl groups by using 15 mM iodoacetamide (IAA) in 10 mM AMBIC at room temperature for 45 mins in the dark. For digestion, samples were mixed with 50 ng/ $\mu\text{l}$  of sequencing grade trypsin (1:20 ratio) (Promega, Germany) and incubated at 37  $^{\circ}\text{C}$  overnight. Prior to LC-MS/MS analysis, the digested samples must be dried and protonated with 0.1 % formic acid before injection into LC-MS/MS.



## 11. Liquid chromatography-tandem mass spectrometry (LC-MS/MS)

The LC-MS/MS was utilized to identify and quantify the peptides obtained from the digested whole-cell lysates. The tryptic peptide samples were prepared for injection into an Ultimate3000 Nano/Capillary LC System (Thermo Scientific, UK) coupled to a Hybrid quadrupole Q-ToF impact II<sup>TM</sup> (Bruker Daltonics) equipped with a Nano-captive spray ion source. Briefly, peptides were enriched on a  $\mu$ -Precolumn 300  $\mu\text{m}$  i.d. x 5 mm C18 Pepmap 100, 5  $\mu\text{m}$ , 100 A (Thermo Scientific, UK), separated on a 75  $\mu\text{m}$  I.D. x 15 cm and

packed with Acclaim PepMap RSLC C18, 2  $\mu\text{m}$ , 100 $\text{\AA}$ , nanoViper (Thermo Scientific, UK). Solvent A and B containing 0.1% formic acid in water and 0.1 % formic acid in 80% acetonitrile, respectively, were supplied on the analytical column. A gradient of 5–55% solvent B was used to elute the peptides at a constant flow rate of 0.30  $\mu\text{l}/\text{min}$  for 30 min. Electrospray ionization was carried out at 1.6kV using the CaptiveSpray. Mass spectra (MS) and MS/MS spectra were obtained in the positive-ion mode over the range (m/z) 150–2200 (Compass 1.9 software, Bruker Daltonics).

## 12. Bioinformatics and proteomics data analysis

MaxQuant 1.6.6.0 was used to quantify the proteins in individual samples using the Andromeda search engine to correlate MS/MS spectra to the Uniprot *Homo sapiens* database (131). The following parameters were used for data processing: maximum of two miss cleavages, a mass tolerance of 20 ppm for the main search, trypsin as digesting enzyme, carbamidomethylation of cysteine as a fixed modification, and the oxidation of methionine and acetylation of the protein N-terminus as variable modifications. Only peptides with a minimum of 7 amino acids, as well as at least one unique peptide, were required for protein identification. Only proteins with at least two peptides, and at least one unique peptide, were considered as being identified and used for further data analysis.

The gene list enrichment analysis was conducted using Enrichr software (132). Protein organization and biological action were investigated conforming to protein analysis through evolutionary relationships (Panther software) protein classification (133). A Venn diagram (analyzed by jVenn software) was used to show the differences between protein

lists originating from different differential analyses (134). The Search Tool for Retrieval of Interacting Genes/Proteins (STRING) software version 11 was used to analyze the common and the forecasted functional interaction networks between identified proteins (135). Cytoscape 3.7.2 was utilized to analyze the significant nodes from protein-protein interaction networks (136). The significant nodes analysis was modified from Rezaei-Tavirani (2017) (137). The degree values which were determined by an amount of interacted proteins with the node are analyzed, and the top 10% of the nodes based on degree value were selected as significant nodes. The heatmap visualization and statistical analyses were conducted using the MultiExperiment Viewer (MeV) in the TM4 suite software (138).

### **13. Proliferation assay**

MTT assay was used to determine the antiproliferative activity of the non-toxic concentrations of gigantol. Cells were seeded at a density of  $2 \times 10^3$  cells per well in 96-well plates. When the cells adhered, the medium was replaced with 5-20  $\mu\text{M}$  of gigantol or vehicle in complete medium. MTT assay was performed at the time 0-, 24-, 48-, 72-hour after treatment. A growth rate of each treatment group was normalized by its own MTT result at the time 0-hour. The growth rates were compared to the untreated at each time point.

### **14. Colony formation assay**

Cells were seeded at a density of 500 cells per well in a 6-well plate. When the cells adhered, the medium was replaced with 5-20  $\mu\text{M}$  of gigantol or vehicle in complete

medium. The medium with or without gigantol was replaced every 3 days. After an incubation for 10 days, the cells were fixed and stained with crystal violet staining solution. The cells were photographed, and the colonies with > 50 cells were counted. The numbers of colonies of gigantol-treated groups were compared to the control groups.

## 15. Western Blot Analysis

Western blot analysis was used for protein level determination. This assay was utilized to confirm the protein levels, both total and phosphorylated forms, of the signal proteins defined from the proteomic analysis.

Cells were lysed with RIPA lysis buffer containing 20 mM Tris-HCl (pH 7.5), 150 mM NaCl, 1 mM Na<sub>2</sub>EDTA, 1 mM EGTA, 1% NP-40, 1% sodium deoxycholate, 2.5 mM sodium pyrophosphate, 1 mM beta-glycerophosphate, 1 mM Na<sub>3</sub>VO<sub>4</sub>, 1 µg/mL leupeptin, and cocktail protease inhibitor mixture for 30 minutes on ice. The protein contents of the cell lysates were evaluated by Lowry assay. Samples with equal amounts of protein (30-60 µg) were run in the SDS-PAGE before they were transferred onto 0.45 mm nitrocellulose membranes (Bio-Rad, Hercules, California, United States). Transferred membranes were blocked for 1 hour in 5% non-fat dry milk in Tris-buffered saline with Tween 20 (25mM Tris-HCl, pH 7.5, 125 mM NaCl, and 0.05% Tween 20) and incubated overnight with specific primary antibodies against CD133, ALDH1A1, total Akt, phosphorylated Akt (Ser473), total STAT3, phosphorylated STAT3 (Ser727), and GAPDH (Table 3). Membranes were washed three times with Tris-buffered saline with Tween 20 and incubated with appropriate horseradish peroxidase-labeled secondary antibodies for 2 hours at room temperature. The

immune complexes were detected by SuperSignal™ West Pico PLUS Chemiluminescent Substrate (Thermo Scientific) or Immobilon Western Chemiluminescent HRP Substrate (Millipore) and imaged with ImageQuant LAS 4000 biomolecular imager.

**Table 3.** The details of antibodies used in Western blot analysis.

Antibodies	Source	MW (kDa)	Dilution
Anti-CD133	Rabbit	97	1:1000
Anti-ALDH1A1	Rabbit	55	1:1000
Anti-Akt (pan)	Rabbit	60	1:1000
Anti-phospho-Akt (Ser473)	Rabbit	60	1:1000
Anti-STAT3	Mouse	79, 86	1:2000
Anti-phospho-STAT3 (Ser727)	Rabbit	79, 86	1:1000
Anti-GSK-3 $\beta$	Mouse	46	1:1000
Anti-phospho-GSK-3 $\beta$ (Ser9)	Rabbit	46	1:1000
Anti-c-Myc	Rabbit	57-65	1:1000
Anti-GAPDH	Rabbit	37	1:1000
Anti-ubiquitin (HRP conjugated)	Mouse		1:2000
Anti-rabbit IgG (HRP-linked)	Goat		1:5000
Anti-mouse IgG (HRP-linked)	Horse		1:5000

## 16. Cycloheximide (CHX) chasing assay

Cells were treated with 20  $\mu$ M gigantol with or without 50  $\mu$ g/ml CHX for 0, 15, 30, 45, 60 and 90 min. The treated cells were collected and lysed with RIPA buffer containing the protease inhibitor cocktail. Western blot analysis was performed for detecting c-Myc protein levels. Protein band intensities were analyzed using the ImageJ software, and the c-Myc protein half-life was calculated.

## 17. Immunoprecipitation Assay

Cells were pretreated with 10  $\mu$ M MG132 for 1 hour and then treated with 20  $\mu$ M of gigantol or left untreated for 1 hour. The cells were collected and lysed with RIPA buffer containing the protease inhibitor cocktail. Then, Immunoprecipitation was performed by using Dynabeads™ Protein G Immunoprecipitation Kit from Thermo Fisher Scientific Inc. (Waltham, MA, USA). Magnetic beads were prepared and resuspended with the primary antibody of c-Myc (1:50) in a binding buffer for 10 min. A suspension of the magnetic bead-antibody complex was mixed with cell lysate and incubated at 4 °C overnight to allow c-Myc antigen to bind with magnetic bead-antibody complex. After that, the magnetic bead-antibody-antigen complex was washed three times using 200  $\mu$ l of washing buffer, separated on the magnet between each wash, and the supernatant was removed. Elution Buffer was added for releasing the antibody-antigen complex from magnetic beads. The supernatant contained the antibody-antigen complex was then used to perform Western blot analysis for detecting the ubiquitinated c-Myc protein.

## 18. Statistical analysis.

One-way analysis of variance (one-way ANOVA) or student's *t*-test was performed to conduct statistical analysis (GraphPad Prism 7.0). Data are expressed as mean  $\pm$  standard deviation (SD), and values of  $p < 0.05$  are indicative of significant differences.



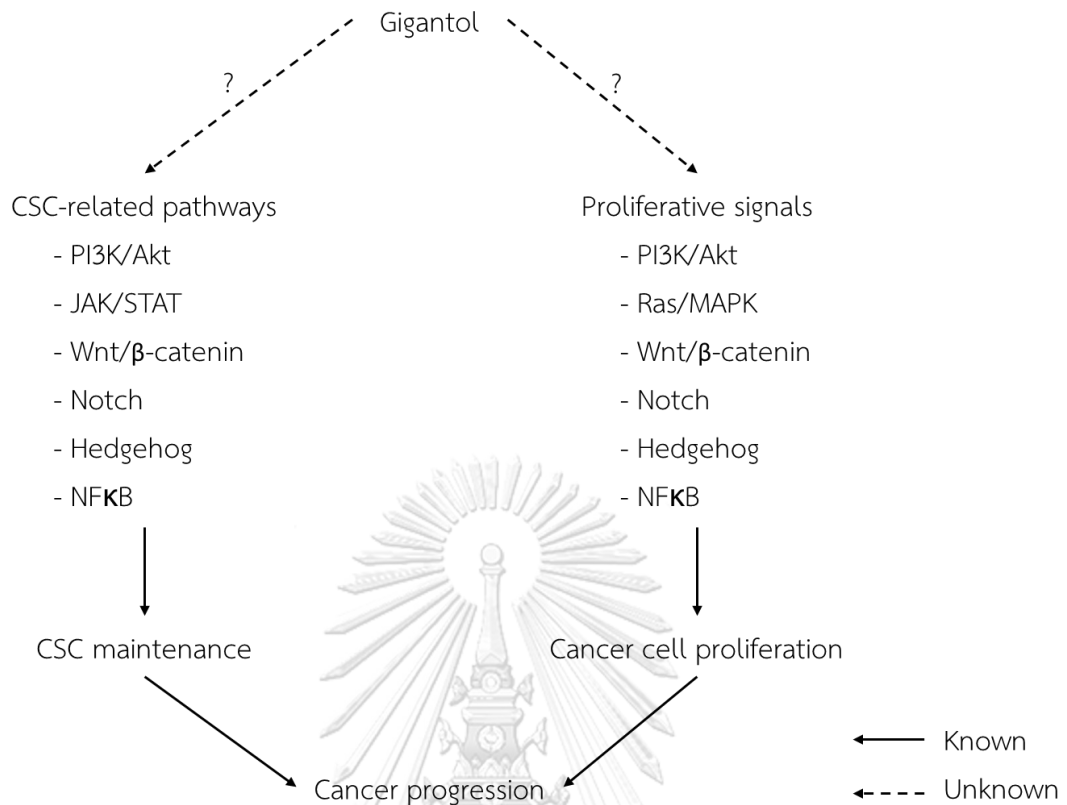


**Figure 8.** Schematic diagram of conceptual framework.

## EXPERIMENTAL DESIGN

### Part I: Determination of the non-toxic concentration of gigantol in human lung cancer cell lines

#### 1. Evaluation the cytotoxicity of gigantol in human lung cancer cell lines

A definition of the toxic concentration used in this study is the concentration of a compound that induces cell death in a mode of apoptosis or necrosis. In order to elucidate the possible tumor suppression activity of gigantol, the concentrations of the compound that caused no toxicity within 24 hours to the cancer cells are selected. MTT assay is used for a cell viability test, and the co-staining of Hoechst 33342 / propidium iodide is used for a mode of cell death determination.

The viable cell in a condition of MTT assay is a lived cell with well-functioned mitochondria. The resulting product of the reaction of MTT and mitochondrial reductase (NADH), which is a formazan crystal, refers to the cell number. Thus, MTT assay can widely use for a cytotoxicity test of compounds except for a compound that directly inhibits mitochondria function because the decreased formazan does not refer to the survived cell number. Once the cytotoxic concentrations are determined, the nuclear co-staining is performed to elucidate that the viable cell loss is a result of antiproliferation, apoptosis, or necrosis. The selected non-cytotoxic concentration is a concentration that neither significantly inhibits cells nor induce cell death.

Cytotoxicity test was performed to determine the concentrations of gigantol that cause no toxic effect on lung cancer cell lines. Cells were treated with 0-200  $\mu\text{M}$  of

gigantol for 24 hours. Percentage of cell viability was calculated. Additionally, the toxic effect of gigantol at 48 hours was performed to investigate the viability rate of H460 cells which was the treatment condition used in cell preparation in xenograft experiment.

Besides, the toxic effect of gigantol was performed in normal lung epithelial cells, BEAS-2B cells, in order to compare the toxicity of gigantol towards cancer and normal lung cells.

To confirm the viability of the lung cancer cells, apoptotic and necrotic cell death were determined by Hoechst 33342 and propidium iodide staining, respectively, compared to the control. Concentrations which did not cause significantly reduction of cell viability and did not cause apoptosis or necrosis were used in the following experiments.

## **Part II: Investigation of effects of non-toxic concentration of gigantol on cell proliferation and tumorigenicity in human lung cancer H460 cell line**

### **1. Investigation on the effect of gigantol on proliferation of human lung cancer cell lines**

Since cell proliferation is a fundamental behavior of cancer cells in tumorigenesis, the effect of gigantol on proliferation of lung cancer cells was investigated with non-toxic concentrations of gigantol. MTT assay was performed at 0, 24, 48, and 72 hours of gigantol treatment. Relative cell proliferation was calculated as a ratio versus 0 hour of treatment and the ratios of treated groups were compared to the control at the same time point.

Colony formation assay was also performed to confirm the anti-proliferative effect of gigantol. The cancer cells were seeded in 6-well plates and incubated with non-toxic

concentrations of gigantol for 10 days. The colonies were stained with crystal violet and counted compared to the untreated control. This experimental design proof the effect of gigantol on the proliferation activity of the total population (CSC and non-CSC) of the cancer cells.

## 2. Investigation on the effects of gigantol on tumorigenicity in human lung cancer

### H460 cell line using *in vivo* model

The *in vivo* subcutaneous xenograft in nude mice experiment is designed base on the assumption that the CSC-suppressed lung cancer cells by gigantol have lower tumorigenicity than the untreated cells. The lung cancer cells used in this experiment were validated by Western blot analysis that the stemness was suppressed before the xenograft inoculation, as evidenced by a reduction of CD133 and ALDH1A1 levels. Because the spontaneous metastasis was not observed, and a posttreatment was not administrated, the multiple tumor xenografts could be performed.

#### 2.1 Gross tumor evaluation

H460 cells were pretreated with vehicle or 20  $\mu$ M of gigantol before inoculated into each flank of a nude mouse. The growing tumors were observed daily. Once the tumors reached endpoint size, the mouse was sacrificed, and the control and pretreated tumors were collected. Tumor weights were investigated and then tumors were subjected to paraffin embedding for further histological investigation.

## 2.2 Investigation on intratumor histology

The tumor slides were performed hematoxylin and eosin staining and then intratumor histology was examined. Intratumoral structure, such as necrotic areas, were detected.

## 2.3 Immunohistochemistry

Ki-67 is used as a marker for cells with a high proliferative rate. The expression of Ki-67 is associated with tumor aggressiveness (139). Alpha smooth muscle actin ( $\alpha$ -SMA), a differentiation marker of smooth muscle cells, is abundantly found in vascular pericytes (140).  $\alpha$ -SMA is also found in normal and cancer cells with high EMT-like phenotype (141). The immunohistochemistry staining of Ki-67 and  $\alpha$ -SMA was performed to reveal the aggressiveness or the phenotypic alteration of the tumors.

## Part III: Investigation of effects of gigantol on underlying mechanisms involved in CSC-like phenotype and cell proliferation in human lung cancer H460 cell line

### 1. Effects of gigantol on CSC-regulating pathways

#### 1.1 Determination the CSC maintenance related pathway affected by gigantol from the proteomics data

Proteomics analysis is used for determining the effects of gigantol on common CSC-regulating pathways. The same lung cancer cell lysates used in this experiment must be validated by Western blot analysis that the stemness is suppressed, as evidenced by a

reduction of CD133 and ALDH1A1 levels, before undergoing the protein digestion process. The differential expression of proteins was determined, and these proteins were further analyzed with the common CSC signals-relating bioinformatics data.

## **1.2 Validation of key signal proteins of the CSC-related pathways affected by gigantol**

Protein levels of the key signals from the CSC-related pathways affected by gigantol were validated using Western blot analysis. Since the function of kinase proteins depended on their post-translational modification, such as phosphorylated form at the specific sites, the active forms of the key signal kinases were also validated.

## **2. Effects of gigantol on underlying mechanisms of lung cancer cell proliferation inhibition**

### **2.1 Determination of effects of gigantol on cell proliferation regulating pathways using proteomics data**

Proteomics analysis was used for determining the effects of gigantol on proliferation-regulatory proteins. The enrichment analysis was utilized to determine the protein set that involved in cell proliferation using Enrichr software. The obtained protein set was further analyzed for the key proteins in response to gigantol treatment.

### **2.2 Validation of key proteins of the proliferation-regulatory pathways affected by gigantol**

Protein levels of the key proteins which dominantly regulated cell proliferation affected by gigantol were validated using Western blot analysis. Also, related pathways of the key proteins were investigated through bioinformatics analysis using STRING software.

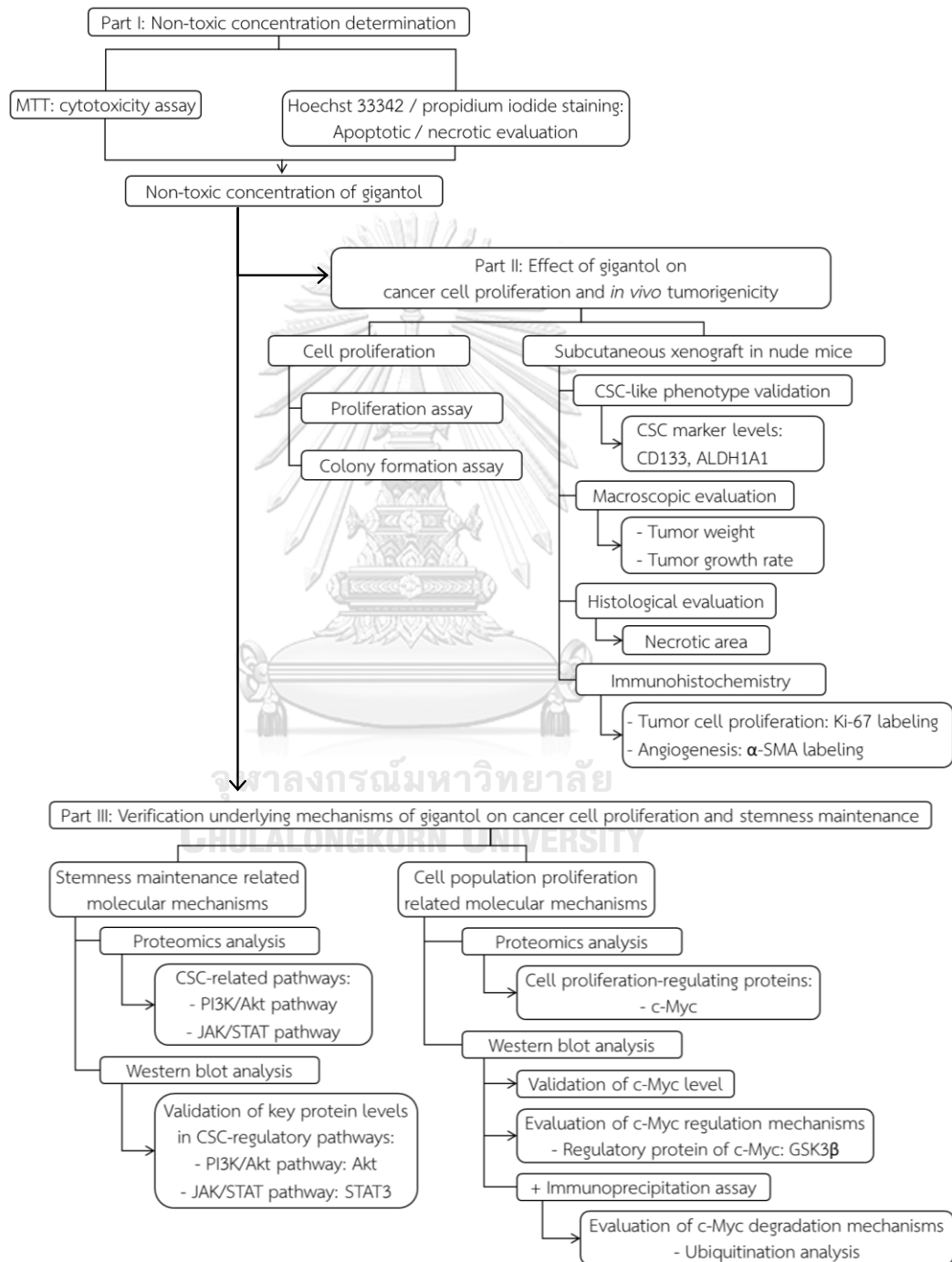


**Figure 9.** Schematic diagram of the experimental design

## CHAPTER IV

### RESULTS

#### Part I: Non-cytotoxic concentration evaluation of gigantol in human lung cancer cell lines

##### 1. Effect of gigantol on cytotoxicity of human lung cancer cell lines

Lung cancer cells were treated with gigantol in various concentrations (0 – 200  $\mu\text{M}$ ) for 24 hours and MTT colorimetric assay was performed to evaluate cytotoxic effect of gigantol. Treatment of three lung cancer cells with 5-20  $\mu\text{M}$  of gigantol for 24 hours had a nonsignificant effect on survival of the cells, while a significant reduction of cell survival could be first detected in response to gigantol at a concentration of 50  $\mu\text{M}$  (Figure 10A). Moreover, cell viability evaluation revealed that gigantol exhibited less toxicity to human lung epithelial cells BEAS-2B as compared with lung cancer cells (Figure 10B).

Although the result of MTT assay showed that 20  $\mu\text{M}$  gigantol had no toxic effect to lung cancer cells, cell morphology was observed to approve the cell viability. Confirmation of cell death, either via apoptosis or necrosis, was detected under a fluorescent microscope after staining with Hoechst 33342 and propidium iodide (PI), as described in the Materials and Methods section. The nuclear staining results revealed that condensed and fragmented nuclei of apoptosis cells could be observed only in the cells treated with gigantol more than 50  $\mu\text{M}$  (Figure 11A and 11B). It is worth indicating that



treatment with gigantol at all concentrations (0 to 200  $\mu\text{M}$ ) caused no necrosis (Figure 11A).

Non-toxic concentrations of gigantol (20  $\mu\text{M}$ ) were used in subsequent experiments.

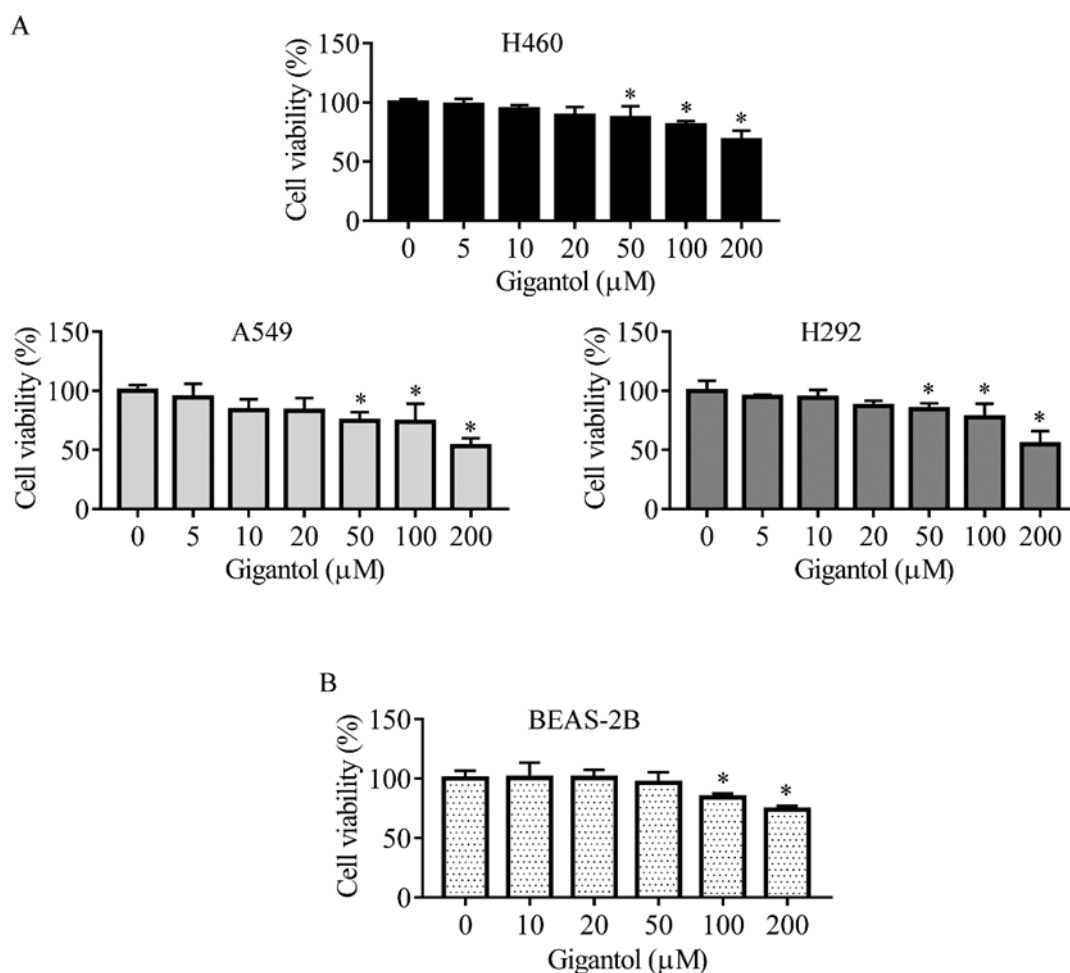


**Figure 10.** Cytotoxic effect of gigantol on lung cancer cells. The cells were treated with 0-200  $\mu\text{M}$  of gigantol or vehicle for 24 hours and then analyzed by MTT assay for cell viability. The percentages of viable cells were compared to their untreated controls. (A) Graphs showing the percentages of lung cancer cells, H460, A549, and H292, viability. (B) Graphs showing the percentages of normal lung epithelial cells, BEAS-2B, viability. The viability of untreated cells was counted as 100% viability (\*  $p < 0.05$ , compared with the untreated cells,  $n = 5$ ).

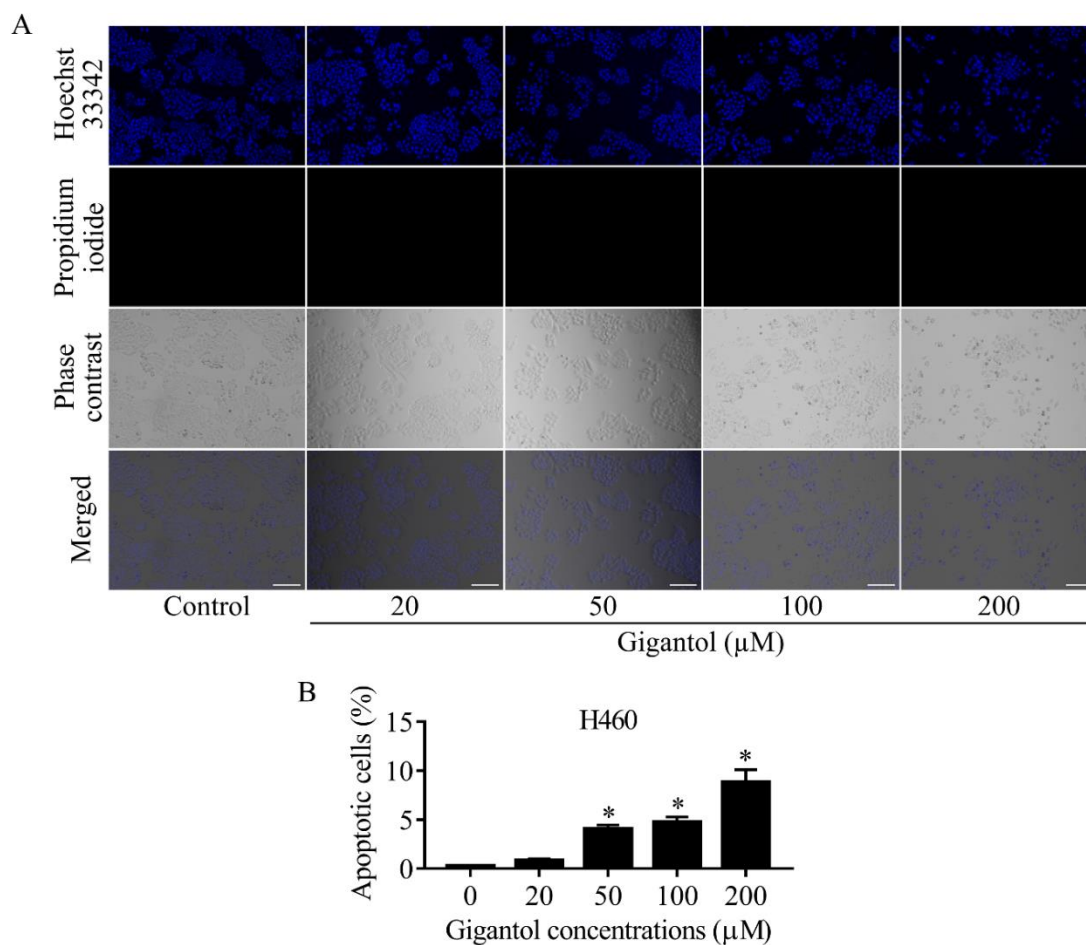


**Figure 11.** (A) Photographs of Hoechst 33342, Propidium iodide (PI), and phase contrast fields showing cancer cells morphologies after 24 hours of gigantol treatment, the scale bars represent 100  $\mu\text{m}$  and the magnification is 100 $\times$ . (B) Graph showing the percentages of apoptotic cell death after 24 hours of gigantol exposure. Necrotic cells could not be detected. (\*  $p < 0.05$ , compared with the untreated cells,  $n = 5$ )

## Part II: Investigation of effects of non-toxic concentration of gigantol on cell proliferation and tumorigenicity in human lung cancer H460 cell line

### 1. Investigation on the effect of gigantol on proliferation of human lung cancer cell lines

Since proliferation of the cancer cells is the fundamental biological process of tumorigenicity, anti-proliferative effect of gigantol was evaluated in lung cancer cells using MTT colorimetric assay. Lung cancer cells were treated with non-cytotoxic concentrations of gigantol (10 – 20  $\mu\text{M}$ ) and were measured the cell viability at indicated time (0, 24, 48, 72 hours).

Gigantol at 5-20  $\mu\text{M}$  was further investigated for the anti-proliferative activity. The cells were cultured in growth medium in the presence or absence of gigantol for 1-3 days. The proliferation assay revealed that gigantol at 20  $\mu\text{M}$  significantly reduced proliferation after 1 days of cultivation in H460 and A549 cells, however, gigantol at lower concentrations (5-10  $\mu\text{M}$ ) significantly suppressed proliferation at day 3. Whilst, in H292 cells, gigantol at 5-20  $\mu\text{M}$  showed anti-proliferative effect after 2 days of treatment (Figure 12). Moreover, the anti-proliferative activity of gigantol was confirmed using colony formation assay of all tested cells as described in Materials and Methods. The average colony numbers of the untreated control group were counted as 100%. The percentage of relative colony numbers of the gigantol-treated groups showed that gigantol at 5-20  $\mu\text{M}$  were able to suppress lung cancer cell growth significantly in a dose-dependent manner (Figure 13A and 13B). Results from these two assays proved that gigantol had an anti-

proliferative effect against lung cancer cell growth. For the concentration at 20  $\mu\text{M}$  of gigantol showed the strongest anti-proliferative effect in both assays, this concentration was used for the further proteomics analysis.

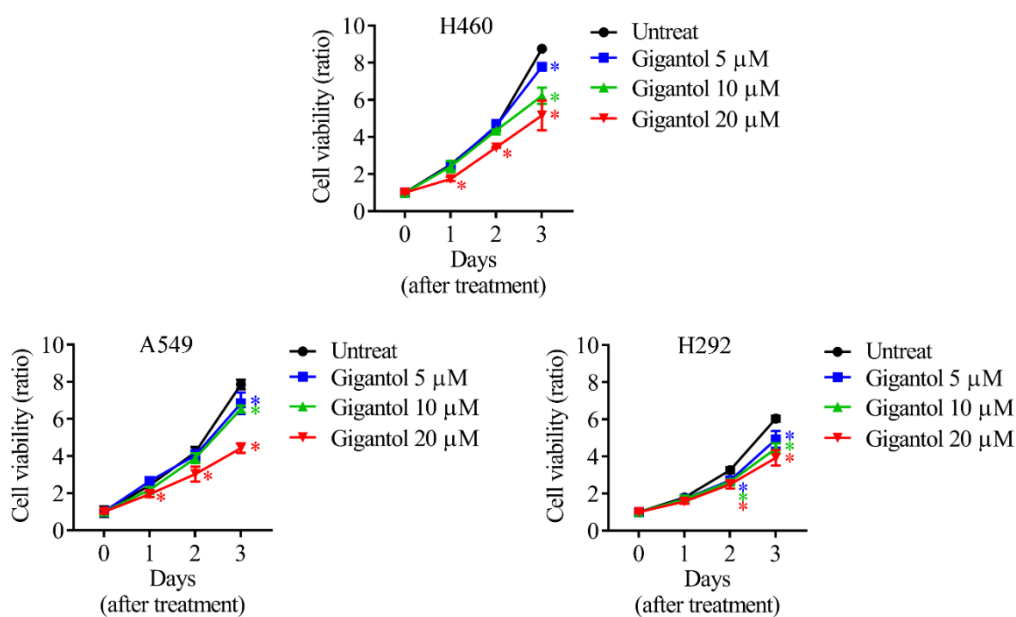


**Figure 12.** Anti-proliferative effect of gigantol was evaluated. Lung cancer cells were treated with 0-20  $\mu\text{M}$  gigantol for 3 days and the MTT assay was performed every 24 hours. The cell viability at day 1-3 was compared to the day 0 viability within group, and data was plotted as a growth rate of each treatment group (The cell viability at day 0 was counted as 1-fold). Relative growth of the gigantol-treated cells was compared with control cells within the same time of gigantol exposure (\*  $p < 0.05$ , compared with the untreated cells at each time point,  $n = 4$ ).

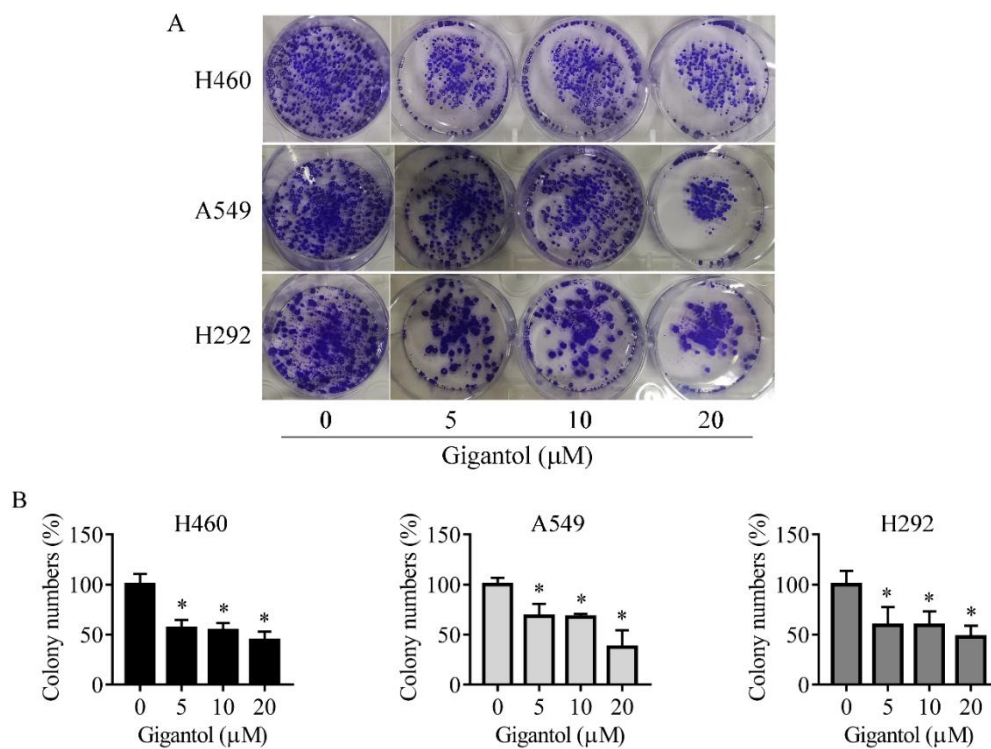


**Figure 13.** Colony formation assay was performed to confirm an anti-proliferative effect of gigantol. Lung cancer cells were treated with 0-20  $\mu\text{M}$  gigantol for 10 days and then were stained with crystal violet. The colonies with > 50 cells were counted. (A) Photographed images of the stained colonies treated with 0-20  $\mu\text{M}$  gigantol. (B) The percentage of treated cells was calculated relative to the untreated cells. All data represented mean  $\pm$  SD (\*  $p < 0.05$ , compared with the untreated cells,  $n = 3$ ).

## 2. Evaluation the suppressive capability of gigantol on tumorigenicity of human lung cancer cells using an *in vivo* subcutaneous xenograft model

### 2.1 Validation of the stemness in gigantol-treated lung cancer cells used in the *in vivo* experiment

Before H460 cells were subjected to a xenograft inoculation, the lung cancer cells were validated for CSC phenotype reduction by gigantol using Western blot analysis of CSC markers, CD133 and ALDH1A1. Cells were treated with 20  $\mu\text{M}$  gigantol for 24 hours and the cells were harvested for protein level measurement. Figure 14 showed that the cancer cells used for tumor xenograft experiment were valid because the gigantol-treated cells had lower stemness than the control group.

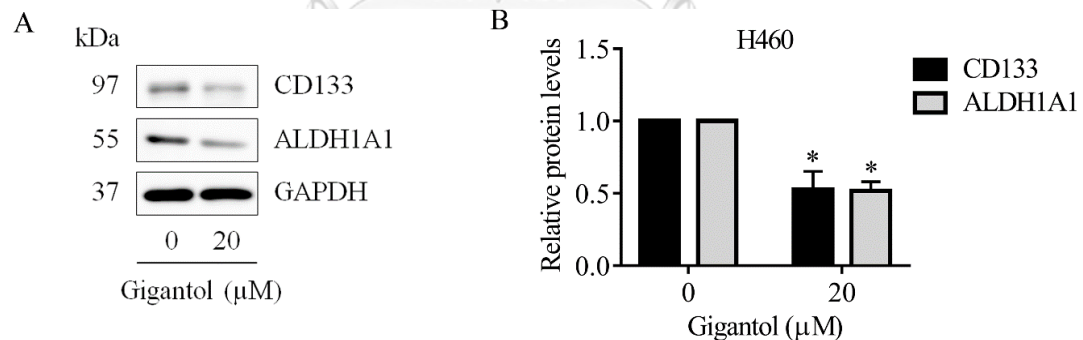


**Figure 14.** (A) The protein expression of CSC markers, CD133 and ALDH1A1, in H460 cells treated with 20  $\mu\text{M}$  gigantol was validated by Western blot analysis. (B) the immunoblot signal intensities were quantified by densitometry. Data represent means  $\pm$  SD. (\*  $p < 0.05$  as compared with the control group,  $n = 3$ ).

## 2.2 Investigation the effects of gigantol on tumor growth and gross tumors in subcutaneous xenograft model using nude mice model

After injection of lung cancer cells into two flanks of each mouse, most mice generated palpable tumors on day seven and most control tumors had reached their endpoint size on day 13. Figure 15 demonstrates that every mouse had a similar growth rate (indicated by body weight) within a normal range. The growing tumors were measured using Vernier caliper and the estimated tumor volumes were calculated. Figure 16A showed the growth rate of each tumor and Figure 16B showed the mean tumor growth rates, which was similar between the control and the treatment groups. At day 13 after inoculation, tumors were dissected (Figure 17A), and tumor weights and tumor sizes were measured, and the estimated volumes were calculated. The gigantol-treated tumors had lower tumor weights as compared with their own control tumors, except for mouse 3. However, the average weights of the tumors were not significantly different between groups (Figure 17B; control group mean =  $966 \pm 345.3$  mg, gigantol group mean =  $698 \pm 345.5$  mg,  $n = 5$ ,  $p = 0.2152$ , Student's *t*-test). Likewise, Tumor volumes of the gigantol groups were lower than the control groups, but the average volume of the gigantol group was not significantly different to the control group (Figure 17C; control group mean =  $1394 \pm 460.7$  mm<sup>3</sup>, gigantol group mean =  $1081 \pm 519.2$  mm<sup>3</sup>,  $n = 5$ ,  $p = 0.2155$ , Student's *t*-test). The tumor densities were compared, and the results showed that the gigantol groups had lower tumor densities than their paired untreated controls (Figure 18; control group mean =  $0.685 \pm 0.089$  mg/mm<sup>3</sup>, gigantol group mean =  $0.633 \pm 0.071$  mg/mm<sup>3</sup>,  $n = 5$ ,  $p = 0.4444$ , Student's *t*-test).

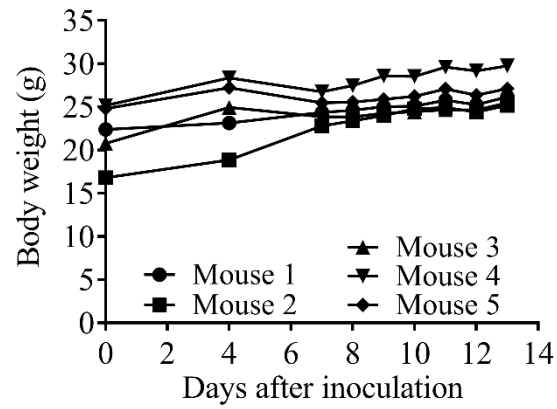


**Figure 15.** Graph showing mice body weights starting at the day of cancer cell inoculation until the day of termination.





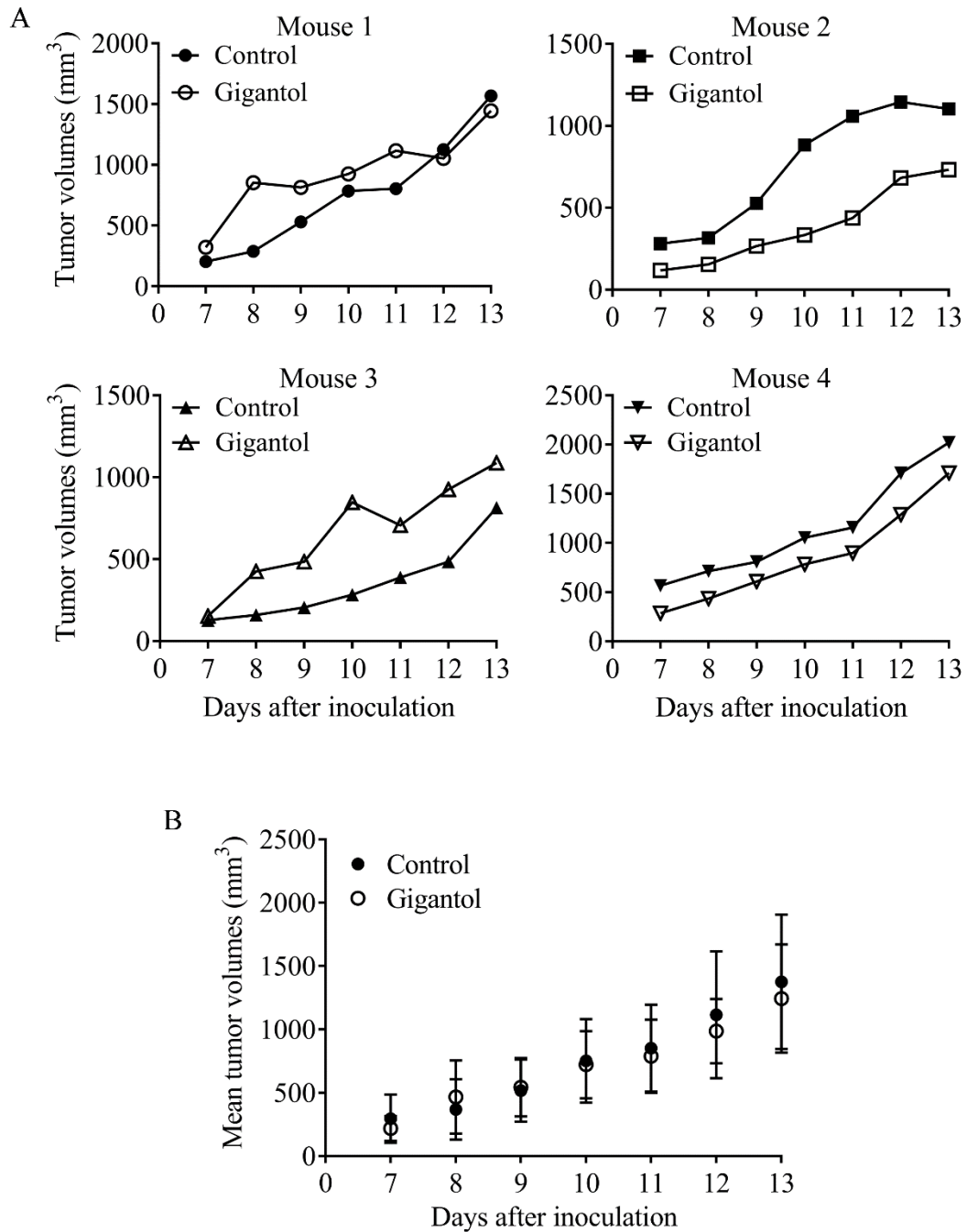


**Figure 16.** (A) Four graphs demonstrating the individual tumor growth rate of each mouse (tumor growth of mouse 5 could not be accomplished because the gigantol-treated tumor was not palpable and measured until the day of termination). (B) Graph presenting the mean tumor growth rate of the control and gigantol groups.

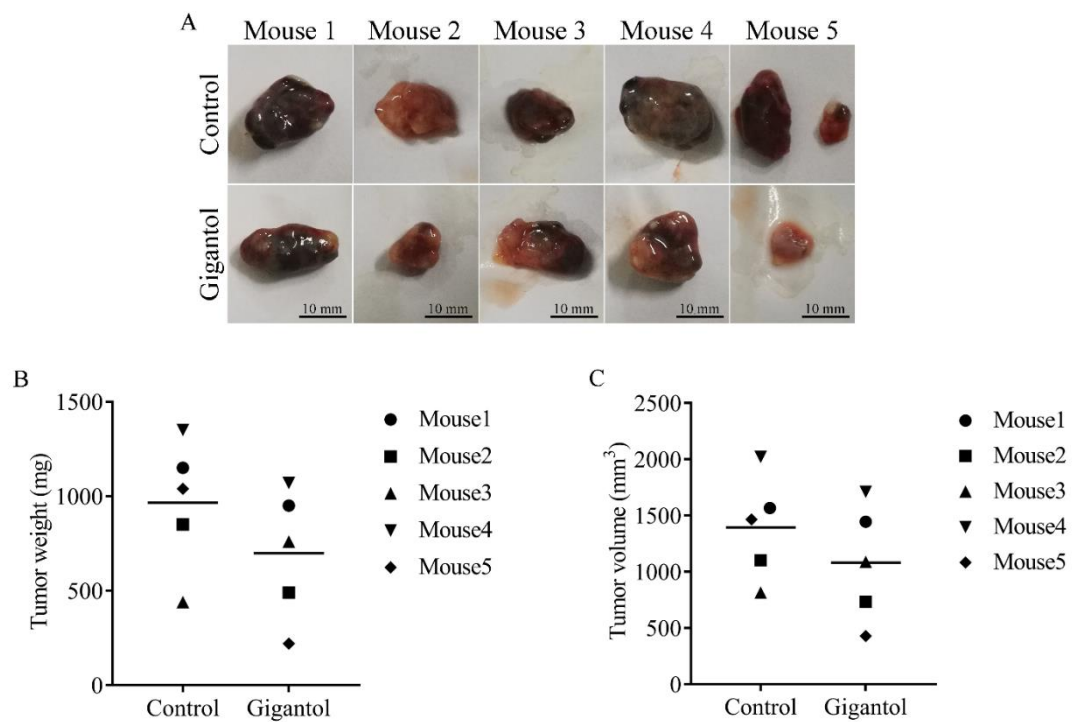


**Figure 17.** (A) Untreated (upper row) and gigantol-treated (lower row) tumors were dissected and photographed at day 13 after inoculation. Scale bars represent 10 mm in length. (B) Graph showing the control and gigantol tumor weights with the grouped means. The 5 different markers represent each pair of tumors (n = 5). (C) Graph showing the control and gigantol tumor volumes with the grouped means. The 5 different markers represent each pair of tumors (n = 5).

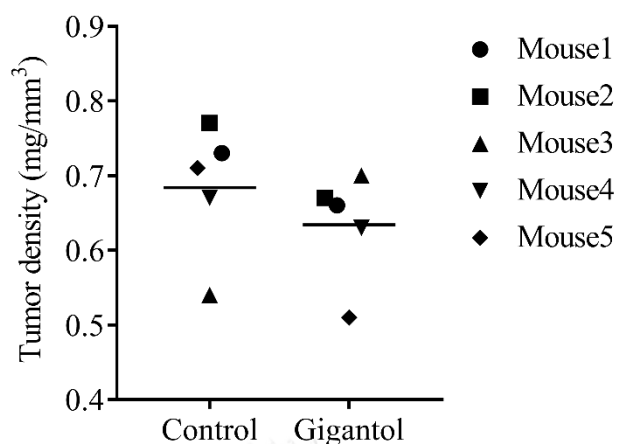
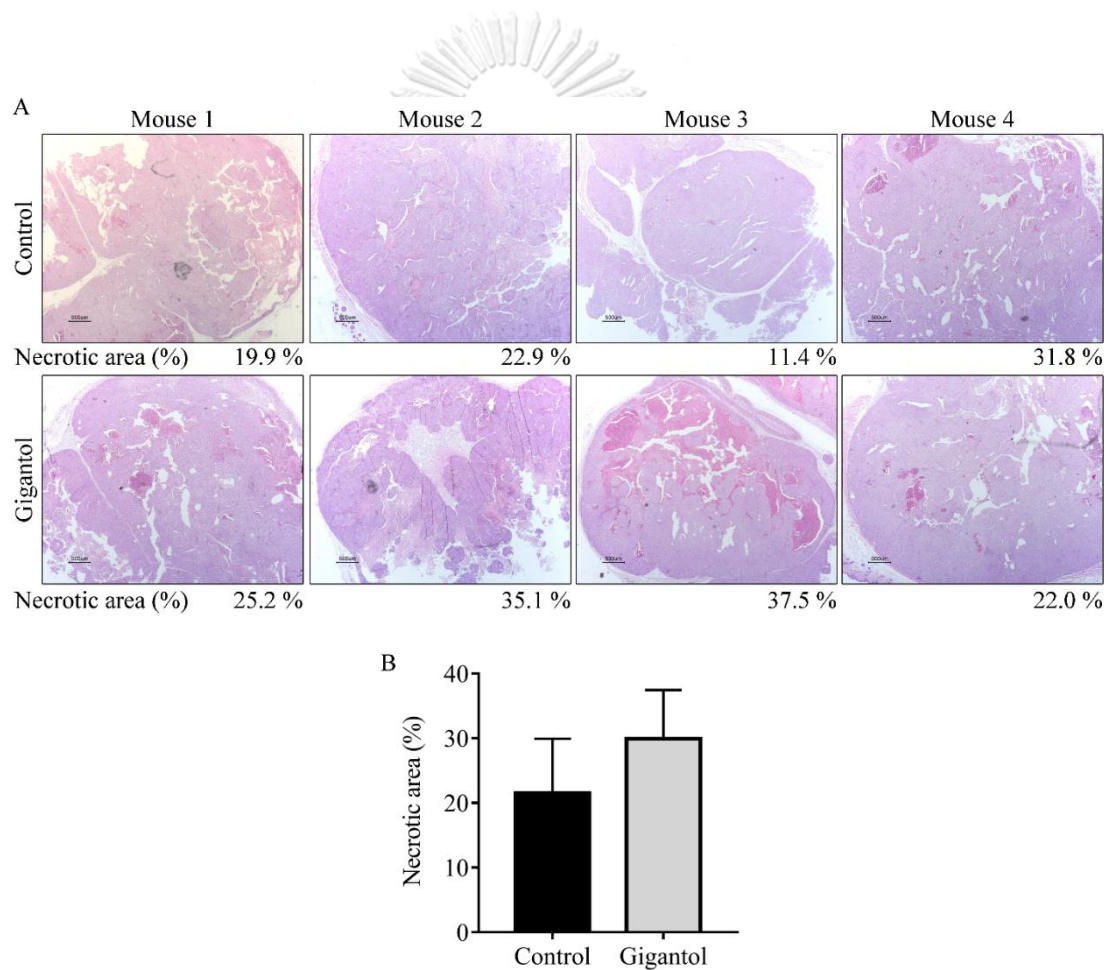


**Figure 18.** Tumor density was calculated as weight by volume. Graph showing the control and gigantol tumor densities with the grouped means. The 5 different markers represent each pair of tumors (n = 5).

### 2.3 Histological observation showed lower viable tumor areas in the gigantol-treated tumors

Having shown that gigantol pretreatment caused tumors with a lesser density as compared with the untreated control, we wish to emphasize this phenomenon as previous studies have indicated that changes in tumor density, as indicated by CT imaging showing a loss of tumor mass, can be a potential assessment for anti-cancer drug action (142, 143). Cross-section slices of the tumors were co-stained by hematoxylin and eosin (H&E), and, then, were photographed. The macro-morphology of the tumor structure was similar among all the tumors (small nodules packed within a tumor lobe, surrounded with fibrous tissues), whereas the percentage of intact and non-viable tumor cells of the two groups were dramatically different. Figure 19A demonstrates that while the control tumors

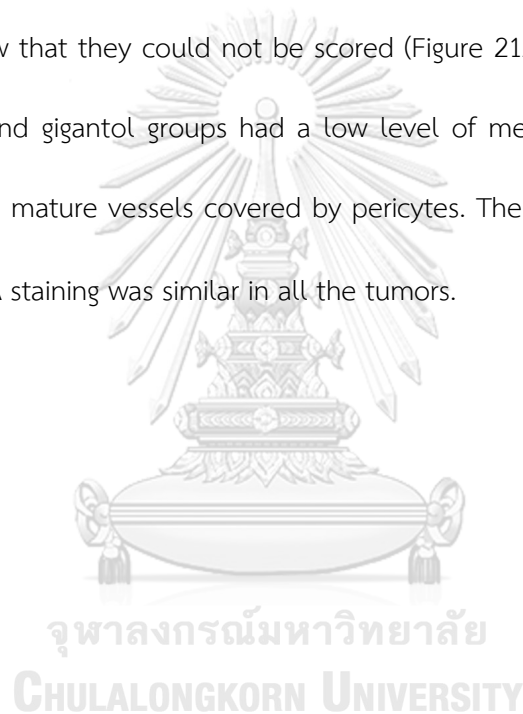
exhibited a dense viable tumor mass, the gigantol tumors showed a substantial loss of tumor mass, as indicated by a hollowing with the magenta staining of cells or pale pink cells without nuclear staining. Figure 19A showed that tumors from gigantol-pretreated cells had more necrotic area compared to their own control tumor, except mouse 4. By the way, the average necrotic area between the two groups was not significantly different (Figure 19B).



**Figure 19.** (A) Hematoxylin and eosin staining showing intratumor morphology (20 $\times$ ). Percentages of necrotic areas as compared with their total areas are shown at the lower-right edge of each picture. Scale bars at the lower-left edge of each picture represent 500  $\mu$ m lengths. (B) Graph showing percentages of control and gigantol tumors (n = 4).

## 2.4 Gigantol suppresses tumor cells proliferation but not tumor vasculature

Two pairs of tumors were selected for Ki-67 and  $\alpha$ -smooth muscle actin ( $\alpha$ -SMA) immunohistochemistry (IHC) staining. The hot spots and cold spots of Ki-67 positive cells are shown in Figure 20A. The mean percentage of Ki-67 positive cells of the control group was  $62.45 \pm 0.3951$  and that of the gigantol-treated group was  $49.49 \pm 0.7348$  ( $p$ -value = 0.0041, Student's  $t$ -test,  $n = 2$ , Figure 20B). The  $\alpha$ -SMA signals from cancer cells in all tumors were so low that they could not be scored (Figure 21A). This result indicated that both the control and gigantol groups had a low level of mesenchymal-like phenotypes. Figure 21B presents mature vessels covered by pericytes. The number of vessels per area detected by  $\alpha$ -SMA staining was similar in all the tumors.



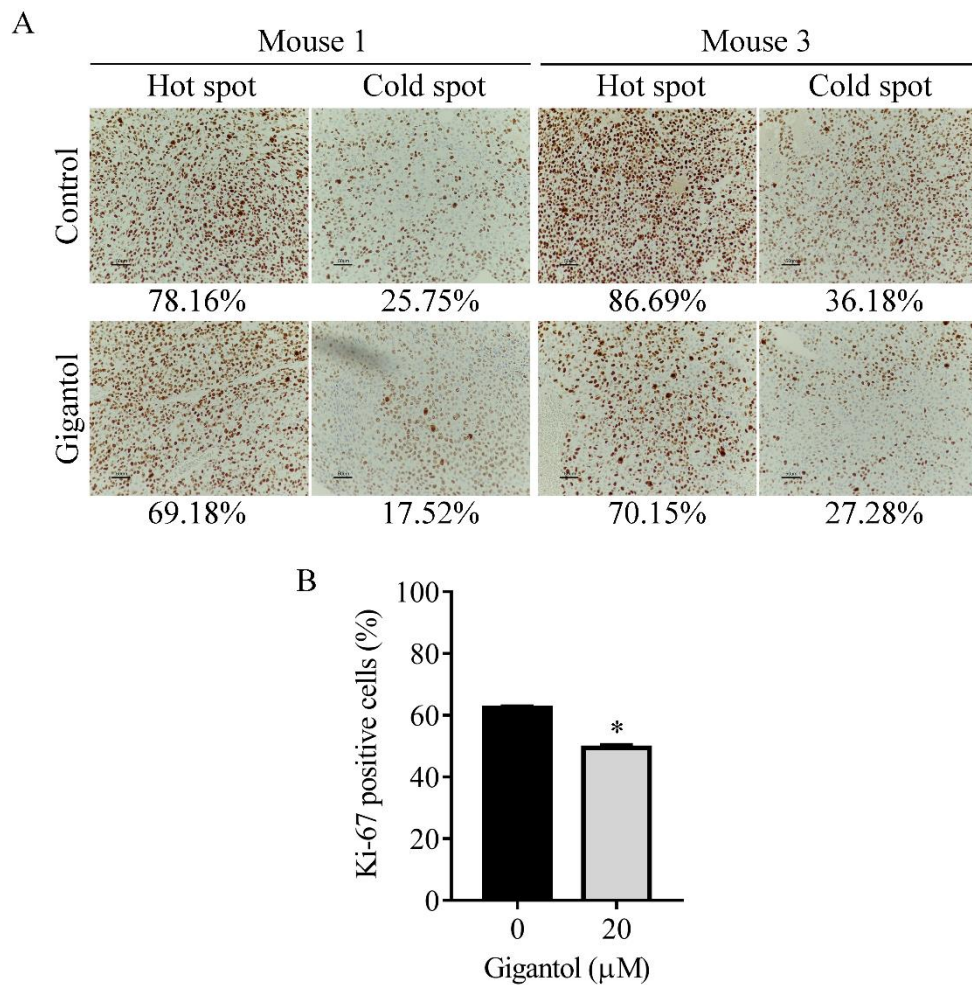


**Figure 20.** (A) Immunohistochemistry (IHC) staining demonstrating 200-fold magnified pictures of hot spots and cold spots from the control and gigantol-treated tumors. The percentages of Ki-67 positive cells as compared with total cells are displayed under their pictures. (B) Graph showing the means of %Ki-67 positive cells. (\*  $p < 0.05$  as compared with the control group, Student's t-test,  $n = 2$ ).



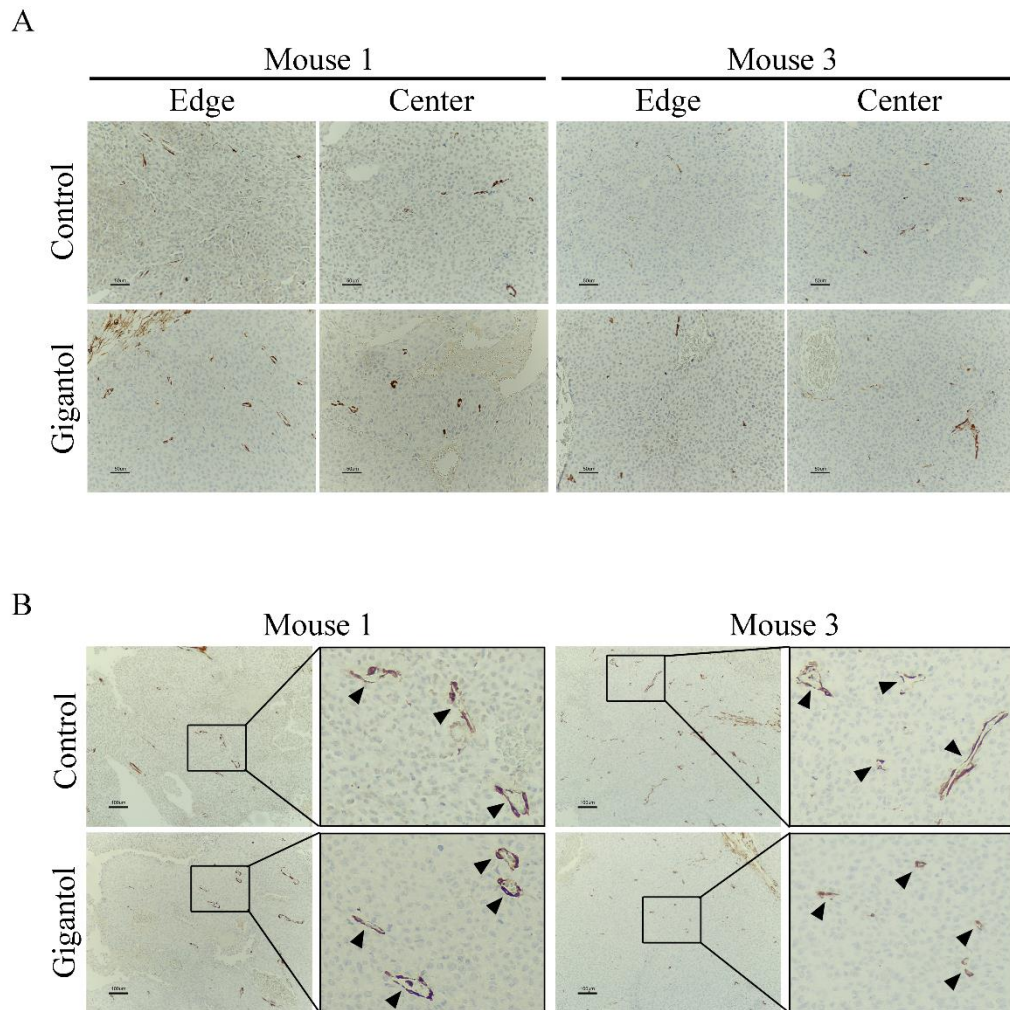


**Figure 21.** (A)  $\alpha$ -SMA IHC staining of cancer cells in both edge and center areas of tumors showing no difference of signal levels (200 $\times$ ). The numbers of mature tumor vessels per areas between the control and gigantol groups were not different. (B) Pictures showing vessel distribution among the tumor mass (100 $\times$ ). Arrow indicates a vessel (400 $\times$ ).

### Part III: Investigation of effects of gigantol on underlying mechanisms involved in CSC-like phenotype and cell proliferation in human lung cancer H460 cell line

#### 1. Investigation on CSC-related signaling pathways affected by gigantol

Whole cell lysates of untreated and gigantol-treated H460 cells were subjected to the proteomic LC-MS/MS system and quantitative proteomics analysis was performed with MaxQuant software using Andromeda database. In total, 4351 proteins were identified from the control cells, while 3745 proteins were identified from the gigantol-treated cells. The proteomics profiles were subjected to further bioinformatic analysis as described in the proteomic workflow (Figure 22). The protein lists from the control and gigantol-treated cells were input to a Venn diagram and 2373 proteins (54.54% of total proteins from control group) were identified as being only from the control cells, 1767 proteins (47.18% of total proteins from gigantol-treated group) only from the gigantol-treated cells, and 1978 proteins from both groups (Figure 23A). The down- and up-regulated protein lists were categorized into three ontologies, molecular function, biological process, and cellular component using Panther software (conducted on 8 October 2019). The most overrepresented molecular functions were binding (38.3% down- and 35.6% up-regulated proteins) and catalytic activity (32.0% down- and 35.6% up-regulated proteins) (Figure 23B). The most overrepresented biological process categories were cellular process (31.8% down- and 32.6% up-regulated proteins), and metabolic process (21.0% down- and 19.8% up-regulated proteins) (Figure 23C). The most overrepresented cellular component



categories were cell (39.4% down- and 40.2% up-regulated proteins) and organelle (33.6% down- and 32.2% up-regulated proteins) (Figure 23D). The differentially expressed proteins were subjected to further bioinformatic analysis.

The two protein lists of down- and up-regulated proteins were input to Enrichr software to identify the enriched biological processes associated with CSC regulation (conducted on 8 October 2019). Enrichment terms from the Gene Ontology (GO) biological process of down-regulated proteins in gigantol-treated cells are involved in macromolecule biosynthesis, DNA-templated transcription, gene expression, protein phosphorylation, cytoskeleton organization, and telomere maintenance. In contrast, enrichment biological processes of up-regulated proteins in gigantol-treated cells are involved in intracellular signal transduction, protein phosphorylation, gene expression, and protein biosynthesis processes (Table 4).

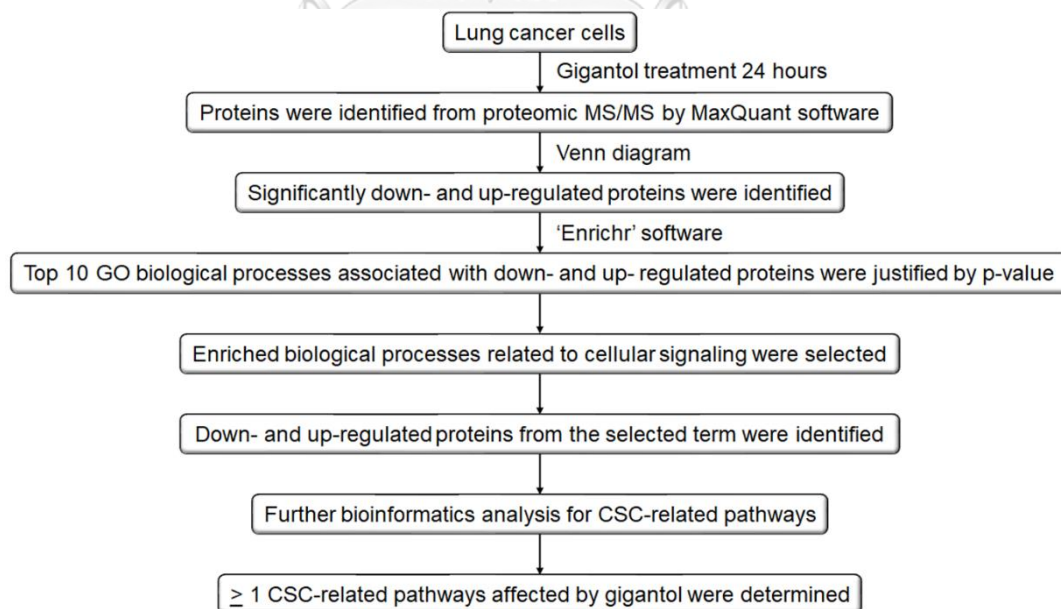


**Figure 22.** Schematic diagram showed the proteomic workflow for verification of the CSC-related signaling pathways affected by gigantol.

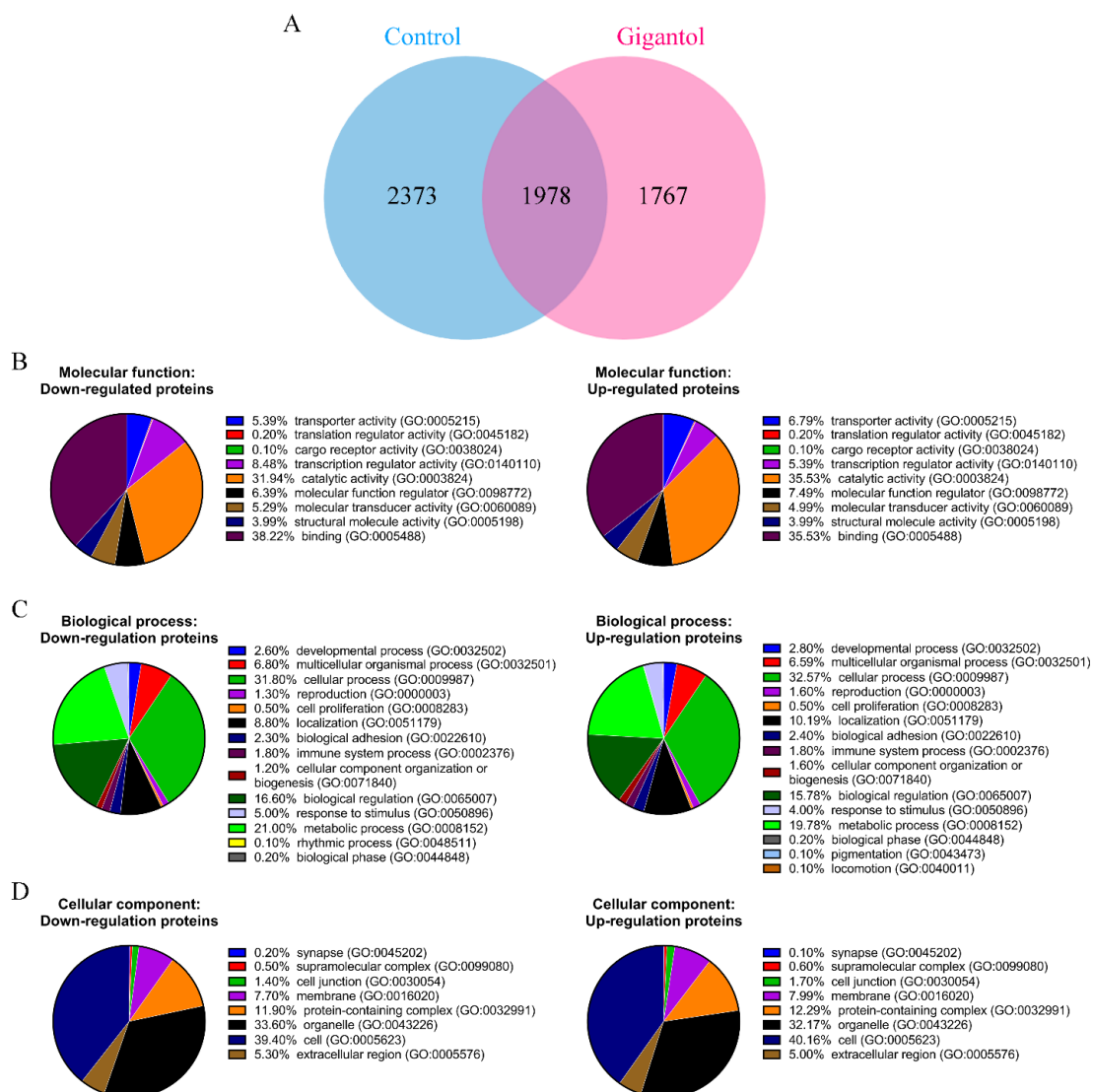


**Figure 23.** H460 cells were treated with 20  $\mu$ M of gigantol or its vehicle (0.004% DMSO) for 24 hours before the whole-cell lysates were collected. The experiment was performed in biological triplicates. (A) Venn diagram showing the difference in proteins expressions between the control and gigantol-treated H460 cells. Three functional classifications of the 2373 down- and 1767 up-regulated proteins affected by gigantol treatment using Panther software: (B) molecular function, (C) biological process, and (D) cellular component.

**Table 4.** First 10 ranking enrichment terms from the GO biological process of down- and up-regulated proteins in gigantol-treated cells.

<b>Enriched biological processes associated with the down-regulated proteins</b>		
<b>Term</b>	<b>Overlap</b>	<b>p-Value</b>
regulation of cellular macromolecule biosynthetic process (GO:2000112)	129/632	2.65E-10
regulation of nucleic acid-templated transcription (GO:1903506)	121/608	4.65E-09
protein phosphorylation (GO:0006468)	97/471	2.82E-08
regulation of transcription, DNA-templated (GO:0006355)	254/1599	3.09E-07
regulation of gene expression (GO:0010468)	174/1038	9.47E-07
phosphorylation (GO:0016310)	76/387	5.61E-06
protein autophosphorylation (GO:0046777)	41/176	1.44E-05
cytoskeleton organization (GO:0007010)	29/127	3.49E-04
membrane depolarization during action potential (GO:0086010)	13/39	3.58E-04
regulation of telomere maintenance (GO:0032204)	10/26	4.67E-04
<b>Enriched biological processes associated with the up-regulated proteins</b>		
<b>Term</b>	<b>Overlap</b>	<b>p-Value</b>
regulation of intracellular signal transduction (GO:1902531)	62/423	4.82E-05
protein phosphorylation (GO:0006468)	67/471	6.24E-05
ribosomal large subunit biogenesis (GO:0042273)	16/64	1.02E-04
cyclic purine nucleotide metabolic process (GO:0052652)	10/31	2.17E-04
regulation of gene expression (GO:0010468)	124/1038	2.75E-04
nucleotide biosynthetic process (GO:0009165)	9/27	3.40E-04
DNA replication checkpoint (GO:0000076)	7/17	3.59E-04
RNA splicing, via transesterification reactions with bulged adenosine as nucleophile (GO:0000377)	37/237	4.55E-04
regulation of mRNA processing (GO:0050684)	9/29	6.19E-04
mRNA processing (GO:0006397)	42/284	6.22E-04

### 1.1 Determination the CSC maintenance related signaling pathways affected by gigantol from the proteomics data

Kinases are vital enzymes that regulate intracellular signaling. Several oncogenes and tumor suppressor genes are kinase enzymes or proteins linked to protein kinase activity. Therefore, the most interesting GO term involved with cellular signaling and found in the enrichment analysis results of both down- and up- regulated proteins was “protein phosphorylation (GO:0006468)”. There were 97 proteins that were down-regulated and 67 proteins that were up-regulated by gigantol associated with protein phosphorylation as listed in Table 5.

**Table 5.** List of genes involved with protein phosphorylation and differentially regulated by gigantol treatment in H460 lung cancer cells.

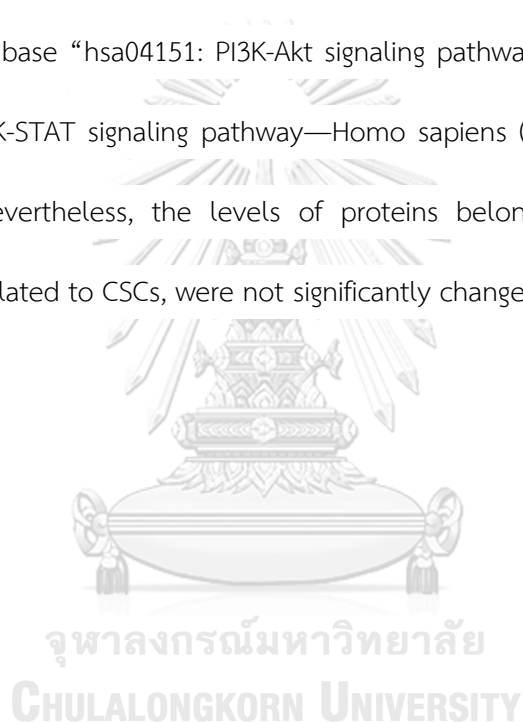
Down-regulated genes	Up-regulated genes
<p><i>MYLK4, IGF1R, RPS6KA4, LIPE, AKT2, CHEK1, PIM1, NEK2, PIM2, NEK3, PSKH1, PRKCG, CDKL2, CDKL3, PDGFRA, MORC3, CDKL5, DAPK1, EPHA8, DAPK3, ADAM10, VRK2, PRKAB1, CDC25B, DGKQ, ULK3, BTK, ALPK3, SIK2, TXK, WNK4, PIK3R4, PRKCZ, GRK1, NUAK2, IRAK2, MARK4, MARK1, CDK17, PLK4, NEK7, DCLK2, PTK2, CLK3, CDK9, CDK8, BMP2, FES, WNK2, CDK12, CDK13, CDK14, MAP3K11, ALK, SMG1, DYRK3, FLT4, MAST1, PIK3CD, IKBKB, TLK2, TLK1, JAK2, JAK3, JAK1, KSR1, TGFBR3, HCK, LATS2, PIK3CA, MYO3A, BIRC6, SGK3, TLR4, PRKAA2, CAMKK2, PHKG1, ERBB4, ERBB2, PTK2B, RICTOR, MAPK6, CAMK2G, MAP4K4, NTRK2, GTF2H1, CDC42BPA, MAPK15, MTOR, HIPK2, SBK1, TAOK3, CAMK4, STK17B, NEK10, ATP13A2, CSNK1A1L</i></p>	<p><i>CCNT1, MAST3, STK19, PIK3CB, PPP4R1, FASTK, RPS6KA2, AKT1, PDK3, PIM3, EPHB4, MAP3K5, MUSK, MINK1, PRPF4B, PASK, BAZ1B, MASTL, ERN1, LATS1, MELK, KIT, BMP2K, TLR9, BIRC5, ULK2, PRKD1, CSNK1G2, EPHA3, TLR3, DDR2, BRSK1, NIM1K, LTK, PNCK, PKN3, ROCK2, STK39, STK4, STK3, AURKA, MAPK8, IRAK1, STK36, ABL1, MAP3K20, ABL2, MAP3K21, MAPK1, FNIP2, PAK2, MAP3K3, INSR, LIMK1, ELP1, EIF2AK4, CDC42BPB, SNRK, TEC, ABI2, CDK2, CDK10, PKN2, PTPN6, TEK, CDK15, BMPR1A</i></p>

The 97 proteins that were down-regulated and 67 proteins that were up-regulated in gigantol-treated cells obtained from the GO term “protein phosphorylation (GO: 0006468)” were separately input to the STRING software (conducted on 8 October 2019). The resulting networks were presented (Figure 24A and 25A), and the hub proteins were determined. The top 10% of the down-regulated proteins that had the highest number of protein interactions were MTOR, PIK3CA, JAK1, JAK2, PIK3CD, ERBB2, CHEK1, IGF1R, PTK2, ALK, and JAK3. Whereas, the top 10% of the up-regulated proteins that had the highest number of protein interactions were AKT1, MAPK1, ABL1, MAPK8, CDK2, and PAK2.

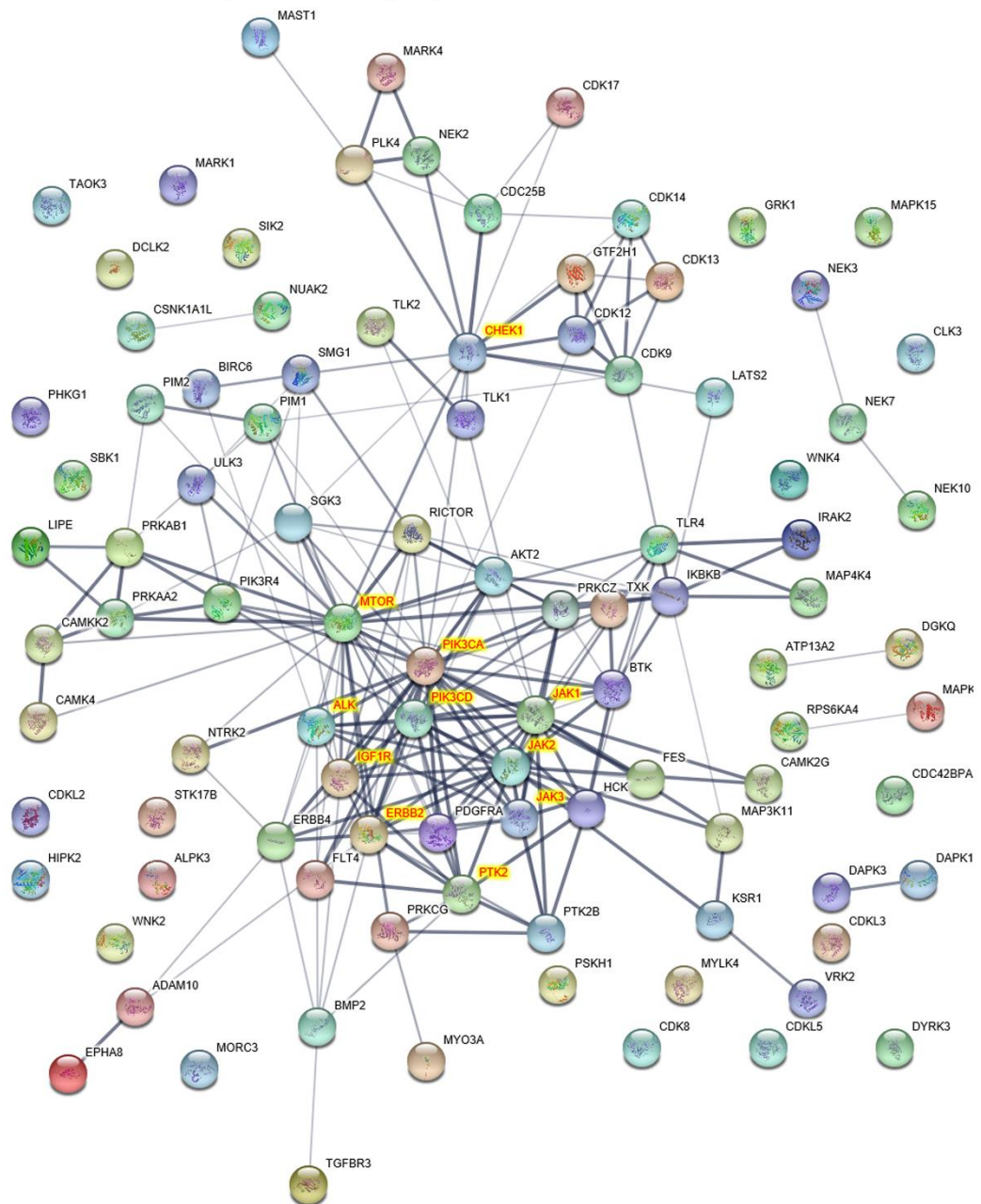
The hub proteins of both down- and up-regulated proteins were then analyzed for the pathways involved in CSCs using STRING. According to the Kyoto Encyclopedia of Genes and Genomes (KEGG) pathways database (<https://www.genome.jp/kegg/>), the enriched signaling pathways that enriched among the hub proteins that were down-regulated by gigantol treatment primarily were the PI3K/Akt and JAK/STAT signaling pathways (Figure 24B). These pathways were indicated as signaling pathways regulating the pluripotency of stem cells. Whereas, the hub proteins of the up-regulated proteins were related to the ErbB signaling pathway (Figure 25B). Interestingly, gigantol down-regulated two major signaling pathways involved in CSC-like phenotype, including PI3K/Akt and JAK/STAT pathways, but did not up-regulated the signaling pathways related to CSC maintenance.

To confirmed that the target pathways of gigantol were crucial for CSC maintenance, the list of proteins involved in CSC regulation was extracted from the KEGG pathway database, using the term “hsa04550: Signaling pathways regulating pluripotency of

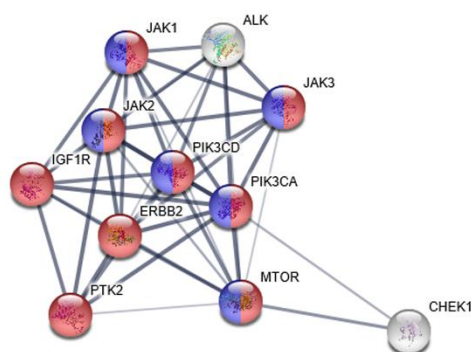
stem cells—Homo sapiens (human)”, and mapped with the H460 proteomic profiles (conducted on 28 October 2019.). In total, 50 proteins were represented in the KEGG pathways, 12 proteins were significantly up-regulated, 20 proteins were significantly down-regulated, and 18 proteins were not significantly altered by gigantol (Figure 26). Remarkably, the down-regulated proteins affected by gigantol were mostly linked to the PI3K/Akt and JAK/STAT pathways (protein lists of the two pathways were obtained from KEGG pathway database “hsa04151: PI3K-Akt signaling pathway—Homo sapiens (human)” and “hsa04630: JAK-STAT signaling pathway—Homo sapiens (human)”; conducted on 28 October 2019.). Nevertheless, the levels of proteins belonging to the Wnt pathway, another pathway related to CSCs, were not significantly changed.



A Hub proteins are highlighted at the center of the network



B



Signaling pathways enriched in down-regulated hub proteins:  
 Red node = PI3K/Akt signaling pathway  
 Blue node = JAK/STAT signaling pathway

**Figure 24.** (A) Networks presenting the functional protein-protein interactions of the 97 down-regulated proteins related to the GO term “protein phosphorylation” (GO:0006468). The 11 hub proteins are identified and highlighted with red font and yellow edge. (B) PPI network of 11 hub proteins. According to the KEGG pathways database, PI3K-Akt signaling pathway (hsa04151) and JAK-STAT signaling pathway (hsa04630) were enriched in the network.





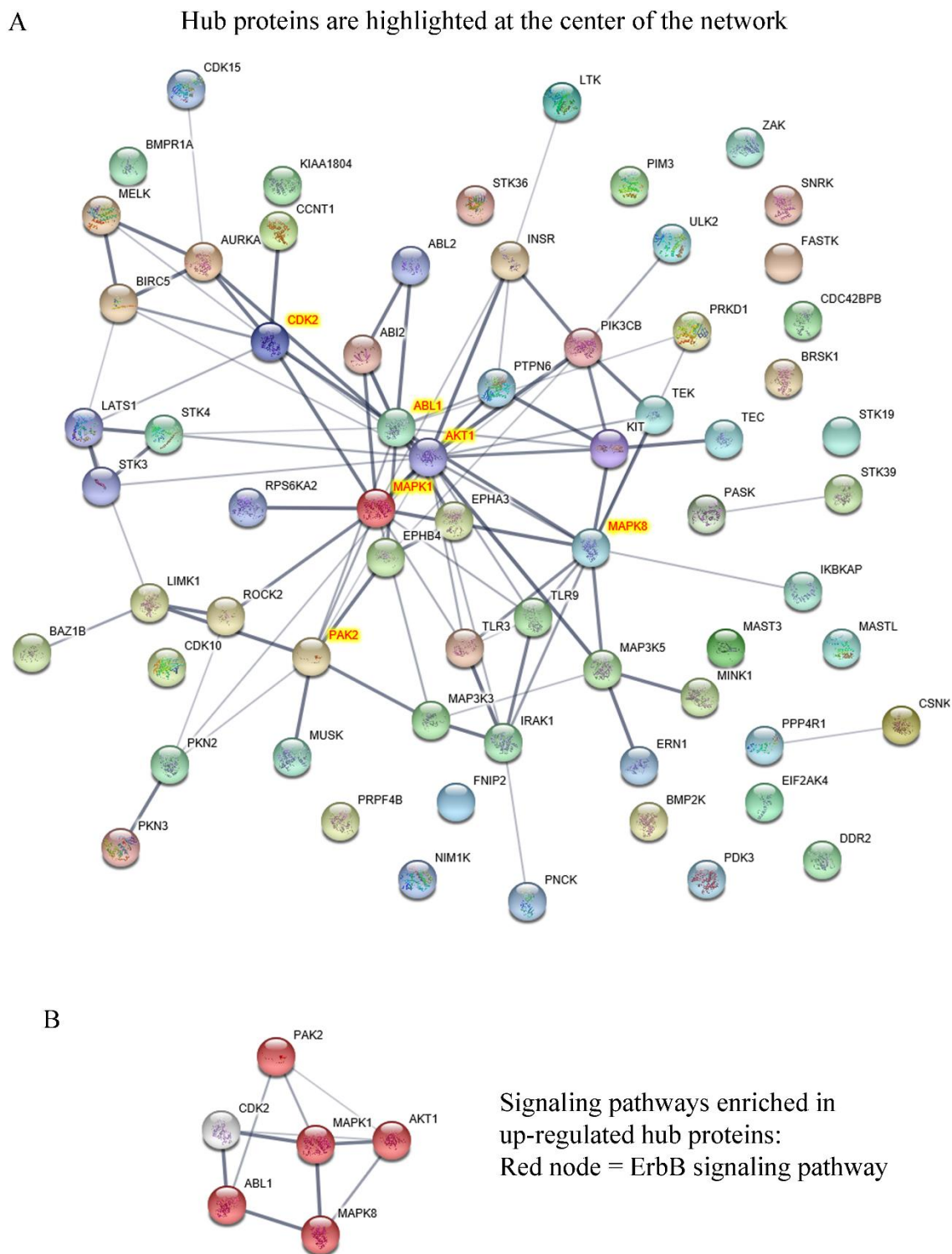


**Figure 25.** (A) Networks presenting the functional protein-protein interactions of the 67 up-regulated proteins related to the GO term “protein phosphorylation” (GO:0006468). The 6 hub proteins are identified and highlighted with red font and yellow edge. (B) PPI network

of 6 hub proteins. According to the KEGG pathways database, ErbB signaling pathway (hsa04012) were enriched in the network.

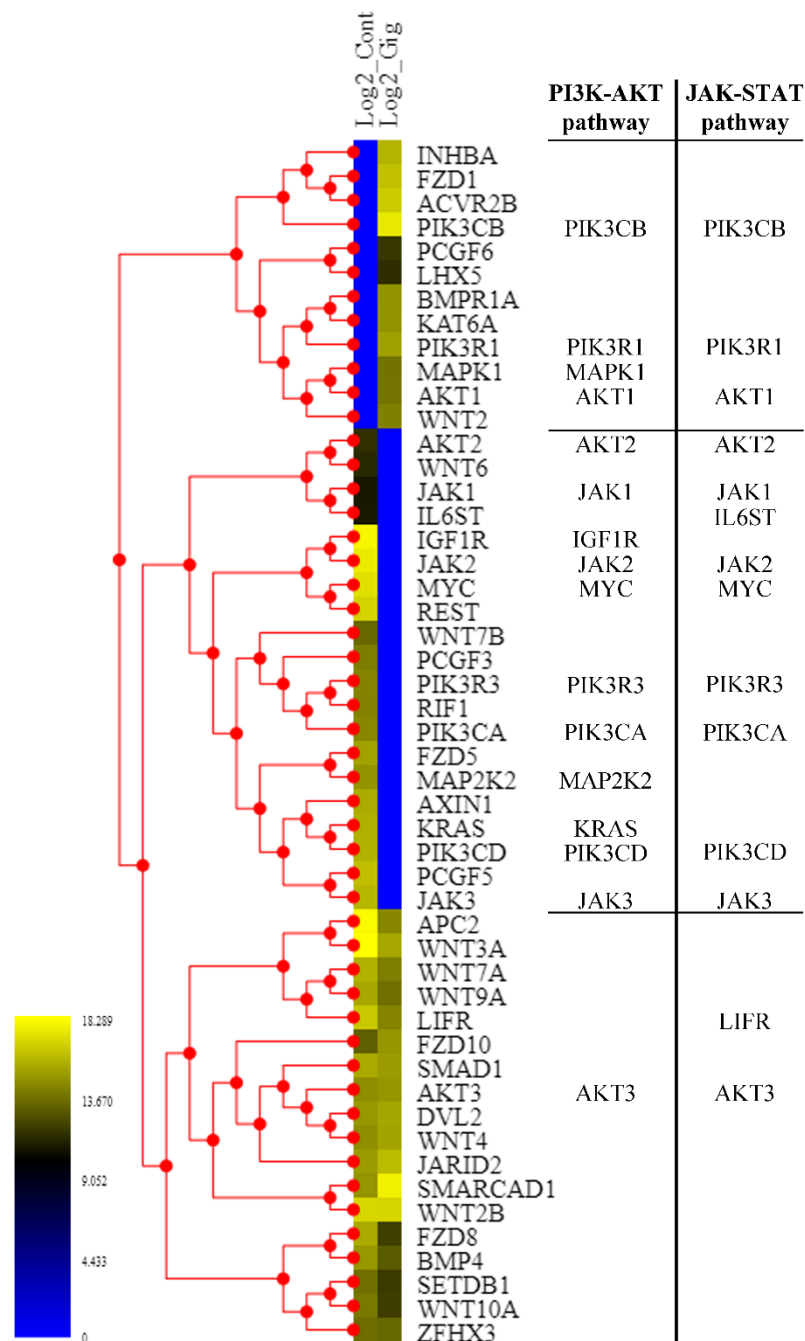


**Figure 26.** Heatmap representing the levels of proteins associated with the signaling pathways regulating the pluripotency of stem cells in the control and gigantol-treated

H460 cells (left and right columns of the heatmap, respectively). Proteins belonging to PI3K/Akt and JAK/STAT pathways are listed to the right.

## 1.2 Validation of key signal proteins of the CSC-related pathways affected by gigantol

To confirm, the key proteins of PI3K/Akt and JAK/STAT pathways including Akt, phosphorylated Akt (Ser473), STAT3, phosphorylated STAT3 (Ser727), and CSC markers were determined by Western blot analysis using the same cell population of proteomics and xenograft experiments. The band density of active form of Akt (phosphorylated Akt) and active STAT3 (phosphorylated STAT3) was normalized with their own total forms in order to determine the levels of activation. The results showed that gigantol could inhibit the activation of Akt and STAT3. In addition, the CSC makers (CD133 and ALHD1A1) were found to be significantly reduced in response to gigantol treatment (Figure 27A and 27B).

Moreover, the effect of gigantol on PI3K/Akt, JAK/STAT, and CSC markers was confirmed in other lung cancer cells, A549 and H292 (Figure 28A and 28B). The results showed that the CSC markers, as well as, the activation of Akt and STAT3 were decreased by gigantol in a dose-dependent pattern in all tested cells. It was quite clear that the PI3K/Akt and JAK/STAT signaling pathways were the target pathways of gigantol on CSC maintenance in NSCLCs.

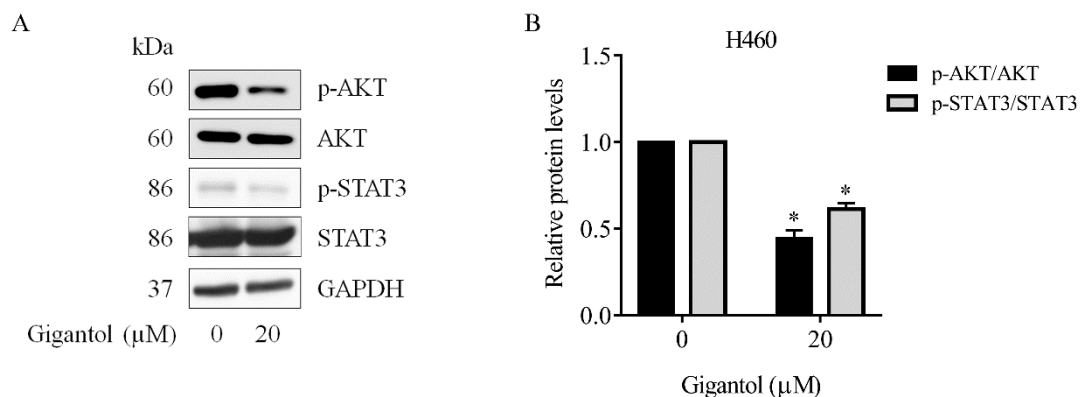


**Figure 27.** (A) The H460 cell lysates used in proteomics analysis were validated for protein levels of phosphorylated Akt (Ser473) and phosphorylated STAT3 (Ser727), the active forms of key kinases of PI3K/Akt and JAK/STAT3 pathways, and their total forms by Western blot analysis. (B) the immunoblot signal intensities were quantified by densitometry. Data represent means  $\pm$  SD. (\*  $p < 0.05$  as compared with the control group,  $n = 3$ ).

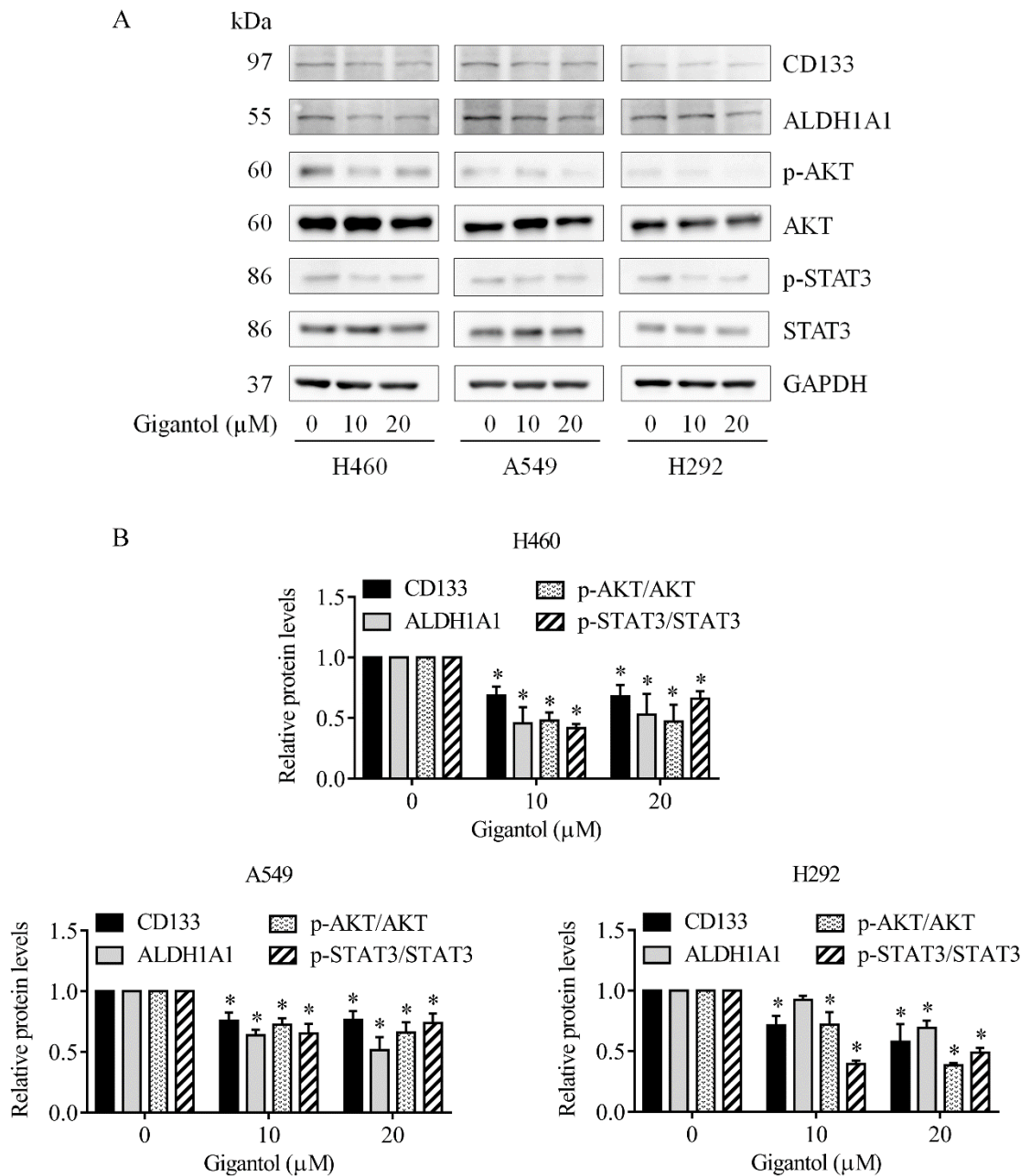


**Figure 28.** (A) The effects of gigantol on Akt, STAT3, and CSC markers were determined in other two lung cancer cell lines, A549 and H292 using Western blot analysis. (B) the relative protein levels were quantified. Data represent means  $\pm$  SD. (\*  $p < 0.05$  as compared with the control group,  $n = 3$ ).

## 2. Investigation on regulatory mechanisms of gigantol on lung cancer cell proliferation

### 2.1 Determination of effects of gigantol on proliferative signals using proteomics data

Having shown that gigantol negatively regulates proliferation of lung cancer cells, the key underlying mechanisms were next identified using proteomic analysis. The analysis process of the H460 proteomics data was demonstrated as a flowchart in Figure 29. The analysis identified 1,767 proteins that were up-regulated and 2,373 proteins that were down-regulated in gigantol-treated versus control cells. The proteins with differential expression were analyzed by the enrichment analysis tool, Enrichr (conducted on 27 April 2020). The GO annotations based on GO Consortium database were investigated and it was found that the GO termed “regulation of cell proliferation (GO:0042127)” was the meaningful GO annotation associated with regulatory signaling of cell proliferation. Gigantol altered the expression of 156 proteins involved in the regulation of cell proliferation, which were 96 down-regulated proteins and 60 up-regulated proteins, as listed in Table 6. Subsequently, the hub proteins were clarified.

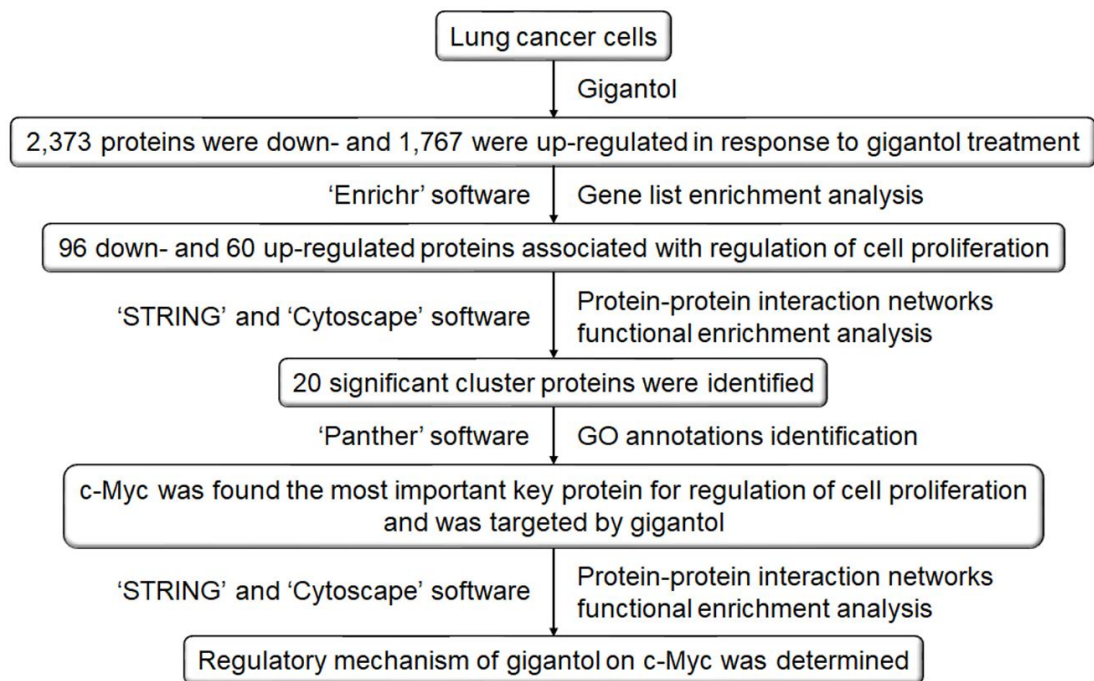


**Figure 29.** The flowchart showed bioinformatic analysis process of proteomic profiles obtained from the untreated and gigantol-treated lung cancer cells.

**Table 6.** List of genes associated with regulation of cell proliferation and differentially regulated by gigantol treatment in H460 lung cancer cells.

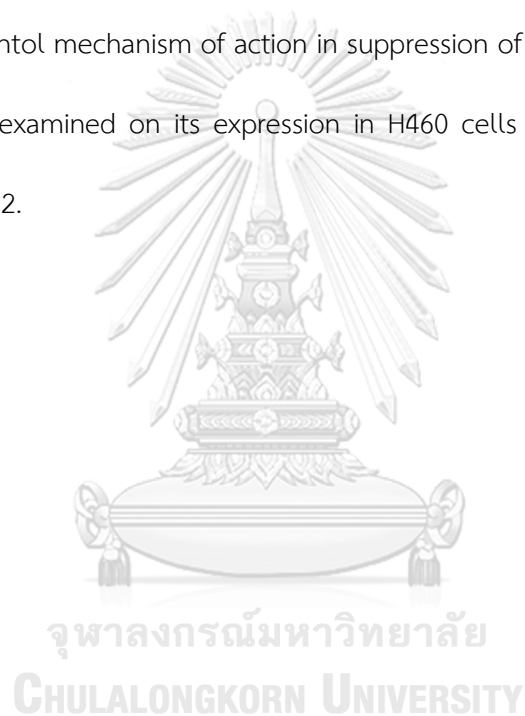
Down-regulated genes	Up-regulated genes
<p><i>COL18A1, TES, ATP8A2, BNC1, FLT4, PINX1, AKR1B1, ADRA1D, CTCF, PTPRK, ADRA1A, FGF3, IGF1R, MYC, AKT2, PIM2, CAPN1, JAK2, ARID2, JAK3, RBM5, JAK1, ENPP7, PDGFRA, TIPIN, PRMT1, MAGI2, P3H1, ADAM10, TSC1, GAB2, NCCRP1, TMEM250, GTPBP4, ADRA2A, CDC25B, HCK, COL4A3, BTK, RAPGEF2, HCLS1, BIRC6, SGK3, NUPR2, ARHGEF2, IL6ST, HDAC4, HDAC2, ZBTB49, TXK, CUL2, NOP2, DLL1, RELA, TBRG4, PKHD1, ERBB4, PDGFD, SH3BP4, PTK2B, UTP20, STX3, ZNF268, TCFL5, JAG2, NTRK2, EGLN3, XRCC6, JUP, NOS3, IL31RA, TNFRSF10B, SMAD6, PTPN14, ST18, PTK2, TNFRSF10D, BMP5, CUL4A, MLXIPL, GDF9, BMP2, REST, AGO3, BCL6, DLG3, PRC1, FES, WNK2, DLC1, STRN, KRAS, CDK13, BAP1, EIF4G1, MXD4</i></p>	<p><i>PTPRU, TENM1, CDCA7L, CHD5, BRCA1, PKD2, PPP1R9B, MECP2, UFL1, ADAMTS1, ADORA3, RPS6KA2, NAMPT, CHP2, AKT1, KCNH1, EDN1, GNL3, SSTR5, TIAM1, IL1A, ADAM17, GAREM1, ADGRB1, KIT, BIRC5, IRF6, KIF20B, BLK, CEBPA, HDAC1, TNFRSF11B, TTK, THBS1, PRDX3, MNT, SCIN, PDGFC, ABL1, ABL2, WNT2, STOX1, TRPM4, EGF, CNBP, INSR, FN1, VEGFD, CDC6, INHBA, TBX2, TEC, CCPG1, DNAJA3, DLG5, CDK2, CDK10, PTPN6, NOX1, BMPR1A</i></p>

## 2.2 Gigantol targets c-Myc in lung cancer cells.

To justify the most important hub protein that controlled cell proliferation, the differentially expressed proteins were subjected to protein-protein interaction (PPI) networks functional enrichment analysis using STRING (Figure 30; conducted on 27 April, 2020), and the number of PPIs was analyzed using the function ‘network analyzer’ of Cytoscape software. The top 20 proteins that had the highest interactions with other proteins in the network were determined, namely AKT1, MYC (or c-Myc), FN1 (or fibronectin), EGF, KRAS, JAK2, KIT (or c-KIT), BRCA1, HDAC1, IGF1R, JAK1, ABL1, CDK2, NOS3



(or eNOS), PTK2 (or FAK), HDAC2, ERBB4, BMP2, PDGFRA, and INSR (Figure 30). Then, their molecular functions were determined from GO annotation using Panther software (conducted on 27 April 2020). The analysis result revealed that, among these candidates of gigantol's target, c-Myc had the most abundant protein-protein interactions in the network (> 50 PPIs) and was down-regulated by gigantol (Figure 31). Besides, it was the only one that had a transcription factor activity (Table 7 and 8). This result suggested that c-Myc was a key player of gigantol mechanism of action in suppression of cell proliferation. Therefore, c-Myc was further examined on its expression in H460 cells and other two lung cancer cells, A549 and H292.



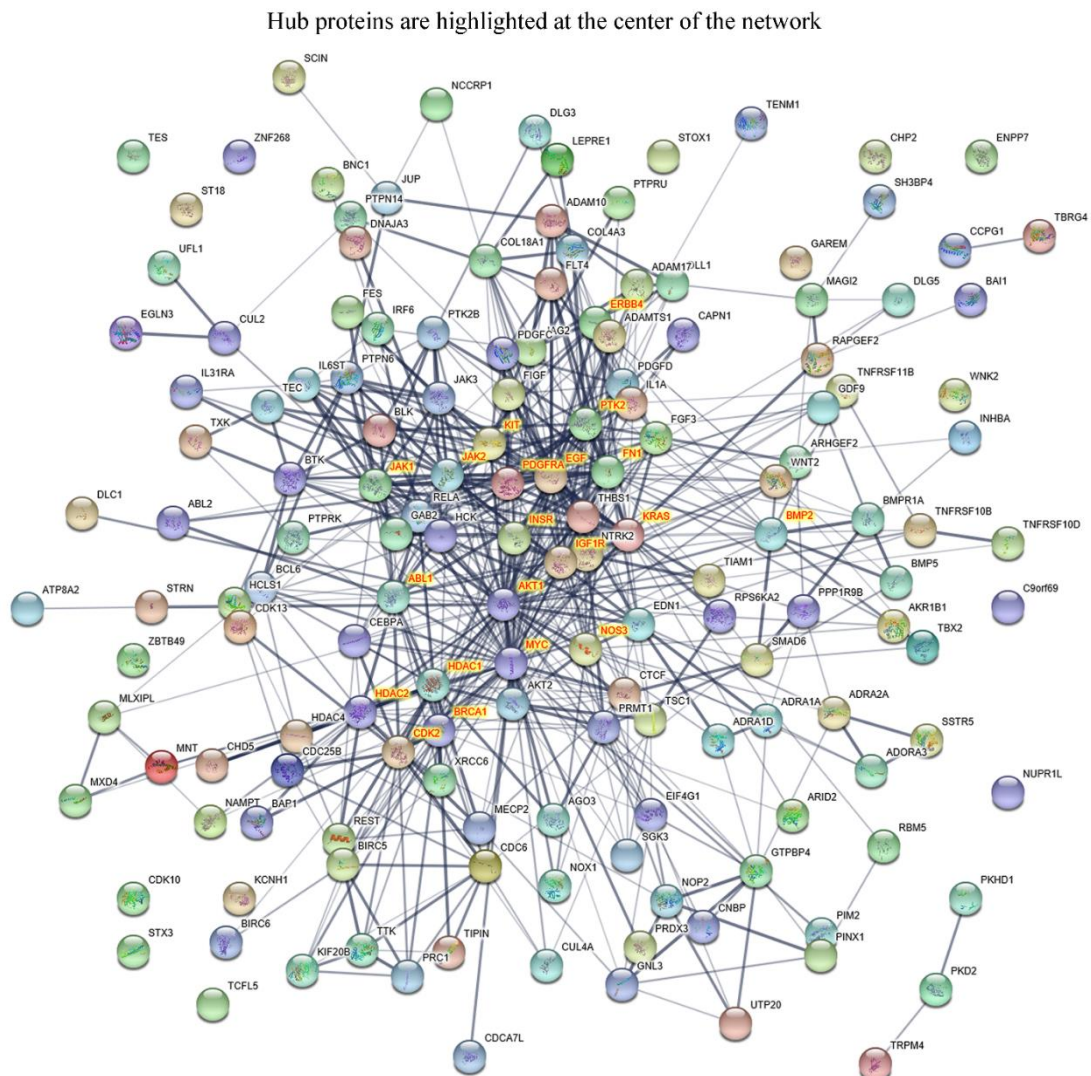


**Figure 30.** The protein-protein interaction network of the differentially expressed proteins demonstrated relationship between the 156 proteins associated with regulation of cell proliferation. Located in the center of the network, the proteins of which gene names were highlighted with red font and yellow edge were the top 20 proteins with the highest number of PPIs.

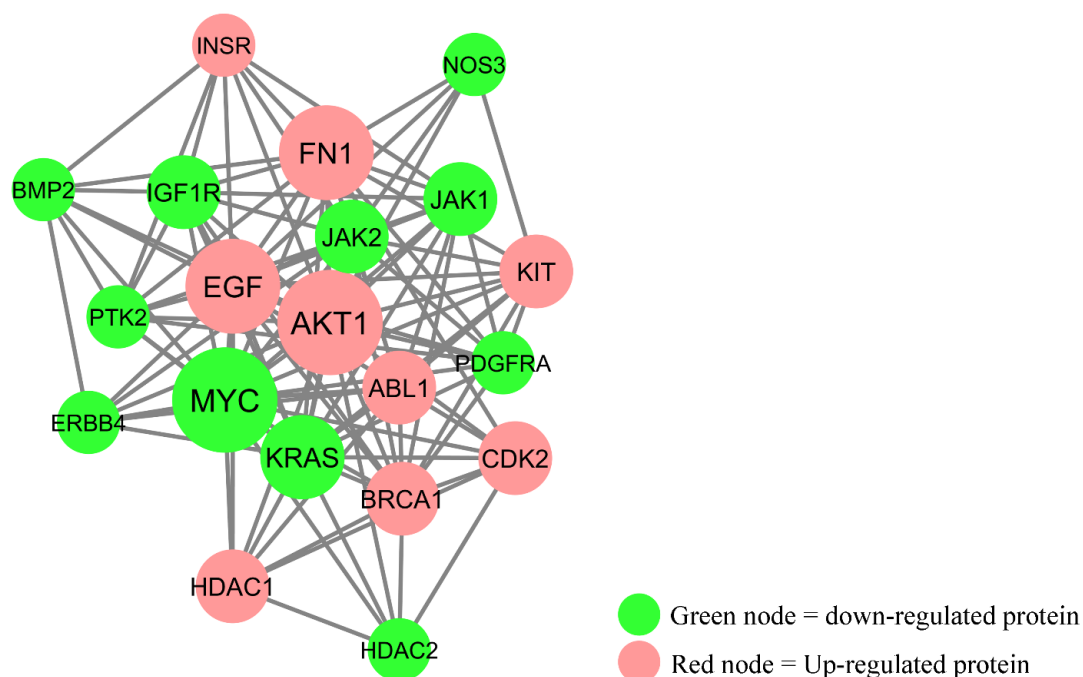


**Figure 31.** PPI network of 20 hub proteins demonstrated regulation status and significance level of the proteins. The bigger node means the higher PPI numbers.

**Table 7.** Hub proteins that controls cell proliferation which were down-regulated by gignatol treatment in H460 lung cancer cells.

Gene name	Molecular functions
MYC	transcription regulator activity; binding
KRAS	catalytic activity; binding
JAK2	catalytic activity; binding
IGF1R	molecular transducer activity; catalytic activity; binding
JAK1	catalytic activity; binding
NOS3	catalytic activity; binding
PTK2	catalytic activity; binding
HDAC2	catalytic activity
ERBB4	catalytic activity; binding
BMP2	molecular function regulator; binding
PDGFRA	molecular transducer activity; catalytic activity; binding

**Table 8.** Hub proteins that controls cell proliferation which were up-regulated by gignatol treatment in H460 lung cancer cells.

Gene name	Molecular functions
AKT1	catalytic activity
FN1	binding
EGF	molecular transducer activity; binding
KIT	catalytic activity; binding
BRCA1	catalytic activity
HDAC1	catalytic activity
ABL1	catalytic activity; binding
CDK2	molecular transducer activity; catalytic activity; binding
INSR	molecular transducer activity; catalytic activity; binding

The proteomic and protein interaction analysis have pointed out that c-Myc was the dominant regulatory protein on cell proliferation in response to gignatol treatment. Then, we confirmed the validity of such protein in gignatol-treated cells. The cells were similarly treated with non-toxic concentrations of gignatol and c-Myc level was determined by Western blot analysis. Figure 32A showed that c-Myc was dramatically decreased in response gignatol treatment. Gignatol at 10 and 20  $\mu\text{M}$  significantly decreased c-Myc levels in all tested cells, while gignatol at 5  $\mu\text{M}$  significantly decreased c-Myc levels of H460 and A549 cells (Figure 32B). In total, gignatol suppressed c-Myc expression in a dose-dependent manner. This result confirmed that gignatol down-regulated c-Myc protein in lung cancer cells.

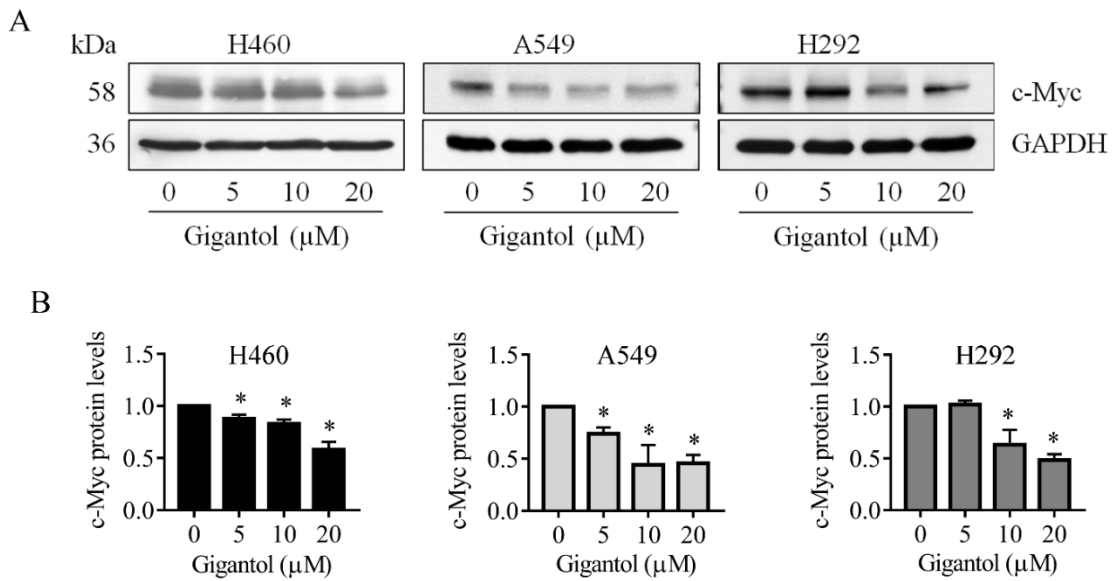


**Figure 32.** (A) Lung cancer cells were treated with gigantol 0-20  $\mu\text{M}$  for 24 hours. Western blot analysis was performed for determined c-Myc levels. GAPDH levels were used to confirm equal loading of each protein sample. (B) The band intensities of treatment groups were compared to the control group and present as fold-change. Data represented mean  $\pm$  SD (\*  $p < 0.05$ , compared with the untreated control,  $n = 3$ ).

### 2.3 Gigantol suppresses c-Myc through an inhibition of GSK3 $\beta$ phosphorylation.

Having shown that gigantol inhibit cell proliferation via c-Myc suppression, the underlying mechanisms of c-Myc protein level modulation were next verified. Figure 33 demonstrated a curated pathway of c-Myc regulation. Well-established evidences revealed that cellular c-Myc is regulated mainly via ubiquitin-proteasomal degradation and the phosphorylation at Thr58 by GSK3 $\beta$  was prerequisite for c-Myc ubiquitination. However, GSK3 $\beta$  function was regulated via phosphorylation at Ser9. Once GSK3 $\beta$  was

phosphorylated and became inactivated, c-Myc protein was more stable and the cellular c-Myc level was increased, resulting to cell proliferation (12). Therefore, the activation status of GSK3 $\beta$  was further investigated by Western blot analysis. Cells were treated with gigantol 0-20  $\mu$ M for 24 h and whole cell lysates were harvested. The levels of phosphorylated and total forms of GSK3 $\beta$  were validated. Western blot results showed that gigantol at 5-20  $\mu$ M significantly decreased the level of inactive GSK3 $\beta$  (phosphorylated GSK3 $\beta$  at Ser9), but rarely affected the total form of GSK3 $\beta$  in all tested cells (Figure 34A). The ratio of relative protein levels of p-GSK3 $\beta$  versus GSK3 $\beta$  was calculated to justify the inactivation level of GSK3 $\beta$  (Figure 34B). The ratios indicated that GSK3 $\beta$  inactivation was significantly reduced by gigantol in a dose-dependent manner. This result suggested that the increase of c-Myc degradation was triggered by surge of active GSK3 $\beta$ .

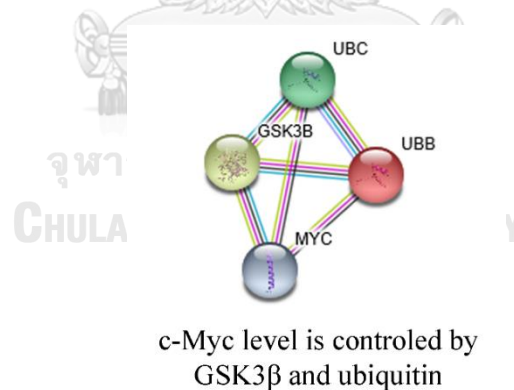


**Figure 33.** PPI network from curated data showed relationship between c-Myc, GSK3 $\beta$ , and ubiquitin.

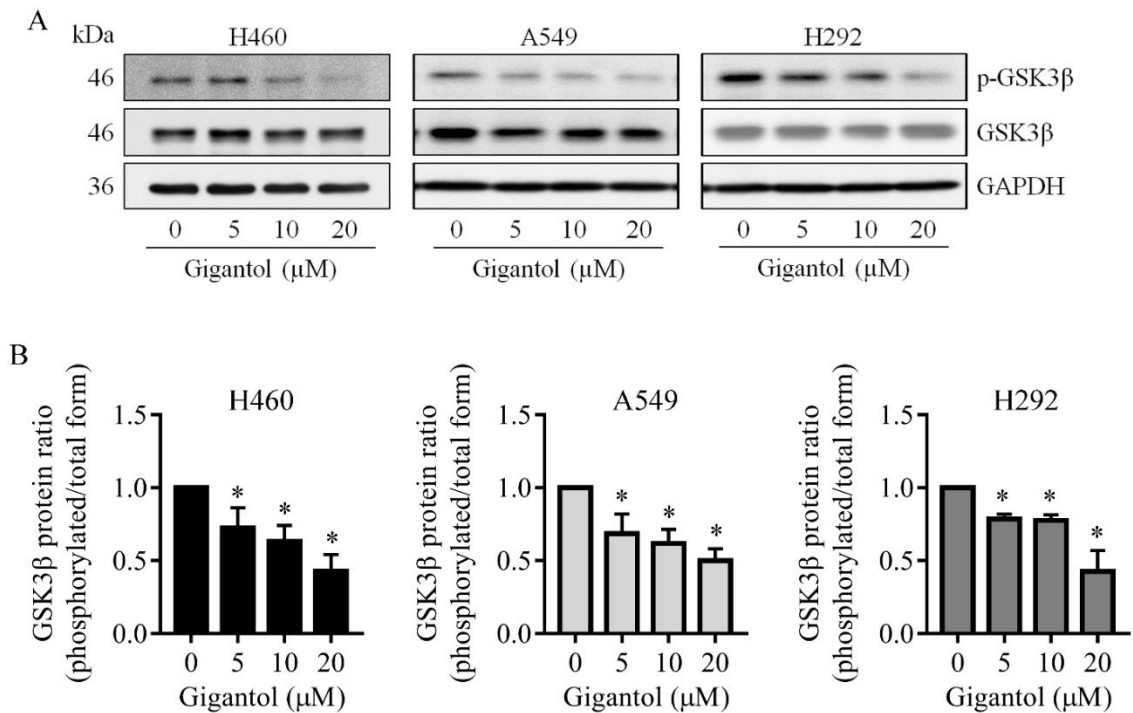


**Figure 34.** (A) Western blot analysis was performed to determine the protein levels of phosphorylated (Ser9) and total form of GSK3 $\beta$ . GAPDH levels were used to confirm equal loading of each protein sample. (B) The band intensities of treatment groups were compared to the control group and presented as fold-change. Data represented mean  $\pm$  SD (\*  $p < 0.05$ , compared with the untreated control,  $n = 3$ ).

#### 2.4 Gigantol destabilized c-Myc via ubiquitination facilitated proteasomal degradation.

Next, gigantol-induced c-Myc degradation was proved using cycloheximide chasing assay. Gigantol at the concentration of 20  $\mu$ M was used in this assay for it reduced more c-Myc protein level compared to the 5 or 10  $\mu$ M. Western blot analysis result showed that gigantol significantly decreased c-Myc protein level at time 15, 30, 45, and 60 minutes after the treatment compared to their untreated control at the same time points in all tested

cells (Figure 35A and 35B). The c-Myc half-life was calculated from an equation obtained from a regression curve. The c-Myc half-lives of untreated H460, A549, and H292 cells were  $44.30 \pm 7.58$ ,  $38.63 \pm 3.75$ , and  $38.52 \pm 7.45$  minutes, while the half-lives of gigantol-treated H460, A549, and H292 cells were  $26.41 \pm 3.24$ ,  $26.55 \pm 2.69$ , and  $26.73 \pm 3.06$  minutes, respectively (Figure 35C). This data indicated that gigantol reduced c-Myc half-life significantly.

To prove that this decrease in c-Myc stability was through proteasomal degradation of the protein, we utilized MG132, a potent selective proteasome inhibitor. The lung cancer cells were pretreated with MG132 0-20  $\mu\text{M}$  for 1 hour and then were left untreated or treated with gigantol for 1 h. The treatment of all concentrations of MG132 drastically increased the c-Myc level, which confirmed that c-Myc protein was degraded mainly through proteasomal degradation pathway (Figure 36A and 36B). Treatment of the lung cancer cells with gigantol for 1 h significantly decreased c-Myc level, while the pretreatment of MG132 (5–20  $\mu\text{M}$ ) reversed an effect of gigantol on c-Myc down-regulation (Figure 36A and 36B). Taken together, it could be concluded that gigantol induced c-Myc proteasomal degradation.

Then, ubiquitination level of c-Myc was observed using immunoprecipitation and Western blot analysis of the c-Myc-ubiquitin complex (Ub-c-Myc) in the lung cancer cells treated with gigantol and untreated control cells. After pretreating the cells with 10  $\mu\text{M}$  MG132 for 1 h, the cells were left untreated or treated with 20  $\mu\text{M}$  gigantol for another 1 h, the c-Myc protein was selectively isolated from cell lysates by the c-Myc antibody. Then, unwanted proteins were washed out and only c-Myc complex was analyzed for



conjugated ubiquitin through Western blot analysis. Figure 37A and 37B showed that gigantol treatment dramatically enhanced the formation of the c-Myc-ubiquitin complex compared to the baseline complex in untreated controls of all tested cells. This result indicated that the mechanism of action of gigantol was through the induction of c-Myc degradation via ubiquitin-proteasomal degradation.



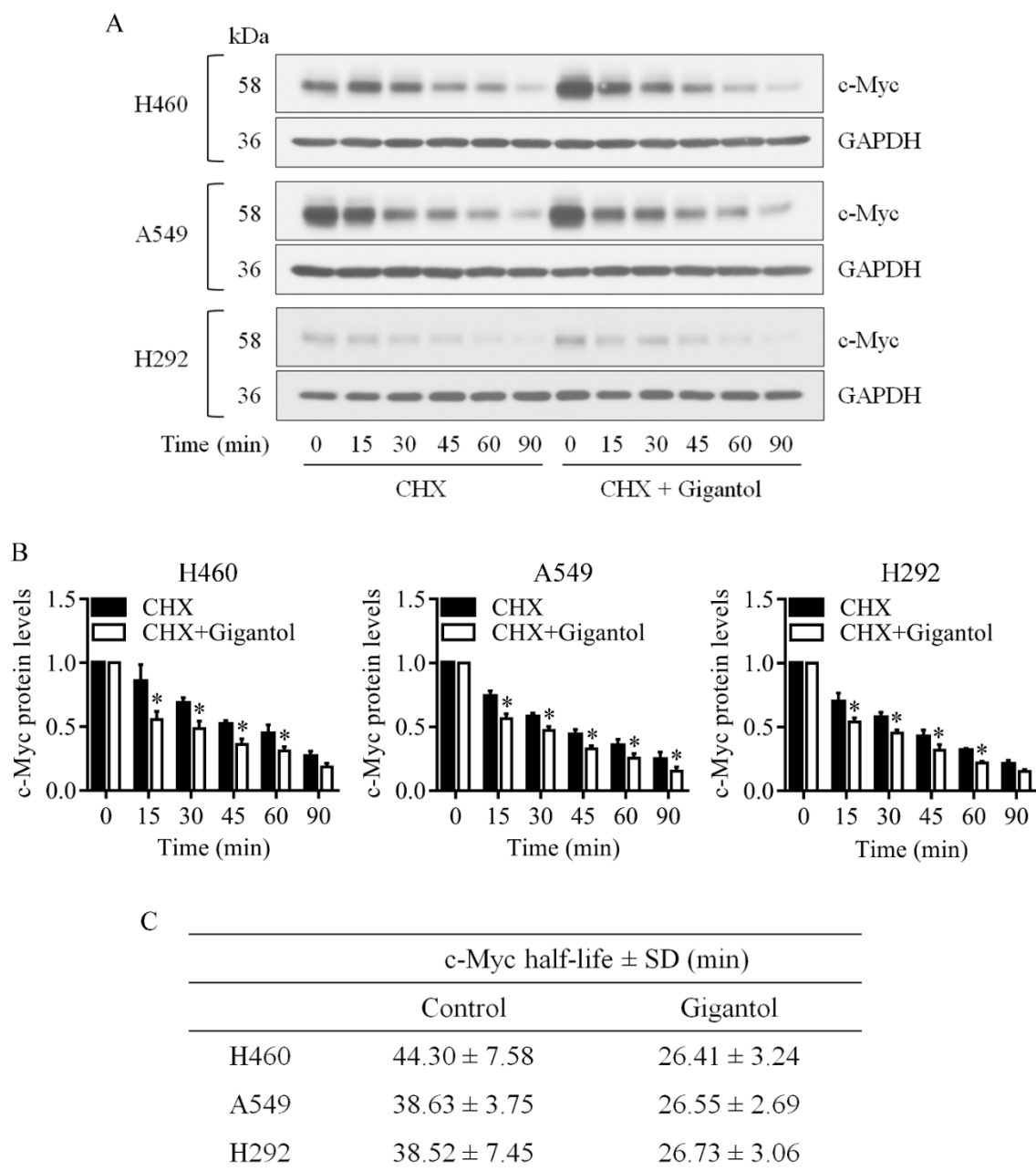


**Figure 35.** Cycloheximide (CHX) chasing assay was performed to measure c-Myc stability. Lung cancer cells were treated with gigantol 20  $\mu$ M with or without 50  $\mu$ g/ml CHX as indicated by the time (minutes). (A) Western blot analysis was performed for determined c-Myc levels. GAPDH levels were used to confirm equal loading of each protein sample. (B) The relative protein levels were calculated by densitometry (\*  $p < 0.05$ , compared with the untreated control at the same time,  $n=3$ ). (C) c-Myc half-lives were calculated.

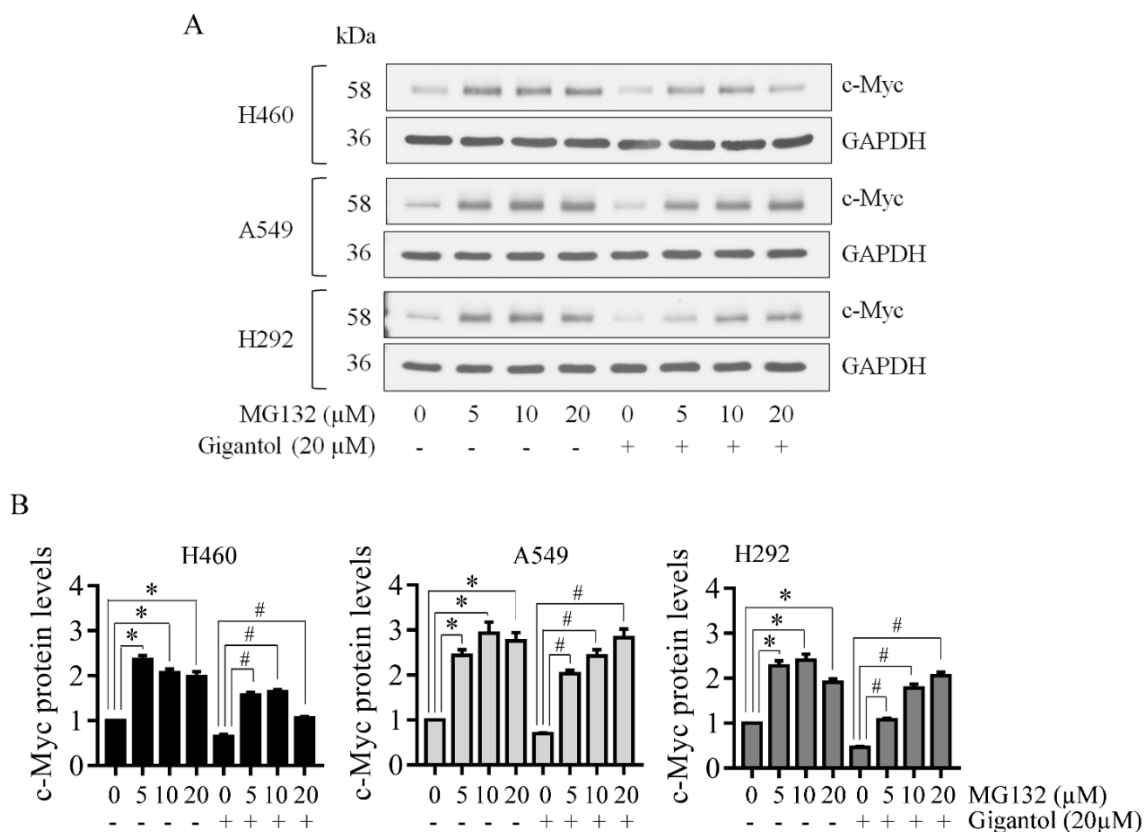


**Figure 36.** (A) Lung cancer cells were treated with MG132 (0–20  $\mu\text{M}$ ) with or without gigantol (20  $\mu\text{M}$ ) for 1 h. c-Myc levels were measured using Western blot analysis. GAPDH levels were used to confirm equal loading of each protein sample. (B) The band intensities were calculated by densitometry compared to the untreated control cells (\*  $p < 0.05$ , compared with the untreated cells, #  $p < 0.05$ , compared with the non-MG132 gigantol-treated cells). All data represented the mean  $\pm$  SD ( $n = 3$ ).

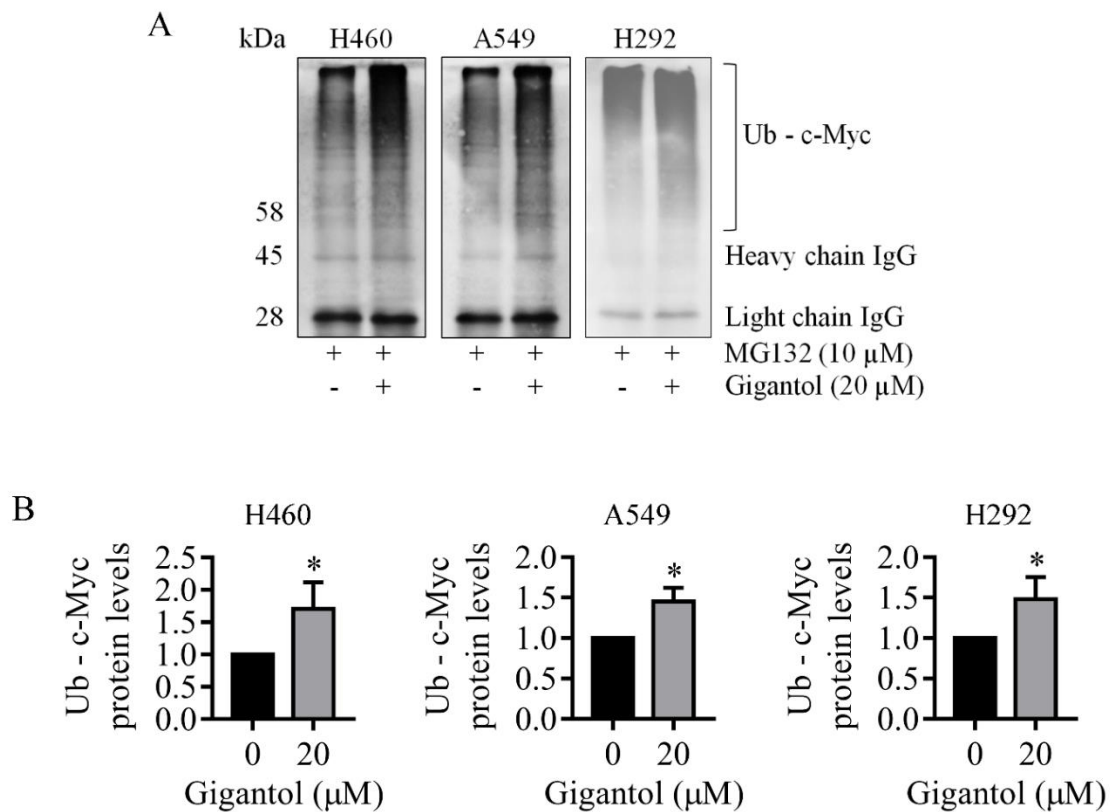


**Figure 37.** (A) Lung cancer cells were treated with MG132 (10  $\mu$ M) with or without gigantol (20  $\mu$ M) for 1 h. Then, protein lysates were collected subsequent to c-Myc immunoprecipitation, and the ubiquitinated protein levels were measured by Western blotting. (D) Ubiquitinated c-Myc (Ub - c-Myc) levels were quantified using densitometry (\*  $p < 0.05$ , compared with the untreated control). All data represented the mean  $\pm$  SD (n = 3).

## CHAPTER V

### DISCUSSION

According to the increasing trend of cancer incidence and mortality, the development of novel anti-cancer therapies is highly needed. Among malignant tumors, lung cancer has been shown to be the main cause of cancer-related mortality and treatment failure (43), leading to the requirement for effective therapeutic options. Previous studies have reported the potential anti-cancer activities of gigantol, one of the most widely studied bibenzyls. Gigantol has exhibited cytotoxicity against various types of cancer cells, such as breast, liver, and lung cancer cells (36, 144, 145). Moreover, gigantol could attenuate certain aggressive phenotypes that bring about tumor progression and metastasis, including proliferation, migration, invasion, anoikis-resistance, and anchorage-independent growth (37-40).

The phenotypes that promote tumorigenicity of lung cancer, including proliferative and CSC-like phenotypes, were studied. Until now, an anti-proliferative effect of gigantol has not been explored. This experiment is in line with abovementioned data and further support the anti-cancer properties of gigantol in suppression of lung cancer cell growth. The non-toxic concentrations were used for an anti-proliferation evaluation. Proliferation assay and colony formation assay were performed. The proliferation assay demonstrated that gigantol reduced the growth rate of total population of lung cancer cells in a dose-dependent manner (Figure 12). Also, the colony formation assay was performed and the colony with > 50 cells (around 7 doubling times) were counted as a normally growing colony. After 10 days of gigantol incubation, the results showed that gigantol decreased

the number of lung cancer cells with a colony formation capacity in a dose-dependent pattern (Figure 13A and 13B). In total, gigantol inhibited lung cancer cells proliferation effectively.

Recent evidence has suggested that CSCs functions as a seed of tumors. Not only do the CSCs use their ability of self-renewal and differentiation for tumor establishing, but also implicate cancer progression, metastasis, and disease relapse (13). Regarding this matter, several previous reports unraveled new information that gigantol could suppress CSC activity and discontinue their role in maintaining tumor (14, 146). This finding is quite in agreement with the previous study indicating that CSCs play a key role in tumor maintenance. This study revealed the effect of gigantol of CSC-like phenotype suppression on the tumor initiation, growth, and maintenance based on the concept that the cells at the first step of tumor initiation had lesser CSC property than the control untreated cells.

In this study, the lung cancer cells were treated with a non-toxic concentration of gigantol prior to inoculation into mice subcutaneous skins. The same populations of gigantol-treated cells were subjected to proteomics. The concept of the *in vivo* xenograft was to compare the ability to form and maintain a tumor between the untreated control and gigantol-treated H460 cells. This experiment revealed the effects of gigantol on the cancer cells whether the CSC or other survival signals were suppressed by the treatment at the time of inoculation. The pretreatment procedure excluded the direct anticancer effect of the compound on the tumor cell after mice implantation. This experimental design displays the clear mechanism of gigantol treatment in attenuation of the stemness and CSC-supportive PI3K/Akt/mTOR and JAK/STAT3 signals at the time of tumor initiation

(Figure 14 and 27). Although this experiment used only a single treatment with low dose, gigantol could slightly inhibit the tumor growth rate (Figure 16B). Tumors from the gigantol-pretreated cells had lower weights and volumes compared to the controls (Figure 17B and 17C). The tumor densities were calculated in order to confirm that the tumor weight correlated to its volume. The results revealed that the tumor densities of the gigantol group were also lower than the control group (Figure 18). This result raised an assumption that there would be some loss of tumor mass in gigantol tumor group. Thus, the histological tumor integrity was determined. Previous studies have either demonstrated or proposed that the tumor density can be a promising assessment of anti-cancer drug evaluation as they have given more accuracy on the assessment of an anti-cancer drug response and have contributed to better treatment outcomes (142, 143, 147). The cross-sectional histology of the tumors was observed to assess the integrity of intact cell viable areas as compared with the cell death areas as recommended in the guideline (148). Interestingly, the results indicated that most of the gigantol-treated tumors had a dramatic loss of tumor mass as compared with those of the untreated controls (Figure 19). Consistently, the intratumor structure and tumor phenotype of Ki-67 labeling showed that the gigantol-treated tumors had lower proliferative cancer cells (Figures 20). However, the EMT properties of cancer cells observed by  $\alpha$ -SMA staining was not altered by treatment with gigantol (Figure 21A). Also, the angiogenic capability of both groups of tumors was not different (Figure 21B). The phenotypic observation revealed that the pretreatment with gigantol did not have an effect on tumor neoangiogenesis. Further investigation on gigantol-mediated stromal cell-induced angiogenesis is thus suggested.

This *in vivo* experiment was designed in a manner of a pharmacological study that minimized the confounding factors in the system and focused on the effect of gigantol on the cancer cells. It could assume from the results that gigantol treatment altered the tumor-promoting activities of the cells prior to the process of tumor inoculation and such alteration attenuated the ability of the cancer cell to grow and maintain a tumor, resulting in a reduced tumor mass with viable cancer cell loss. Lung cancer cell line used for an evaluation on CSC suppression of gigantol was NCI-H460, which is the metastatic lung adenocarcinoma cell. Generally, the standard control cells with CSC-enriched population and the cell population with low stemness profile should be included in the study to confirm an importance of CSC in tumorigenicity and validate the tumor morphologies between the two groups. However, the standard controls were not performed in this study because it is well-established that original population of H460 cells consisted of a high proportion of CSCs. Previous studies demonstrated that the proportion of CSC (CD133-positive or ALDH-high) was around 1-3 % in H460 cell line (149). Although the results helped us scope the direct action of the compound on lung cancer cells, further investigation is necessary, including the injection of the substance into a tumor or animal after tumor formation to gain more insights.

Then, the underlying mechanisms of gigantol that suppressed cell proliferation, tumor formation, and cancer stemness were investigated utilizing proteomics technique and bioinformatics analysis. The down- and up-regulated proteins from the gigantol-treated cells were subjected to an enrichment analysis using Enrichr software in order to screening for the most affected biological processes associated with cellular signaling. The



enrichment analysis results in Table 4 revealed that the top 10 biological processes associated with the down- and up-regulated proteins mainly involved in protein or DNA synthesis (regulation of cellular macromolecule biosynthesis process; regulation of nucleic acid-templated transcription; regulation of transcription, DNA-templated; regulation of gene expression; ribosomal large subunit biogenesis; cyclic purine nucleotide metabolic process; nucleotide biosynthesis process; DNA replication checkpoint; RNA splicing, via transesterification reactions with bulged adenosine as nucleotide; regulation of mRNA processing; mRNA processing) and protein phosphorylation (protein phosphorylation; phosphorylation; protein autophosphorylation). The biological process that related to cellular signaling should be the protein phosphorylation, which enriched in both down- and up-regulated proteins. Therefore, the proteins listed in this term were subjected for further analysis for the involved signaling pathways (Table 5).

The hub proteins, also known as the significant nodes, were identified as the top 10% of the proteins with the highest PPIs. The down- and up-regulated significant proteins associated with protein phosphorylation were performed an enrichment analysis again using KEGG pathways database by STRING software in order to clarify the enriched pathways. The results showed that the signaling pathways enriched in down-regulated significant proteins were PI3K/Akt and JAK/STAT pathways, while the signaling pathway enriched in up-regulated significant proteins was ErbB pathway (Figure 24B and 25B).

Bioinformatics analysis demonstrated that PI3K/Akt/mTOR and JAK/STAT were among the most affected proteins in response to gigantol treatment. The key kinase signals belonging to the PI3K/Akt/mTOR axis, including phosphoinositide 3-kinases (PI3Ks,  $\alpha$  and  $\delta$

isoforms) and mammalian target of rapamycin (mTOR), were significantly decreased in the gigantol-treated cells (Figure 24A). Both isoforms of PI3K can activate phosphatidylinositol (3,4,5)-trisphosphate (PIP3), an upstream activator of Akt (150). In addition, PI3K can trigger an Akt-independent mechanism, which transduces signals through serine/threonine-protein kinase Sgk3 (SGK3) and mTOR complex 2 (mTORC2), of which principle downstream targets were SGK1 and PKC (151). The activation of mTORC2 promotes cell survival, proliferation, mobility and metabolism (152). Consistently, the proteomic results showed the suppression of key proteins of the PI3K-mediated Akt-independent pathway, such as PIK3CA, PIK3CD, SGK3, MTOR, and RICTOR, which were simultaneously down-regulated (Figure 24A).

Janus kinase 1 and 2 (JAK1 and JAK2) are transducers of the heteromeric receptors of interleukin 6 and 10 (IL-6 and IL-10), which activate signal transducer and activator of transcription 3 (STAT3). STAT3 was shown to mediate cancer cell survival, proliferation, angiogenesis, and metastasis, as well as maintaining the CSC phenotypes (19, 153). Although the STAT3 protein could not be detected in the proteomic profiles due to its low abundance, its downstream target genes, including cyclin D1 and c-Myc, were down-regulated (24). JAK3 is an upstream regulator of STAT5 and STAT6. An accumulating data exercise revealed that inhibition of the JAK3 signaling could reduce cancer progression (154). It is possible that the suppression of JAK/STAT signaling by gigantol should attenuate CSC in lung cancer.

In addition, the mitogen-activated protein kinase 8 (MAPK8) or c-Jun N-terminal kinase (JNK) protein level was found to be induced by gigantol treatment (Figure 25A). JNK

plays a role in controlling cancer cell death. The activation of JNK is necessary for intrinsic and extrinsic apoptosis, and autophagic cell death (155). JNK signaling has been reported as a vital molecular mechanism of many anti-cancer-agents-induced cancer cell death and inactivation of such a protein led to cancer cell resistance to death stimuli (156, 157). An early up-regulation of JNK by gigantol before the cancer cells encountered the stressful conditions in the tumor possibly led to stress induced JNK hyperactivation, which subsequently promoted the expression of proapoptotic proteins (155). However, the protein level, in case of kinase protein, might not represent its function because proteomic profile could not distinguish its active form (phosphorylated form) from its total form. The further validation of these up-regulated kinases, as well as, their functions on lung tumor was recommended.

In order to confirm that these signaling pathways associated with CSC-like phenotype of the lung cancer cells, KEGG pathways database was examined, and the term “Signaling pathways regulating pluripotency of stem cells” was the only meaningful one. The genes listed in this term were mapped with the gigantol-mediated down- and up-regulated proteins, and the results revealed that the pathways represented in this term were still the PI3K/Akt and JAK/STAT pathways (Figure 26). Therefore, expression levels of Akt and STAT3, the key signals of PI3K/Akt and JAK/STAT, respectively, were validated by Western blot analysis. The Western blot results from the protein lysate of H460 showed that total Akt and STAT3 did not change, but the active forms of Akt (Ser473 phosphorylated Akt) and STAT3 (Ser727 phosphorylated STAT3) were significantly decreased in gigantol-treated cells (Figure 27). This result confirmed that gigantol-treated

cells had been inhibited the CSC-related pathways prior to subject to the proteomics analysis and subcutaneous xenograft experiment. Moreover, the effect of gigantol on Akt and STAT3 function was performed in more lung cancer cell lines, A549 and H292, using Western blot analysis. The results showed that gigantol also inhibited all tested cells in a dose-dependent manner (Figure 28).

Cancer cell growth is a consequence of activation of oncoproteins as well as dysregulation of proliferative proteins. Here it was demonstrated that c-Myc was key protein affected by the treatment of gigantol using proteomics and bioinformatics approaches (Figure 29). Based on the enrichment analysis results, the GO biological processes termed “regulation of cell proliferation” was the nearest term related to the cell proliferation (Table 6). Hub proteins were defined because such proteins would affect to several effectors or signaling pathways and caused a big impact to overall cellular processes. Changes of hub proteins by the treatment would affect the cancer cell proliferation. The top 20 hub proteins were identified as potential candidates for gigantol’s target (Figure 30). Since the proliferation assay and colony formation assay indicated that gigantol inhibited cancer cell growth, hence, the target in response to the gigantol treatment should be the proteins that facilitated cell proliferation and were down-regulated by gigantol, or the up-regulated proteins which inhibited cell proliferation. It appeared that c-Myc, which was a pro-proliferative protein, was the down-regulated protein with the most abundant PPIs (Figure 31). Furthermore, c-Myc was a transcription factor, of which its function correlated with its expression level (Table 7). Thus, a little change in c-Myc protein level might cause a large effect on cell division processes. c-Myc is

a well-known proto-oncogene which controls several proteins involved in cell cycle and is crucial for cancer cell growth (7). Moreover, PI3K/Akt, MAPK, or JAK/STAT pathways induced cancer proliferation through c-Myc regulation (158-160). Therefore, it could be considered c-Myc as a target of gigantol-mediated proliferation inhibition. c-Myc expression level was validated in lung cancer cells, and the Western blot analysis demonstrated that c-Myc levels in gigantol treated cells was significantly decreased (Figure 32). The protein analysis confirmed that gigantol reduced cellular c-Myc level in lung cancer cells.

The mechanisms that caused c-Myc level attenuation were also investigated. It was known that GSK3 $\beta$  promoted proteasomal degradation of c-Myc by phosphorylating c-Myc at Thr58 and enhancing c-Myc degradation via ubiquitin-proteasome pathway (Figure 33). Also, c-Myc was positively regulated by Akt via Akt-mediated GSK3 $\beta$  inactivation (12). Previous studies demonstrated that gigantol inhibited Akt function by decrease an active form of Akt (phosphorylated Akt at Ser473) in lung cancer (37), so it was possible that gigantol could enhance GSK3 $\beta$  function. Nevertheless, an effect of gigantol on GSK3 $\beta$  was unclear. So, this assumption was proved by Western blot analysis. The results indicated that gigantol treatment reduced the level of Ser9 p-GSK3 $\beta$  (the inactive form) but not total GSK3 $\beta$  (Figure 34). It suggested that gigantol attenuated GSK3 $\beta$  inactivation, which led to an increase of active form of GSK3 $\beta$  (non-phosphorylated form) and accelerated c-Myc degradation, as demonstrated by the reduction of c-Myc half-life in the cycloheximide chasing assay (Figure 35). An inhibition of proteasomal degradation experiment was performed using MG132 and the results confirmed that c-Myc degraded mainly through proteasomal pathway. MG132-treated cells showed higher c-Myc level because c-Myc

degradation was blocked and c-Myc accumulated in the cells (Figure 36). Moreover, MG132 was able to reverse an inhibitory effect of gigantol on c-Myc level (Figure 36), which proved that gigantol destabilized c-Myc through proteasomal degradation. Next, the level of ubiquitin-c-Myc conjugation was verified for ubiquitination was required for the recognition of the proteasome. The immunoprecipitation followed by Western blot analysis was performed and the results indicated that c-Myc ubiquitination was significantly increased in gigantol treated cells (Figure 37). This data strongly proved that c-Myc degradation was increased by gigantol since ubiquitination was the critical process for prompting the ubiquitin-proteasomal degradation.

Data from several studies revealed that certain oncoproteins like c-Myc is overexpressed and activated in cancers (161-163). In general, c-Myc protein regulates biological functions, namely proliferation, apoptosis, and differentiation. It is called a master transcription factor since c-Myc participates up to 15% of transcription of the entire genome (164). In cancer, the overexpression of c-Myc correlates with poor prognosis and unfavorable patient survival (165), and the transient silencing of c-Myc is shown to sufficiently inhibit cancer cell proliferation (9). The previous data have pointed out that c-Myc is critical protein for enhancing tumor growth and inhibition of such a protein may offer an effective strategy for management of the disease. An inducible MYC transgenic mice model revealed that c-Myc inhibition caused regression of established lung tumors. Once the systemic c-Myc was enhanced after being suppressed by continuous doxycycline treatment, proliferative cells were dramatically increased, indicating by BrdU staining, and significantly decreased immediately after c-Myc inhibition by re-introducing doxycycline. As

well, apoptotic cells, indicating by TUNEL staining, were observed in c-Myc inhibited tumor but not in normally expressed c-Myc tumor (166). The similar effect of c-Myc inhibition was also found in other type of cancer. The transient inhibition of c-Myc in the transgenic mice with hepatocellular tumor resulted to cancer cell differentiation into hepatocyte-like phenotype accompanied with apoptosis and completely regression of the tumors was observed (167). So far, c-Myc is a potential target for cancer treatment as it plays prominent roles in tumorigenesis and cancer progression. Various strategies for modulating c-Myc expression were suggested, such as targeting the up-stream signaling pathways which destabilized c-Myc protein level (7). Natural flavonoids that modulated c-Myc were intensively explored. For example, taxifolin was demonstrated to inhibit osteosarcoma cell proliferation and suppress tumor growth in nude mice xenograft model through an Akt/c-Myc inhibition (168). In line with above context, the present study provides a detail of key molecular mechanism of gigantol on c-Myc suppression and supports gigantol for potential use and development for cancer treatment.

In conclusion, gigantol inhibited PI3K/Akt and JAK/STAT3 signaling pathways and decreased c-Myc function through the facilitating of GSK3 $\beta$ -mediated c-Myc ubiquitin-proteasomal degradation. These signals inhibition caused the suppression of CSC-like phenotype and proliferative capacity of lung cancer cells, resulting to attenuation of tumor formation *in vivo* (Figure 38). This finding provided more insight information of gigantol mechanisms on tumor formation which supported further development of gigantol as an anticancer drug.

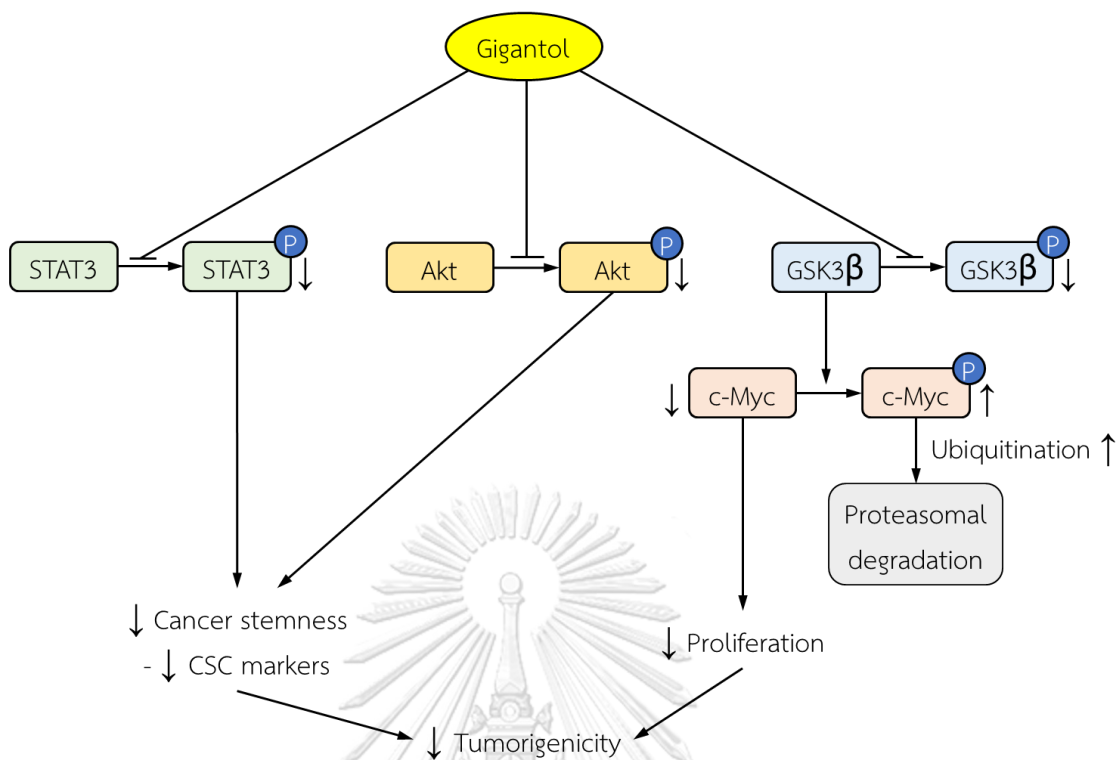


**Figure 38.** Schematic diagram summarizes the effects of gigantol on tumorigenicity and cell proliferation of lung cancer cells



## REFERENCES



จุฬาลงกรณ์มหาวิทยาลัย  
**CHULALONGKORN UNIVERSITY**

1. Hanahan D, Weinberg RA. Hallmarks of cancer: the next generation. *Cell*. 2011;144(5):646-74.
2. van Diest PJ, van der Wall E, Baak JP. Prognostic value of proliferation in invasive breast cancer: a review. *J Clin Pathol*. 2004;57(7):675-81.
3. Miura K, Hamanaka K, Koizumi T, Kawakami S, Kobayashi N, Ito KI. Solid component tumor doubling time is a prognostic factor in non-small cell lung cancer patients. *J Cardiothorac Surg*. 2019;14(1):57.
4. Eymin B, Gazzeri S. Role of cell cycle regulators in lung carcinogenesis. *Cell Adh Migr*. 2010;4(1):114-23.
5. Yuan M, Huang L-L, Chen J-H, Wu J, Xu Q. The emerging treatment landscape of targeted therapy in non-small-cell lung cancer. *Signal Transduct Target Ther*. 2019;4(1):61.
6. Kohno M, Pouyssegur J. Targeting the ERK signaling pathway in cancer therapy. *Ann Med*. 2006;38(3):200-11.
7. Chen H, Liu H, Qing G. Targeting oncogenic Myc as a strategy for cancer treatment. *Signal Transduct Target Ther*. 2018;3:5.
8. Lim DY, Shin SH, Lee M-H, Malakhova M, Kurinov I, Wu Q, et al. A natural small molecule, catechol, induces c-Myc degradation by directly targeting ERK2 in lung cancer. *Oncotarget*. 2016;7(23):35001-14.
9. Liu X, Wu C, Wu Y, Tang Y, Du J. c-Myc silencing impedes cell proliferation and enhances cytotoxicity of cisplatin in non-small cell lung cancer. *Int J Clin Exp Pathol*. 2016;9(9):9199-9205.

10. Evangelisti C, Chiarini F, Paganelli F, Marmioli S, Martelli AM. Crosstalks of GSK3 signaling with the mTOR network and effects on targeted therapy of cancer. *Biochim Biophys Acta Mol Cell Res.* 2020;1867(4):118635.
11. Zheng H, Saito H, Masuda S, Yang X, Takano Y. Phosphorylated GSK3 $\beta$ -ser9 and EGFR are Good Prognostic Factors for Lung Carcinomas. *Anticancer Res.* 2007;27(5B):3561-9.
12. Sears RC. The Life Cycle of C-Myc: From Synthesis to Degradation. *Cell Cycle.* 2004;3(9):1131-5.
13. Ayob AZ, Ramasamy TS. Cancer stem cells as key drivers of tumour progression. *J Biomed Sci.* 2018;25(1):20.
14. Battle E, Clevers H. Cancer stem cells revisited. *Nat Med.* 2017;23:1124–34.
15. Carney D, Gazdar A, Bunn JP, Guccion J. Demonstration of the stem cell nature of clonogenic tumor cells from lung cancer patients. *Stem cells.* 1982;1(3):149-64.
16. Gomez-Casal R, Bhattacharya C, Ganesh N, Bailey L, Basse P, Gibson M, et al. Non-small cell lung cancer cells survived ionizing radiation treatment display cancer stem cell and epithelial-mesenchymal transition phenotypes. *Mol Cancer.* 2013;12(1):94.
17. Garber K. Cancer stem cell pipeline flounders. *Nat Rev Drug Discov.* 2018;17(11):771-3.
18. Papadimitrakopoulou V. Development of PI3K/AKT/mTOR pathway inhibitors and their application in personalized therapy for non-small-cell lung cancer. *J Thorac Oncol.* 2012;7(8):1315-26.
19. Loh CY, Arya A, Naema AF, Wong WF, Sethi G, Looi CY. Signal Transducer and Activator of Transcription (STATs) Proteins in Cancer and Inflammation: Functions and Therapeutic Implication. *Front Oncol.* 2019;9:48.

20. Lawlor MA, Alessi DR. PKB/Akt. *J Cell Sci.* 2001;114(16):2903.
21. Wang M, Liu ZM, Li XC, Yao YT, Yin ZX. Activation of ERK1/2 and Akt is associated with cisplatin resistance in human lung cancer cells. *J Chemother.* 2013;25(3):162-9.
22. Oo AKK, Calle AS, Nair N, Mahmud H, Vaidyanath A, Yamauchi J, et al. Up-Regulation of PI 3-Kinases and the Activation of PI3K-Akt Signaling Pathway in Cancer Stem-Like Cells Through DNA Hypomethylation Mediated by the Cancer Microenvironment. *Transl Oncol.* 2018;11(3):653-63.
23. Hambardzumyan D, Becher OJ, Rosenblum MK, Pandolfi PP, Manova-Todorova K, Holland EC. PI3K pathway regulates survival of cancer stem cells residing in the perivascular niche following radiation in medulloblastoma in vivo. *Genes Dev.* 2008;22(4):436-48.
24. Galoczova M, Coates P, Vojtesek B. STAT3, stem cells, cancer stem cells and p63. *Cell Mol Biol Lett.* 2018;23:12.
25. Song L, Rawal B, Nemeth JA, Haura EB. JAK1 activates STAT3 activity in non-small-cell lung cancer cells and IL-6 neutralizing antibodies can suppress JAK1-STAT3 signaling. *Mol Cancer Ther.* 2011;10(3):481-94.
26. Bahmad HF, Mouhieddine TH, Chalhoub RM, Assi S, Araj T, Chamaa F, et al. The Akt/mTOR pathway in cancer stem/progenitor cells is a potential therapeutic target for glioblastoma and neuroblastoma. *Oncotarget.* 2018;9(71):33549-61.
27. Shibata M, Hoque MO. Targeting Cancer Stem Cells: A Strategy for Effective Eradication of Cancer. *Cancers (Basel).* 2019;11(5).

28. Chanvorachote P, Chamni S, Ninsontia C, Phiboonchaiyanan PP. Potential Anti-metastasis Natural Compounds for Lung Cancer. *Anticancer Res.* 2016;36(11):5707-17.
29. Shin SA, Moon SY, Kim WY, Paek SM, Park HH, Lee CS. Structure-Based Classification and Anti-Cancer Effects of Plant Metabolites. *Int J Mol Sci.* 2018;19(9):2651.
30. Bhummaphan N, Pongrakhananon V, Sritularak B, Chanvorachote P. Cancer Stem Cell-Suppressing Activity of Chrysotoxine, a Bibenzyl from *Dendrobium pulchellum*. *J Pharmacol Exp Ther.* 2018;364(2):332-46.
31. Tsai AC, Pan SL, Liao CH, Guh JH, Wang SW, Sun HL, et al. Moscatilin, a bibenzyl derivative from the India orchid *Dendrobium loddigesii*, suppresses tumor angiogenesis and growth in vitro and in vivo. *Cancer Lett.* 2010;292(2):163-70.
32. Chen WK, Chen CA, Chi CW, Li LH, Lin CP, Shieh HR, et al. Moscatilin Inhibits Growth of Human Esophageal Cancer Xenograft and Sensitizes Cancer Cells to Radiotherapy. *J Clin Med.* 2019;8(2):187.
33. Won JH, Kim JY, Yun KJ, Lee JH, Back NI, Chung HG, et al. Gigantol isolated from the whole plants of *Cymbidium goeringii* inhibits the LPS-induced iNOS and COX-2 expression via NF-kappaB inactivation in RAW 264.7 macrophages cells. *Planta Med.* 2006;72(13):1181-7.
34. Wu J, Li X, Wan W, Yang Q, Ma W, Chen D, et al. Gigantol from *Dendrobium chrysotoxum* Lindl. binds and inhibits aldose reductase gene to exert its anti-cataract activity: An in vitro mechanistic study. *J Ethnopharmacol.* 2017;198:255-61.

35. Chen MF, Liou SS, Hong TY, Kao ST, Liu IM. Gigantol has Protective Effects against High Glucose-Evoked Nephrotoxicity in Mouse Glomerulus Mesangial Cells by Suppressing ROS/MAPK/NF-kappaB Signaling Pathways. *Molecules*. 2018;24(1):80.
36. Charoenrungruang S, Chanvorachote P, Sritularak B, Pongrakhananon V. Gigantol-induced apoptosis in lung cancer cell through mitochondrial-dependent pathway. *Thai J Pharm Sci*. 2014;38:67-73.
37. Bhummaphan N, Chanvorachote P. Gigantol Suppresses Cancer Stem Cell-Like Phenotypes in Lung Cancer Cells. *Evid Based Complement Alternat Med*. 2015;2015:836564.
38. Charoenrungruang S, Chanvorachote P, Sritularak B, Pongrakhananon V. Gigantol, a bibenzyl from *Dendrobium draconis*, inhibits the migratory behavior of non-small cell lung cancer cells. *J Nat Prod*. 2014;77(6):1359-66.
39. Unahabhokha T, Chanvorachote P, Sritularak B, Kitsongsermthon J, Pongrakhananon V. Gigantol Inhibits Epithelial to Mesenchymal Process in Human Lung Cancer Cells. *Evid Based Complement Alternat Med*. 2016;2016:4561674.
40. Unahabhokha T, Chanvorachote P, Pongrakhananon V. The attenuation of epithelial to mesenchymal transition and induction of anoikis by gigantol in human lung cancer H460 cells. *Tumour Biol*. 2016;37(7):8633-41.
41. Frantzi M, Latosinska A, Mischak H. Proteomics in Drug Development: The Dawn of a New Era? *Proteomics Clin Appl*. 2019;13(2):e1800087.

42. Bray F, Ferlay J, Soerjomataram I, Siegel RL, Torre LA, Jemal A. Global cancer statistics 2018: GLOBOCAN estimates of incidence and mortality worldwide for 36 cancers in 185 countries. *CA Cancer J Clin.* 2018;68(6):394-424.
43. Siegel RL, Miller KD, Jemal A. Cancer statistics, 2019. *CA Cancer J Clin.* 2019;69(1):7-34.
44. Survival of Patients with Stage I Lung Cancer Detected on CT Screening. *New England Journal of Medicine.* 2006;355(17):1763-71.
45. Noone AM, Howlader N, Krapcho M, Miller D, Brest A, Yu M, et al. SEER Cancer Statistics Review, 1975-2015.: National Cancer Institute. Bethesda, MD; [updated November 2017; cited 2018. Available from: [https://seer.cancer.gov/csr/1975\\_2015/](https://seer.cancer.gov/csr/1975_2015/)].
46. Consonni D, Pierobon M, Gail MH, Rubagotti M, Rotunno M, Goldstein A, et al. Lung cancer prognosis before and after recurrence in a population-based setting. *J Natl Cancer Inst.* 2015;107(6):djv059.
47. Pikor LA, Ramnarine VR, Lam S, Lam WL. Genetic alterations defining NSCLC subtypes and their therapeutic implications. *Lung Cancer.* 2013;82(2):179-89.
48. Travis WD, Brambilla E, Nicholson AG, Yatabe Y, Austin JHM, Beasley MB, et al. The 2015 World Health Organization Classification of Lung Tumors: Impact of Genetic, Clinical and Radiologic Advances Since the 2004 Classification. *J Thorac Oncol.* 2015;10(9):1243-60.
49. Adams; VR, Peters SS. Chapter 129: Lung Cancer. In: Joseph T. DiPiro, Robert L. Talbert, Gary C. Yee, Gary R. Matzke, Barbara G. Wells, Posey LM, editors. *Pharmacotherapy: A Pathophysiologic Approach.* 10 ed: McGraws Hill; 2017. p. 2117-32.

50. Ellis PM, Vandermeer R. Delays in the diagnosis of lung cancer. *J Thorac Dis.* 2011;3(3):183-8.
51. Gajra A, Zemla TJ, Jatoi A, Feliciano JL, Wong ML, Chen H, et al. Time-to-Treatment-Failure and Related Outcomes Among 1000+ Advanced Non-Small Cell Lung Cancer Patients: Comparisons Between Older Versus Younger Patients (Alliance A151711). *J Thorac Oncol.* 2018;13(7):996-1003.
52. Sculier JP, Moro-Sibilot D. First- and second-line therapy for advanced nonsmall cell lung cancer. *Eur Respir J.* 2009;33(4):915-30.
53. Maeda H, Khatami M. Analyses of repeated failures in cancer therapy for solid tumors: poor tumor-selective drug delivery, low therapeutic efficacy and unsustainable costs. *Clin Transl Med.* 2018;7(1):11.
54. Bonnet D, Dick JE. Human acute myeloid leukemia is organized as a hierarchy that originates from a primitive hematopoietic cell. *Nat Med.* 1997;3(7):730-7.
55. Al-Hajj M, Wicha MS, Benito-Hernandez A, Morrison SJ, Clarke MF. Prospective identification of tumorigenic breast cancer cells. *Proceedings of the National Academy of Sciences.* 2003;100(7):3983-8.
56. Tirino V, Desiderio V, Paino F, De Rosa A, Papaccio F, La Noce M, et al. Cancer stem cells in solid tumors: an overview and new approaches for their isolation and characterization. *FASEB J.* 2013;27(1):13-24.
57. Rahman M, Deleyrolle L, Vedam-Mai V, Azari H, Abd-El-Barr M, Reynolds BA. The cancer stem cell hypothesis: failures and pitfalls. *Neurosurgery.* 2011;68(2):531-45; discussion 45.



58. Carnero A, Lleona M. The hypoxic microenvironment: A determinant of cancer stem cell evolution. *Inside the Cell*. 2016;1(2):96-105.
59. Korkaya H, Liu S, Wicha MS. Regulation of cancer stem cells by cytokine networks: attacking cancer's inflammatory roots. *Clin Cancer Res*. 2011;17(19):6125-9.
60. Yongsanguanchai N, Pongrakhananon V, Mutirangura A, Rojanasakul Y, Chanvorachote P. Nitric oxide induces cancer stem cell-like phenotypes in human lung cancer cells. *Am J Physiol Cell Physiol*. 2015;308(2):C89-100.
61. Inaba M, Yamashita YM. Asymmetric stem cell division: precision for robustness. *Cell Stem Cell*. 2012;11(4):461-9.
62. Zhu P, Fan Z. Cancer stem cells and tumorigenesis. *Biophys Rep*. 2018;4(4):178-88.
63. Chang JC. Cancer stem cells: Role in tumor growth, recurrence, metastasis, and treatment resistance. *Medicine (Baltimore)*. 2016;95(1 Suppl 1):S20-5.
64. Phi LTH, Sari IN, Yang YG, Lee SH, Jun N, Kim KS, et al. Cancer Stem Cells (CSCs) in Drug Resistance and their Therapeutic Implications in Cancer Treatment. *Stem Cells Int*. 2018;2018:5416923.
65. Jackson EL, Willis N, Mercer K, Bronson RT, Crowley D, Montoya R, et al. Analysis of lung tumor initiation and progression using conditional expression of oncogenic K-ras. *Genes Dev*. 2001;15(24):3243-8.
66. Kim CF, Jackson EL, Woolfenden AE, Lawrence S, Babar I, Vogel S, et al. Identification of bronchioalveolar stem cells in normal lung and lung cancer. *Cell*. 2005;121(6):823-35.

67. Eramo A, Haas TL, De Maria R. Lung cancer stem cells: tools and targets to fight lung cancer. *Oncogene*. 2010;29(33):4625-35.
68. Hardavella G, George R, Sethi T. Lung cancer stem cells-characteristics, phenotype. *Transl Lung Cancer Res*. 2016;5(3):272-9.
69. Ding XW, Wu JH, Jiang CP. ABCG2: a potential marker of stem cells and novel target in stem cell and cancer therapy. *Life Sci*. 2010;86(17-18):631-7.
70. Liang SC, Yang CY, Tseng JY, Wang HL, Tung CY, Liu HW, et al. ABCG2 localizes to the nucleus and modulates CDH1 expression in lung cancer cells. *Neoplasia*. 2015;17(3):265-78.
71. Liu J, Xiao Z, Wong SK-M, Tin VP-C, Ho K-Y, Wang J, et al. Lung cancer tumorigenicity and drug resistance are maintained through ALDH(hi)CD44(hi) tumor initiating cells. *Oncotarget*. 2013;4(10):1698-711.
72. Chambers I. The Molecular Basis of Pluripotency in Mouse Embryonic Stem Cells. *Cloning and Stem Cells*. 2004;6(4):386-91.
73. DeVita VT, Jr., Chu E. A history of cancer chemotherapy. *Cancer Res*. 2008;68(21):8643-53.
74. Liu X, Wang P, Zhang C, Ma Z. Epidermal growth factor receptor (EGFR): A rising star in the era of precision medicine of lung cancer. *Oncotarget*. 2017;8(30):50209-20.
75. Annett S, Robson T. Targeting cancer stem cells in the clinic: Current status and perspectives. *Pharmacol Ther*. 2018;187:13-30.
76. Brown JS, Banerji U. Maximising the potential of AKT inhibitors as anti-cancer treatments. *Pharmacol Ther*. 2017;172:101-15.

77. Wong ALA, Hirpara JL, Pervaiz S, Eu JQ, Sethi G, Goh BC. Do STAT3 inhibitors have potential in the future for cancer therapy? *Expert Opin Investig Drugs*. 2017;26(8):883-7.
78. Prescott JA, Cook SJ. Targeting IKKbeta in Cancer: Challenges and Opportunities for the Therapeutic Utilisation of IKKbeta Inhibitors. *Cells*. 2018;7(9).
79. Schott AF, Landis MD, Dontu G, Griffith KA, Layman RM, Krop I, et al. Preclinical and clinical studies of gamma secretase inhibitors with docetaxel on human breast tumors. *Clin Cancer Res*. 2013;19(6):1512-24.
80. Cortes JE, Gutzmer R, Kieran MW, Solomon JA. Hedgehog signaling inhibitors in solid and hematological cancers. *Cancer Treat Rev*. 2019;76:41-50.
81. Shaw HV, Koval A, Katanaev VL. Targeting the Wnt signalling pathway in cancer: prospects and perils. *Swiss Med Wkly*. 2019;149:w20129.
82. Matsui WH. Cancer stem cell signaling pathways. *Medicine (Baltimore)*. 2016;95(1 Suppl 1):S8-S19.
83. Xia P, Xu X-Y. PI3K/Akt/mTOR signaling pathway in cancer stem cells: from basic research to clinical application. *Am J Cancer Res*. 2015;5(5):1602-9.
84. Lara PN, Jr., Longmate J, Mack PC, Kelly K, Socinski MA, Salgia R, et al. Phase II Study of the AKT Inhibitor MK-2206 plus Erlotinib in Patients with Advanced Non-Small Cell Lung Cancer Who Previously Progressed on Erlotinib. *Clin Cancer Res*. 2015;21(19):4321-6.
85. Papadimitrakopoulou V, Lee JJ, Wistuba II, Tsao AS, Fossella FV, Kalhor N, et al. The BATTLE-2 Study: A Biomarker-Integrated Targeted Therapy Study in Previously Treated

- Patients With Advanced Non-Small-Cell Lung Cancer. *J Clin Oncol*. 2016;34(30):3638-47.
86. Wong AL, Soo RA, Tan DS, Lee SC, Lim JS, Marban PC, et al. Phase I and biomarker study of OPB-51602, a novel signal transducer and activator of transcription (STAT) 3 inhibitor, in patients with refractory solid malignancies. *Ann Oncol*. 2015;26(5):998-1005.
87. Chiang AC, Rudin CM, Spira AI, Jotte RM, Gadgeel SM, Mita AC, et al. Updated results of phase 1b study of tarextumab (TRXT, anti-Notch2/3) in combination with etoposide and platinum (EP) in patients (pts) with untreated extensive-stage small-cell lung cancer (ED-SCLC). *J Clin Oncol*. 2016;34(15\_suppl):8564-.
88. Tsao AS, Wistuba I, Xia D, Byers L, Diao L, Wang J, et al. Germline and Somatic Smoothed Mutations in Non-Small-Cell Lung Cancer Are Potentially Responsive to Hedgehog Inhibitor Vismodegib. *JCO Precision Oncology*. 2017(1):1-10.
89. Hill MM, Hemmings BA. Inhibition of protein kinase B/Akt: implications for cancer therapy. *Pharmacol Therapeut*. 2002;93(2):243-51.
90. Yang ZZ, Tschopp O, Baudry A, Dümmler B, Hynx D, Hemmings BA. Physiological functions of protein kinase B/Akt. *Biochem Soc Trans*. 2004;32(2):350-4.
91. Kumar CC, Madison V. AKT crystal structure and AKT-specific inhibitors. *Oncogene*. 2005;24(50):7493-501.
92. Romano G. The role of the dysfunctional akt-related pathway in cancer: establishment and maintenance of a malignant cell phenotype, resistance to therapy, and future strategies for drug development. *Scientifica (Cairo)*. 2013;2013:317186.

93. Vivanco I, Sawyers CL. The phosphatidylinositol 3-Kinase AKT pathway in human cancer. *Nat Rev Cancer*. 2002;2(7):489-501.
94. Manning BD, Cantley LC. AKT/PKB signaling: navigating downstream. *Cell*. 2007;129(7):1261-74.
95. Liao Y, Hung M-C. Physiological regulation of Akt activity and stability. *Am J Transl Res*. 2010;2(1):19-42.
96. Rivas S, Gomez-Oro C, Anton IM, Wandosell F. Role of Akt Isoforms Controlling Cancer Stem Cell Survival, Phenotype and Self-Renewal. *Biomedicines*. 2018;6(1).
97. Yang L, Shi P, Zhao G, Xu J, Peng W, Zhang J, et al. Targeting cancer stem cell pathways for cancer therapy. *Signal Transduct Target Ther*. 2020;5(1):8.
98. Yu H, Jove R. The STATs of cancer--new molecular targets come of age. *Nat Rev Cancer*. 2004;4(2):97-105.
99. Harrison DA. The Jak/STAT pathway. *Cold Spring Harb Perspect Biol*. 2012;4(3).
100. Rawlings JS, Rosler KM, Harrison DA. The JAK/STAT signaling pathway. *J Cell Sci*. 2004;117(Pt 8):1281-3.
101. Yu H, Lee H, Herrmann A, Buettner R, Jove R. Revisiting STAT3 signalling in cancer: new and unexpected biological functions. *Nat Rev Cancer*. 2014;14(11):736-46.
102. Murase S, McKay RD. Neuronal activity-dependent STAT3 localization to nucleus is dependent on Tyr-705 and Ser-727 phosphorylation in rat hippocampal neurons. *Eur J Neurosci*. 2014;39(4):557-65.
103. Wen Z, Zhong Z, Darnell JE, Jr. Maximal activation of transcription by stat1 and stat3 requires both tyrosine and serine phosphorylation. *Cell*. 1995;82(2):241-50.

104. Annex 3: Recommendations for the evaluation of animal cell cultures as substrates for the manufacture of biological medicinal products and for the characterization of cell banks. WHO Expert Committee on Biological Standardization. WHO Press, Geneva, Switzerland: World Health Organization; 2013. p. 79-187.
105. Puisieux A, Pommier RM, Morel AP, Laval F. Cellular Pliancy and the Multistep Process of Tumorigenesis. *Cancer Cell*. 2018;33(2):164-72.
106. Bruttel VS, Wischhusen Jr. Cancer Stem Cell Immunology: Key to Understanding Tumorigenesis and Tumor Immune Escape? *Front Immunol*. 2014;5.
107. Noh KH, Kang TH, Kim JH, Pai SI, Lin KY, Hung CF, et al. Activation of Akt as a mechanism for tumor immune evasion. *Mol Ther*. 2009;17(3):439-47.
108. Dutta P, Sabri N, Li J, Li WX. Role of STAT3 in lung cancer. *JAKSTAT*. 2014;3(4):e999503.
109. Galluzzo P, Bocchetta M. Notch signaling in lung cancer. *Expert Rev Anticancer Ther*. 2011;11(4):533-40.
110. Rapp J, Jaromi L, Kvell K, Miskei G, Pongracz JE. WNT signaling - lung cancer is no exception. *Respir Res*. 2017;18(1):167.
111. Giroux-Leprieur E, Costantini A, Ding VW, He B. Hedgehog Signaling in Lung Cancer: From Oncogenesis to Cancer Treatment Resistance. *Int J Mol Sci*. 2018;19(9).
112. Rinkenbaugh AL, Baldwin AS. The NF-kappaB Pathway and Cancer Stem Cells. *Cells*. 2016;5(2).
113. Giovanella BC, Fogh J. The Nude Mouse in Cancer Research. *Adv Cancer Res*. 1985;44:69-120.

114. Okada S, Vaeteewoottacharn K, Kariya R. Application of Highly Immunocompromised Mice for the Establishment of Patient-Derived Xenograft (PDX) Models. *Cells*. 2019;8(8).
115. Workman P, Aboagye EO, Balkwill F, Balmain A, Bruder G, Chaplin DJ, et al. Guidelines for the welfare and use of animals in cancer research. *Br J Cancer*. 2010;102(11):1555-77.
116. Wang J, Luo B, Li X, Lu W, Yang J, Hu Y, et al. Inhibition of cancer growth in vitro and in vivo by a novel ROS-modulating agent with ability to eliminate stem-like cancer cells. *Cell Death Dis*. 2017;8(6):e2887.
117. Okayama T, Kokura S, Ishikawa T, Adachi S, Hattori T, Takagi T, et al. Antitumor effect of pretreatment for colon cancer cells with hyperthermia plus geranylgeranylacetone in experimental metastasis models and a subcutaneous tumor model of colon cancer in mice. *Int J Hyperthermia*. 2009;25(2):141-9.
118. Hanahan D, Weinberg RA. The hallmarks of cancer. *Cell*. 2000;100:57–70.
119. Feitelson MA, Arzumanyan A, Kulathinal RJ, Blain SW, Holcombe RF, Mahajna J, et al. Sustained proliferation in cancer: Mechanisms and novel therapeutic targets. *Seminars in Cancer Biology*. 2015;35:S25-S54.
120. Gabay M, Li Y, Felsher DW. MYC activation is a hallmark of cancer initiation and maintenance. *Cold Spring Harb Perspect Med*. 2014;4(6).
121. Pinkhien T, Petpiroon N, Sritularak B, Chanvorachote P. Batatasin III Inhibits Migration of Human Lung Cancer Cells by Suppressing Epithelial to Mesenchymal Transition and FAK-AKT Signals. *Anticancer res*. 2017;37(11):6281-9.

122. Kowitdamrong A, Chanvorachote P, Sritularak B, Pongrakhananon V. Moscatilin inhibits lung cancer cell motility and invasion via suppression of endogenous reactive oxygen species. *Biomed Res Int.* 2013;2013:765894.
123. Busaranon K, Plaimee P, Sritularak B, Chanvorachote P. Moscatilin inhibits epithelial-to-mesenchymal transition and sensitizes anoikis in human lung cancer H460 cells. *J Nat Med.* 2016;70(1):18-27.
124. Juneja RK, Sharma SC, Tandon JS. A substituted 1,2-diarylethane from *Cymbidium giganteum*. *Phytochemistry.* 1985;24(2):321-4.
125. Guide for the Care and Use of Laboratory Animals -- Portuguese Edition. Washington, DC: The National Academies Press; 1996. 130 p.
126. Sritularak B, Anuwat M, Likhitwitayawuid K. A new phenanthrenequinone from *Dendrobium draconis*. *J Asian Nat Prod Res.* 2011;13(3):251-5.
127. Leary S. AVMA Guidelines for the Euthanasia of Animals: 2013 Edition. American Veterinary Medical Association "AVMA guidelines for the euthanasia of animals: 2013 edition" *Journal of the American Veterinary Medical Association* (2013). 2013;<https://www.avma.org/KB/Policies/Documents/euthanasia.pdf>.
128. Schneider CA, Rasband WS, Eliceiri KW. NIH Image to ImageJ: 25 years of image analysis. *Nat Methods.* 2012;9(7):671-5.
129. Jang MH, Kim HJ, Chung YR, Lee Y, Park SY. A comparison of Ki-67 counting methods in luminal Breast Cancer: The Average Method vs. the Hot Spot Method. *PLoS One.* 2017;12(2):e0172031.



130. Lowry OH, Rosebrough NJ, Farr AL, Randall RJ. Protein measurement with the Folin phenol reagent. *J Biol Chem.* 1951;193(1):265-75.
131. Tyanova S, Temu T, Cox J. The MaxQuant computational platform for mass spectrometry-based shotgun proteomics. *Nat Protoc.* 2016;11(12):2301-19.
132. Kuleshov MV, Jones MR, Rouillard AD, Fernandez NF, Duan Q, Wang Z, et al. Enrichr: a comprehensive gene set enrichment analysis web server 2016 update. *Nucleic Acids Res.* 2016;44(W1):W90-7.
133. Mi H, Muruganujan A, Ebert D, Huang X, Thomas PD. PANTHER version 14: more genomes, a new PANTHER GO-slim and improvements in enrichment analysis tools. *Nucleic Acids Res.* 2019;47(D1):D419-D26.
134. Bardou P, Mariette J, Escudié F, Djemiel C, Klopp C. jvenn: an interactive Venn diagram viewer. *BMC Bioinformatics.* 2014;15(1):293.
135. Szklarczyk D, Gable AL, Lyon D, Junge A, Wyder S, Huerta-Cepas J, et al. STRING v11: protein-protein association networks with increased coverage, supporting functional discovery in genome-wide experimental datasets. *Nucleic Acids Res.* 2019;47(D1):D607-D13.
136. Shannon P, Markiel A, Ozier O, Baliga NS, Wang JT, Ramage D, et al. Cytoscape: a software environment for integrated models of biomolecular interaction networks. *Genome Res.* 2003;13(11):2498-504.
137. Rezaei-Tavirani M, Rezaei-Taviran S, Mansouri M, Rostami-Nejad M, Rezaei-Tavirani M. Protein-Protein Interaction Network Analysis for a Biomarker Panel Related to Human Esophageal Adenocarcinoma. *Asian Pac J Cancer Prev.* 2017;18(12):3357-63.

138. Howe EA, Sinha R, Schlauch D, Quackenbush J. RNA-Seq analysis in MeV. *Bioinformatics*. 2011;27(22):3209-10.
139. Li LT, Jiang G, Chen Q, Zheng JN. Ki67 is a promising molecular target in the diagnosis of cancer (review). *Mol Med Rep*. 2015;11(3):1566-72.
140. Talele NP, Fradette J, Davies JE, Kapus A, Hinz B. Expression of alpha-Smooth Muscle Actin Determines the Fate of Mesenchymal Stromal Cells. *Stem Cell Rep*. 2015;4(6):1016-30.
141. Lee HW, Park YM, Lee SJ, Cho HJ, Kim DH, Lee JI, et al. Alpha-smooth muscle actin (ACTA2) is required for metastatic potential of human lung adenocarcinoma. *Clin Cancer Res*. 2013;19(21):5879-89.
142. Faivre S, Zappa M, Vilgrain V, Boucher E, Douillard JY, Lim HY, et al. Changes in tumor density in patients with advanced hepatocellular carcinoma treated with sunitinib. *Clin Cancer Res*. 2011;17(13):4504-12.
143. Hale MD, Nankivell MG, Mueller W, West NP, Stenning SP, Wright AI, et al. The relationship between tumor cell density in the pretreatment biopsy and survival after chemotherapy in OE02 trial esophageal cancer patients. *J Clin Oncol*. 2014;32(3\_suppl):49-.
144. Chen H, Huang Y, Huang J, Lin L, Wei G. Gigantol attenuates the proliferation of human liver cancer HepG2 cells through the PI3K/AKT/NF-kappaB signaling pathway. *Oncol Rep*. 2017;37(2):865-70.

145. Yu S, Wang Z, Su Z, Song J, Zhou L, Sun Q, et al. Gigantol inhibits Wnt/beta-catenin signaling and exhibits anticancer activity in breast cancer cells. *BMC Complement. Altern Med.* 2018;18:59.
146. Fukunaga-Kalabis M, Roesch A, Herlyn M. From cancer stem cells to tumor maintenance in melanoma. *J Investig Dermatol.* 2011;131:1600–4.
147. Yang D, Woodard G, Zhou C, Wang X, Liu Z, Ye Z, et al. Significance of different response evaluation criteria in predicting progression-free survival of lung cancer with certain imaging characteristics. *Thorac Cancer.* 2016;7:535–42.
148. Lencioni R, Llovet JM. Modified RECIST (mRECIST) assessment for hepatocellular carcinoma. *Semin Liver Dis.* 2010;30:52–60.
149. Wang Y, Jiang M, Du C, Yu Y, Liu Y, Li M, and Luo F. Utilization of lung cancer cell lines for the study of lung cancer stem cells (Review). *Oncol Lett.* 2018;15:6791-8.
150. Thorpe LM, Yuzugullu H, Zhao JJ. PI3K in cancer: Divergent roles of isoforms, modes of activation and therapeutic targeting. *Nat Rev Cancer.* 2015;15:7–24.
151. Lien EC, Dibble CC, Toker A. PI3K signaling in cancer: Beyond AKT. *Curr Opin Cell Biol.* 2017;45:62–71.
152. Liu P, Cheng H, Roberts TM, Zhao JJ. Targeting the phosphoinositide 3-kinase pathway in cancer. *Nat Rev Drug Discov.* 2009;8(8):627–644.
153. Johnson DE, O’Keefe RA, Grandis JR. Targeting the IL-6/JAK/STAT3 signalling axis in cancer. *Nat Rev Clin Oncol.* 2018;15:234–248.

154. Valle-Mendiola A, Weiss-Steider B, Rocha-Zavaleta L, Soto-Cruz I. IL-2 enhances cervical cancer cells proliferation and JAK3/STAT5 phosphorylation at low doses, while at high doses IL-2 has opposite effects. *Cancer Investig.* 2014;32:115–25.
155. Dhanasekaran DN, Reddy EP. JNK-signaling: A multiplexing hub in programmed cell death. *Genes Cancer.* 2017;8:682–94.
156. Hu L, Zhang T, Liu D, Guan G, Huang J, Proksch P, Chen X, Lin W. Notoamide-type alkaloid induced apoptosis and autophagy via a P38/JNK signaling pathway in hepatocellular carcinoma cells. *RSC Adv.* 2019;9:19855–68.
157. Bai Y, Liu X, Qi X, Liu X, Peng F, Li H, et al. PDIA6 modulates apoptosis and autophagy of non-small cell lung cancer cells via the MAP4K1/JNK signaling pathway. *EBioMedicine.* 2019;42:311–25.
158. Buckler JL, Liu X, Turka LA. Regulation of T-cell responses by PTEN. *Immunol Rev.* 2008;224:239-48.
159. Wang Q, Tan R, Zhu X, Zhangn Y, Tan Z, Su B, et al. Oncogenic K-ras confers SAHA resistance by up-regulating HDAC6 and c-myc expression. *Oncotarget.* 2016;7(9):10064-72.
160. Choi JW, Schroeder MA, Sarkaria JN, Bram RJ. Cyclophilin B supports Myc and mutant p53-dependent survival of glioblastoma multiforme cells. *Cancer Res.* 2014;74(2):484-96.
161. Chanvorachote P, Sriratanasak N, Nonpanya N. C-myc Contributes to Malignancy of Lung Cancer: A Potential Anticancer Drug Target. *Anticancer Res.* 2020;40(2):609-18.
162. Xu J, Chen Y, Olopade OI. MYC and Breast Cancer. *Genes Cancer.* 2010;1(6):629-40.

163. Koh CM, Bieberich CJ, Dang CV, Nelson WG, Yegnasubramanian S, De Marzo AM. MYC and Prostate Cancer. *Genes & cancer*. 2010;1(6):617-28.
164. Dang CV, O'Donnell KA, Zeller KI, Nguyen T, Osthus RC, Li F. The c-Myc target gene network. *Sem Cancer Biol*. 2006;16(4):253-64.
165. Seo AN, Yang JM, Kim H, Jheon S, Kim K, Lee CT, et al. Clinicopathologic and prognostic significance of c-MYC copy number gain in lung adenocarcinomas. *Br J Cancer*. 2014;110(11):2688-99.
166. Soucek L, Whitfield J, Martins CP, Finch AJ, Murphy DJ, Sodir NM, et al. Modelling Myc inhibition as a cancer therapy. 2008;455:679-83.
167. Shachaf CM, Kopelman Am, Arvanitis C, Karlsson A, Beer S, Mandl S, et al. MYC inactivation uncovers pluripotent differentiation and tumour dormancy in hepatocellular cancer. 2004;431:1112-7.
168. Chen X, Gu N, Xue C, Li BR. Plant flavonoid taxifolin inhibits the growth, migration and invasion of human osteosarcoma cells. *Mol Med Rep*. 2018;17(2):3239-45.

## APPENDIX

### TABLES OF EXPERIMENTAL RESULTS

**Table 9.** The percentage of H460, A549, H292 and BEAS-2B cell viability was determined by MTT assay after treatment with various concentrations of gigantol for 24 hours.

Gigantol ( $\mu\text{M}$ )	Cell viability (%)			
	H460	A549	H292	BEAS-2B
0	100 $\pm$ 2.73	100 $\pm$ 4.93	100 $\pm$ 8.43	100 $\pm$ 6.60
5	98.05 $\pm$ 4.96	94.32 $\pm$ 11.59	94.84 $\pm$ 1.88	-
10	94.17 $\pm$ 3.66	83.66 $\pm$ 9.20	94.07 $\pm$ 6.68	100.5 $\pm$ 12.87
20	88.88 $\pm$ 7.19	83.02 $\pm$ 10.85	87.18 $\pm$ 4.33	100.6 $\pm$ 6.78
50	86.83 $\pm$ 9.98 *	74.72 $\pm$ 7.26 *	84.46 $\pm$ 4.93 *	96.44 $\pm$ 8.83
100	80.72 $\pm$ 3.63 *	73.74 $\pm$ 15.39 *	77.51 $\pm$ 11.64 *	84.27 $\pm$ 3.21 *
200	68.04 $\pm$ 8.2 *	53.16 $\pm$ 6.63 *	54.89 $\pm$ 11.13 *	73.76 $\pm$ 3.30 *

Value represents means  $\pm$  SD of four independent experiments, \*  $p < 0.05$  versus untreated control.

**Table 10.** The percentage of apoptotic cells of H460 cells was determined by Hoechst 33342 and propidium iodide staining after treatment with various concentrations of gigantol for 24 hours.

Gigantol ( $\mu\text{M}$ )	Apoptotic cells (%)
0	0.29 $\pm$ 0.03
20	0.81 $\pm$ 0.21
50	4.05 $\pm$ 0.41 *
100	4.73 $\pm$ 0.57 *
200	8.81 $\pm$ 1.30 *

Value represents means  $\pm$  SD of three independent experiments, \*  $p < 0.05$  versus untreated control.

**Table 11.** Relative protein levels of CSC markers of H460 cells were determined by Western blot analysis after treatment with various concentrations of gigantol for 24 hours.

Gigantol ( $\mu\text{M}$ )	Relative protein levels	
	CD133	ALDH1A1
0	1 $\pm$ 0.00	1 $\pm$ 0.00
20	0.53 $\pm$ 0.12 *	0.52 $\pm$ 0.06 *

Value represents means  $\pm$  SD of three independent experiments, \*  $p < 0.05$  versus untreated control.

**Table 12.** Body weights of nude mice were observed from day 0 – 13.

Day after inoculation (days)	Body weight (g)				
	Mouse 1	Mouse 2	Mouse 3	Mouse 4	Mouse 5
0	22.41	16.83	20.78	25.17	24.81
4	23.15	18.87	24.95	28.37	27.23
7	24.38	22.82	23.88	26.75	25.48
8	24.63	23.4	23.84	27.48	25.57
9	25.05	24	24.3	28.6	25.9
10	25.1	24.78	24.47	28.53	26.24
11	25.78	24.93	24.69	29.63	27.1
12	25.26	24.43	24.64	29.17	26.38
13	26.18	25.19	25.49	29.76	27.12

**Table 13.** Tumor volumes ( $\text{mm}^3$ ) of untreated and gigantol-pretreated groups were measured using Vernier Caliper on day 7-13.

		Day after inoculation (days)						
		7	8	9	10	11	12	13
Mouse 1	Control	204.6	288.79	529.92	785.47	804.71	1126.1	1566.8
	Gigantol	321.43	853.65	814.64	924.69	1116.8	1053.9	1444.8
Mouse 2	Control	280.88	315.88	527.1	883.33	1058.2	1145.7	1103.1
	Gigantol	117.81	153.97	266.58	332.9	437.45	681.98	732.77
Mouse 3	Control	128.29	159.78	205.88	283.67	389.44	485.13	813.9
	Gigantol	153.36	426.31	485.11	846.74	707.8	925.41	1087
Mouse 4	Control	566.64	713.57	807.18	1054.7	1157.6	1709.7	2021
	Gigantol	286.71	435.58	609.32	782.98	897.52	1288.2	1711.8
Mouse 5	Control	532.57	989.08	1464.4	1183.3	1557.9	1795.2	1463.9
	Gigantol	-	-	-	-	-	-	-

\* The gigantol-pretreated tumor of mouse 5 could not be measured because it was not palpable, and the edge of the tumor could not be verified.

**Table 14.** Means of tumor volume ( $\text{mm}^3$ ) of untreated and gigantol-pretreated groups on day 7-13 were calculated.

Day after inoculation (days)	Mean of tumor volume ( $\text{mm}^3$ )	
	Untreated control	Gigantol-pretreated
7	295.1 $\pm$ 191.4	219.8 $\pm$ 99.37
8	369.5 $\pm$ 239.3	467.4 $\pm$ 288.8
9	517.5 $\pm$ 245.8	543.9 $\pm$ 229.4
10	751.8 $\pm$ 331.3	721.8 $\pm$ 265.7
11	852.5 $\pm$ 342.6	789.9 $\pm$ 288.3
12	1117 $\pm$ 500.5	987.4 $\pm$ 253
13	1376 $\pm$ 530	1244 $\pm$ 426.3



**Table 15.** Tumor weights (mg) of untreated and gigantol-pretreated groups were observed on day 13.

	Tumor weight (mg)	
	Untreated control	Gigantol-pretreated
Mouse 1	1150	950
Mouse 2	850	490
Mouse 3	440	760
Mouse 4	1350	1070
Mouse 5	1040	220
Mean $\pm$ SD (n = 5)	966 $\pm$ 345.3	698 $\pm$ 345.5

**Table 16.** Tumor volume (mm<sup>3</sup>) of dissected untreated and gigantol-pretreated groups measured on day 13.

	Tumor volume (mm <sup>3</sup> )	
	Untreated control	Gigantol-pretreated
Mouse 1	1566.84	1444.77
Mouse 2	1103.09	732.77
Mouse 3	813.9	1087.01
Mouse 4	2020.95	1711.77
Mouse 5	1463.86	427.78
Mean $\pm$ SD (n = 5)	1394 $\pm$ 460.7	1081 $\pm$ 519.2

**Table 17.** Tumor densities of untreated and gigantol-pretreated groups were calculated from dissected tumor weights and volumes measured on day 13.

	Tumor density (mg/mm <sup>3</sup> )	
	Untreated control	Gigantol-pretreated
Mouse 1	0.734	0.6575
Mouse 2	0.7706	0.6687
Mouse 3	0.5406	0.6992
Mouse 4	0.668	0.6251
Mouse 5	0.7105	0.5143
Mean ± SD (n = 5)	0.6847 ± 0.089	0.633 ± 0.071

**Table 18.** The percentage of necrotic areas in Hematoxylin and eosin-stained tumor slides.

	Necrotic area (%)	
	Untreated control	Gigantol-pretreated
Mouse 1	19.9	25.2
Mouse 2	22.9	35.1
Mouse 3	11.4	37.5
Mouse 4	31.8	22.0
Mean ± SD (n = 4)	21.5 ± 8.42	29.95 ± 7.51

The total area of tumor mass was counted as 100% and the necrotic area was calculated as a percentage relative to the total area.

**Table 19.** The percentage of Ki-67 positive cells of the untreated and gigantol-pretreated tumor from mouse 1 and mouse 3 and the mean of percentage of Ki-67 positive cells of the untreated and gigantol-pretreated tumor calculated from the two mice.

	Ki-67 positive cells (%)	
	Untreated control	Gigantol-pretreated
Mouse 1	62.85	48.76
Mouse 3	62.06	50.22
Mean (n = 2)	62.45 ± 0.56	49.49 ± 1.04

The values of mouse 1 and mouse 3 are the average values of hot-spot and cold-spot of the same tumor. The values of mean percentage are the average values of mouse 1 and mouse 3 (means ± SD). \* p < 0.05 versus untreated control.

**Table 20.** Relative ratios of the protein levels of p-Akt (S473) and total Akt and p-STAT3 (S727) and total STAT3 of H460 cells were determined by Western blot analysis after treatment with 20 μM gigantol for 24 hours.

Gigantol (μM)	Relative protein levels	
	p-Akt/Akt	p-STAT3/STAT3
0	1 ± 0.00	1 ± 0.00
20	0.44 ± 0.05 *	0.61 ± 0.03 *

Value represents means ± SD of three independent experiments, \* p < 0.05 versus untreated control.

**Table 21.** Relative protein levels of CSC markers, CD133 and ALDH1A1, and relative ratios of the protein levels of p-Akt (S473) and total Akt and p-STAT3 (S727) and total STAT3 of H460, A549, and H292 cells were determined by Western blot analysis after treatment with various concentrations of gigantol for 24 hours.

	Gigantol ( $\mu$ M)	Relative protein levels			
		CD133	ALDH1A1	p-Akt/Akt	p-STAT3/STAT3
H460	0	1 $\pm$ 0.00	1 $\pm$ 0.00	1 $\pm$ 0.00	1 $\pm$ 0.00
	10	0.69 $\pm$ 0.07 *	0.46 $\pm$ 0.13 *	0.48 $\pm$ 0.07 *	0.42 $\pm$ 0.03 *
	20	0.68 $\pm$ 0.09 *	0.53 $\pm$ 0.17 *	0.47 $\pm$ 0.14 *	0.66 $\pm$ 0.06 *
A549	0	1 $\pm$ 0.00	1 $\pm$ 0.00	1 $\pm$ 0.00	1 $\pm$ 0.00
	10	0.76 $\pm$ 0.07 *	0.64 $\pm$ 0.05 *	0.72 $\pm$ 0.06 *	0.65 $\pm$ 0.08 *
	20	0.77 $\pm$ 0.07 *	0.52 $\pm$ 0.11 *	0.66 $\pm$ 0.08 *	0.74 $\pm$ 0.08 *
H292	0	1 $\pm$ 0.00	1 $\pm$ 0.00	1 $\pm$ 0.00	1 $\pm$ 0.00
	10	0.71 $\pm$ 0.08 *	0.93 $\pm$ 0.03	0.72 $\pm$ 0.1 *	0.39 $\pm$ 0.03 *
	20	0.58 $\pm$ 0.14 *	0.69 $\pm$ 0.06 *	0.39 $\pm$ 0.02 *	0.49 $\pm$ 0.04 *

Value represents means  $\pm$  SD of three independent experiments, \* p < 0.05 versus untreated control.

**Table 22.** Relative growth rates of H460, A549, and H292 cells were determined by MTT assay after treatment with various concentrations of gigantol for 3 days.

	Day after treatment (days)	Gigantol ( $\mu\text{M}$ )			
		0	5	10	20
H460	0	1 $\pm$ 0.20	1 $\pm$ 0.1	1 $\pm$ 0.08	1 $\pm$ 0.06
	1	2.51 $\pm$ 0.15	2.45 $\pm$ 0.11	2.40 $\pm$ 0.31	1.74 $\pm$ 0.11 *
	2	4.55 $\pm$ 0.04	4.60 $\pm$ 0.3	4.35 $\pm$ 0.04	3.43 $\pm$ 0.02 *
	3	8.75 $\pm$ 0.02 *	7.78 $\pm$ 0.06 *	6.22 $\pm$ 0.44 *	5.16 $\pm$ 0.80 *
A549	0	1 $\pm$ 0.28	1 $\pm$ 0.22	1 $\pm$ 0.20	1 $\pm$ 0.10
	1	2.43 $\pm$ 0.21	2.65 $\pm$ 0.10	2.18 $\pm$ 0.16	1.95 $\pm$ 0.16 *
	2	4.21 $\pm$ 0.29	4.04 $\pm$ 0.29	3.89 $\pm$ 0.26	3.03 $\pm$ 0.4 *
	3	7.86 $\pm$ 0.25 *	6.84 $\pm$ 0.59 *	6.54 $\pm$ 0.19 *	4.43 $\pm$ 0.26 *
H292	0	1 $\pm$ 0.12	1 $\pm$ 0.18	1 $\pm$ 0.05	1 $\pm$ 0.07
	1	1.8 $\pm$ 0.04	1.71 $\pm$ 0.17	1.7 $\pm$ 0.19	1.58 $\pm$ 0.12
	2	3.26 $\pm$ 0.17 *	2.7 $\pm$ 0.18 *	2.64 $\pm$ 0.13 *	2.5 $\pm$ 0.22 *
	3	6.04 $\pm$ 0.15 *	4.92 $\pm$ 0.45 *	4.43 $\pm$ 0.27 *	3.93 $\pm$ 0.42 *

Value represents means  $\pm$  SD of four independent experiments, \*  $p < 0.05$  versus untreated control at the same time point.

**Table 23.** The percentage of colony numbers of H460, A549, and H292 cells were determined by colony formation assay after treatment with various concentrations of gigantol for 10 days.

Gigantol ( $\mu\text{M}$ )	Colony number (%)		
	H460	A549	H292
0	100 $\pm$ 10.7	100 $\pm$ 6.66	100 $\pm$ 13.79
5	56.37 $\pm$ 8.4 *	68.2 $\pm$ 12.53 *	59.57 $\pm$ 17.99 *
10	54 $\pm$ 7.79 *	67.47 $\pm$ 3.33 *	59.4 $\pm$ 13.9 *
20	44.33 $\pm$ 8.66 *	37.57 $\pm$ 16.65 *	47.67 $\pm$ 11.2 *

Value represents means  $\pm$  SD of three independent experiments, \*  $p < 0.05$  versus untreated control. The untreated control was counted as 100%.

**Table 24.** Relative protein levels of c-Myc of lung cancer cells were determined by Western blot analysis after treatment with various concentrations of gigantol for 24 hours.

Gigantol ( $\mu\text{M}$ )	Relative protein levels of c-Myc		
	H460	A549	H292
0	1 $\pm$ 0.00	1 $\pm$ 0.00	1 $\pm$ 0.00
5	0.88 $\pm$ 0.04 *	0.74 $\pm$ 0.06 *	1.02 $\pm$ 0.04
10	0.83 $\pm$ 0.04 *	0.44 $\pm$ 0.19 *	0.63 $\pm$ 0.14 *
20	0.58 $\pm$ 0.07 *	0.46 $\pm$ 0.08 *	0.49 $\pm$ 0.05 *

Value represents means  $\pm$  SD of three independent experiments, \*  $p < 0.05$  versus untreated control.

**Table 25.** Relative protein levels of p-GSK3 $\beta$ (S9)/GSK3 $\beta$  of lung cancer cells were determined by Western blot analysis after treatment with various concentrations of gigantol for 24 hours.

Gigantol ( $\mu$ M)	Relative protein levels of p-GSK3 $\beta$ (S9)/GSK3 $\beta$		
	H460	A549	H292
0	1 $\pm$ 0.00	1 $\pm$ 0.00	1 $\pm$ 0.00
5	0.72 $\pm$ 0.14 *	0.69 $\pm$ 0.13 *	0.79 $\pm$ 0.03 *
10	0.63 $\pm$ 0.11 *	0.62 $\pm$ 0.10 *	0.78 $\pm$ 0.04 *
20	0.43 $\pm$ 0.11 *	0.5 $\pm$ 0.08 *	0.43 $\pm$ 0.14 *

Value represents means  $\pm$  SD of three independent experiments, \* p < 0.05 versus untreated control.

**Table 26.** Relative protein levels of c-Myc of lung cancer cells were determined by Western blot analysis after treatment with CHX or CHX with gigantol as indicated time.

	Gigantol ( $\mu$ M)	Time of CHX treatment (minutes)					
		0	15	30	45	60	90
H460	0	1 $\pm$ 0.00	0.86 $\pm$ 0.13	0.69 $\pm$ 0.04	0.52 $\pm$ 0.03	0.45 $\pm$ 0.07	0.27 $\pm$ 0.04
	20	1 $\pm$ 0.00	0.56 $\pm$ 0.06*	0.49 $\pm$ 0.06*	0.36 $\pm$ 0.04*	0.31 $\pm$ 0.03*	0.18 $\pm$ 0.03
A549	0	1 $\pm$ 0.00	0.74 $\pm$ 0.04	0.58 $\pm$ 0.03	0.44 $\pm$ 0.04	0.36 $\pm$ 0.05	0.25 $\pm$ 0.06
	20	1 $\pm$ 0.00	0.57 $\pm$ 0.04*	0.47 $\pm$ 0.03*	0.33 $\pm$ 0.03*	0.26 $\pm$ 0.04*	0.16 $\pm$ 0.03*
H292	0	1 $\pm$ 0.00	0.70 $\pm$ 0.07	0.58 $\pm$ 0.04	0.43 $\pm$ 0.05	0.32 $\pm$ 0.02	0.21 $\pm$ 0.03
	20	1 $\pm$ 0.00	0.54 $\pm$ 0.03*	0.45 $\pm$ 0.03*	0.32 $\pm$ 0.05*	0.22 $\pm$ 0.01*	0.15 $\pm$ 0.02

Value represents means  $\pm$  SD of three independent experiments, \* p < 0.05 versus CHX control at the same time point.

**Table 27.** Relative protein levels of c-Myc of lung cancer cells were determined by Western blot analysis after treatment with MG132 or MG132 with gigantol for 1 hour.

	Gigantol ( $\mu$ M)	MG132 ( $\mu$ M)			
		0	5	10	20
H460	0	1 $\pm$ 0.00	2.36 $\pm$ 0.09 *	2.07 $\pm$ 0.08 *	1.97 $\pm$ 0.11 *
	20	0.65 $\pm$ 0.05	1.57 $\pm$ 0.06 #	1.64 $\pm$ 0.05 #	1.06 $\pm$ 0.03 #
A549	0	1 $\pm$ 0.00	2.44 $\pm$ 0.13 *	2.93 $\pm$ 0.25 *	2.76 $\pm$ 0.19 *
	20	0.70 $\pm$ 0.01	2.03 $\pm$ 0.07 #	2.42 $\pm$ 0.14 #	2.83 $\pm$ 0.19 #
H292	0	1 $\pm$ 0.00	2.28 $\pm$ 0.11	2.4 $\pm$ 0.14	1.91 $\pm$ 0.08
	20	0.46 $\pm$ 0.02	1.08 $\pm$ 0.03	1.78 $\pm$ 0.09	2.05 $\pm$ 0.08

Value represents means  $\pm$  SD of three independent experiments. \*  $p < 0.05$  versus untreated control, #  $p < 0.05$  versus gigantol-treated control.

**Table 28.** Relative protein levels of ubiquitin of lung cancer cells from the c-Myc immunoprecipitated lysates were determined by Western blot analysis after treatment with MG132 or MG132 with gigantol for 1 hour.

	Gigantol ( $\mu$ M)	
	0	20
H460	1 $\pm$ 0.00	1.71 $\pm$ 0.42 *
A549	1 $\pm$ 0.00	1.45 $\pm$ 0.17 *
H292	1 $\pm$ 0.00	1.48 $\pm$ 0.28 *

Value represents means  $\pm$  SD of three independent experiments. \*  $p < 0.05$  versus untreated control.



## VITA

**NAME** Nattanan Losuwannarak

**DATE OF BIRTH** 26 April 1985

**PLACE OF BIRTH** Ubon Ratchathani Province

**INSTITUTIONS ATTENDED** The Faculty of Pharmaceutical Sciences, Chulalongkorn University

**HOME ADDRESS** 842/11 Trok Wat Chan Nai, Khwaeng Bang Khlo, Khet Bang Kho Laem, Bangkok, Thailand 10120

**PUBLICATION** Losuwannarak N, Pasadhika C, Tantisira MH, Tantisira B. Effects of longan seed extract on scopolamine-induced learning and memory deficit in mice. Thai J Pharm Sci. 2009;33:31-8.